F.W. Klaiber, T.J. Wipf, J.C. Nauman, Y-S. Siow

Investigation of Two Bridge Alternatives for Low Volume Roads - Phase II
Volume 2 of 2

Concept 2:
Beam In Slab Bridge

July 2000

Sponsored by the
Iowa Department of Transportation
Highway Division and the
Iowa Highway Research Board

Iowa DOT Project TR-410

Final

REPORT

IOWA STATE UNIVERSITY
OF SCIENCE AND TECHNOLOGY

Department of Civil and Construction Engineering

The opinions, findings, and conclusions expressed in this publication are those of the authors and not necessarily those of the Iowa Department of Transportation

F.W. Klaiber, T.J. Wipf, J.C. Nauman, Y-S. Siow

Investigation of Two Bridge Alternatives for Low Volume Roads - Phase II
Volume 2 of 2

Concept 2:
Beam In Slab Bridge

July 2000

Sponsored by the
Iowa Department of Transportation
Highway Division and the
Iowa Highway Research Board

Iowa DOT Project TR-410

Final

REPORT

IOWA STATE UNIVERSITY
OF SCIENCE AND TECHNOLOGY

Iowa Department of Transportation

Department of Civil and Construction Engineering

ABSTRACT

This project continues the research sponsored by the Project Division of the Iowa DOT and the Iowa Highway Research Board which addresses the numerous bridge problems on the Iowa secondary road system. It is a continuation (Phase 2) of Project HR-382 in which two replacement alternatives (Concept 1 - Steel Beam Precast Units and Concept 2 - modification of the Benton County Beam-in-Slab Bridge (BISB)) were investigated.

Work continued on both of the replacement alternatives in this study, the results of which are presented in two volumes. This volume (Volume 2) presents the results of Concept 2 - Modification of the Beam-in-Slab Bridge, while the continued work on Concept 1 - Steel Beam Precast Units is presented in Volume 1.

In previous research (HR-382) an alternate shear connector (ASC) was developed and subjected to static loading. In this investigation, the ASC was subjected to cyclic loading in both push-out specimens and composite beam tests. Based on these tests, the fatigue strength of the ASC was determined to be significantly greater than that required in typical low volume road single span bridges.

The ASC was also used in the full-scale composite beam specimens tested to determine their service load behavior, ultimate strength and fatigue strength. Two of the specimens had inverted T-beams and one was constructed with an I-beam. Two full-scale two-beam specimens - representing possible bridge systems - were constructed and tested to determine their strength and behavior. These specimens also used the ASC. One of the specimens was very similar to the Canadian steel free deck system, the other - a concrete arch system - was essentially the BISB with concrete removed from the tension side and composite action added.

In all of these tests, the ASC was effective in creating full composite action during the service load tests. None of the specimens experienced a bond failure when loaded to failure. Both the steel-free deck system and concrete arch system - with the ASC for composite action - were determined to meet AASHTO strength and serviceability requirements and thus are viable low volume road bridge systems.

Each of the systems previously described are relatively easy to construct. Use of the ASC rather than welded studs significantly simplifies the work, equipment, and materials required to develop composite action between the steel beams and the concrete deck.

TABLE OF CONTENTS

LIST OF FIGURES ix

LIST OF TABLES xiii

1. INTRODUCTION 1

1.1_ Background 1

1.2_ Objective and Scope of Research 4

1.2.1 Composite Beam Specimens 5

1.2.2 Two-beam Specimens 6

1.2.3 Push-out Fatigue Specimens 7

2. LITERATURE REVIEW 9

2.1 Perfobond Rib Connector 9

2.2 Fatigue Tests 13

2.3 Arching Action and Steel-free Decks 15

3. SPECIMEN DETAILS 19

3.1 Composite Beam Specimens 19

3.1.1 Inverted T-beams 19

3.1.2 I-beam 22

3.2 Two-beam Specimens 24

3.2.1 Steel-free Deck System 25

3.2.2 Concrete Arch System 28

3.3 Push-out Specimens 31

4. TESTING PROGRAM 41

4.1 Composite Beam Tests 41

4.1.1 Load Setup 42

4.1.2 Instrumentation 44

4.1.3 Testing Procedures 47

4.2 Two-beam Tests 49

4.2.1 Load Setup 49

4.2.2 Instrumentation 54

4.2.2.1 Specimen 4 54

4.2.2.2 Specimen 5 57

4.2.3 Testing Procedures 59

4.3 Push-out Specimen Tests 60

4.3.1 Test Setup 60

4.3.2 Testing Procedures 60

4.4 Theoretical Calculations 63

4.4.1 Composite Beam Specimens 63

4.4.2 Two-beam Specimens 64

5. EXPERIMENTAL RESULTS 67

5.1 Composite Beam Results 67

5.1.1 Static Tests 67

5.1.2 Composite Beam Fatigue Test 77

5.2 Two-beam Results 83

5.2.1 Steel-free Deck System 83

5.2.2 Concrete Arch System 94

5.3 Push-out Specimen Fatigue Results 103

5.3.1 Static Tests 109

5.3.2 Fatigue Tests 111

5.3.3 Failure Mechanisms 113

5.3.4 Evaluation of Fatigue Test Results 113

5.3.5 Practical Design Implications 119

6. SUMMARY AND CONCLUSIONS 121

6.1 Composite Beam Specimens 121

6.2 Two-beam Specimens 123

6.3 Fatigue Push-out Specimens 125

7. RECOMMENDED RESEARCH 129

8. ACKNOWLEDGEMENTS 131

9. REFERENCES 133

LIST OF FIGURES

Figure 1.1. Existing and modified BISB systems 3

Figure 3.1. Details of Specimens 1 and 2 20

Figure 3.2. Details of Specimen 3 23

Figure 3.3. Details of Specimen 4 26

Figure 3.4. Details of Specimen 5 29

Figure 3.5. Placement of concrete for Specimen 5 32

Figure 3.6. Push-out specimen for SH1 34

Figure 3.7. Shear hole arrangements used in the push-out tests 35

Figure 3.8.. Photograph of formwork 37

Figure 3.9. Reinforcing bar placed through the shear hole 37

Figure 3.10. Push-out specimen cylinder strength curves 39

Figure 4.1. Load setup for composite beam tests 43

Figure 4.2. Location of strain gages at midspan 45

Figure 4.3. Location of concrete strain gages on top of slab 46

Figure 4.4. Location of steel strain gages on underside of bottom flange 46

Figure 4.5. Side view of instrumentation 47

Figure 4.6. Load setup for two-beam tests 50

Figure 4.7. Load positions on Specimens 4 and 5 52

Figure 4.8. Location of instrumentation on Specimen 4 55

Figure 4.9. Concrete strain gages around wheel footprint at Load Position 1 56

Figure 4.10. Locations of instrumentation on Specimen 5 58

Figure 4.11. Push-out specimen loading arrangement and instrumentation 61

Figure 4.12. Photograph of push-out test set-up 62

Figure 5.1. Specimen 1 service load test results.....69

Figure 5.2. Specimen 3 service load test results.....71

Figure 5.3. Midspan deflections during ultimate load testing of Specimens 1 and 3 73

Figure 5.4. Horizontal slip between steel beam and concrete slab in Specimens 1 and 3 75

Figure 5.5. Specimen 2 service load test results.....78

Figure 5.6. Midspan deflections during fatigue testing of Specimen 2.....80

Figure 5.7. Horizontal slip during fatigue testing of Specimen 2 81

Figure 5.8. Fatigue failure of the steel beam in Specimen 2 82

Figure 5.9. Service load test results for the load at Load Position 1 on Specimen 4 85

Figure 5.10. Deflection under load during service load testing at Load Positions 2 and 3 on Specimen 4.....89

Figure 5.11. Deflections under load during ultimate load testing of Specimen 4.....90

Figure 5.12. Photographs of Specimen 4 failure patterns on top of slab 91

Figure 5.13. Service load test results for the load at Load Position 1 on Specimen 5 95

Figure 5.14. Deflections under load during service load testing at Load Position 2 on Specimen 5.....98

Figure 5.15. Deflections under load during ultimate load testing of Specimen 5.....99

Figure 5.16. Photograph of failure patterns for Specimen 5 101

Figure 5.17. Static load-slip curves for series SH1 106

Figure 5.18. Reinforcing bars from specimens SH1-5 and SH1-12.....107

Figure 5.19. Photograph of specimen SH3-1 after failure 108

Figure 5.20. Photograph of specimen SH3-6 during testing 108

Figure 5.21. Static load-slip curves 109

Figure 5.22. Comparison of fatigue slip-cycle curves.....112

Figure 5.23. Failure of concrete in high stress area.....114

Figure 5.24. Photograph of concrete dowel failed in double shear (specimen SH2-7).....114

Figure 5.25. S-N curves.....116

Figure 5.26. Composite S-N curves 118

LIST OF TABLES

Table 3.1. Push-out specimens concrete properties 38

Table 5.1. Comparison of ultimate moment capacity for Specimens 1 and 3 76

Table 5.2. Comparison of ultimate moment capacity for Specimen 4.....93

Table 5.3. Comparison of Specimen 4 deflections to the maximum allowable.....93

Table 5.4. Comparison of ultimate moment capacity for Specimen 5.....99

Table 5.5. Comparison of Specimen 5 deflections to the maximum allowable.....103

Table 5.6. Summary of series SH1 test results 104

Table 5.7. Summary of series SH2 test results 105

Table 5.8. Summary of series SH3 test results 105

Table 5.9. Experimental and predicted (based on Ref. 10) static strength of ASC 111

Table 5.10. Results of regression analysis 115

1. INTRODUCTION

1.1 Background

According to a recent report by the American Society of Civil Engineers, 30% of Iowa's bridges are rated structurally deficient or functionally obsolete (versus 31.4% nationwide). A structurally deficient bridge is closed or restricted to light loads only because of its deteriorated structural components and may require immediate rehabilitation or strengthening to remain open. A functionally obsolete bridge is one that has older design features and cannot safely accommodate current traffic volumes, vehicle geometries, or weights [2].

In other words, close to one third of Iowa's bridges require strengthening, rehabilitation, or replacement. In many situations it has been determined that replacement is the most effective solution. Since 82% of Iowa's bridges are located on the county road system [25], a significant number of these replacements are county bridges.

Due to rising costs and limited county funds, bridge construction and maintenance has been kept to a minimum, thereby adding to the continuing deterioration of county bridges. In addition, Iowa has the highest percentage of rural bridge maintenance responsibilities at the county level and is one of 16 states in which the federal government is not responsible for bridge maintenance [25]. Economic constraints such as these limit a county engineer's selection of bridge replacement alternatives; thus, selecting a cost-effective alternative is critical.

Through a questionnaire sent to Iowa county engineers in 1993, the need for and interest in a study to evaluate replacement bridges was determined. Seventy six percent of

these responding indicated that such a study would be beneficial or very beneficial. A study was completed in 1993 (HR-365 "Evaluation of Bridge Replacement Alternatives for the County Bridge System"), in which several current replacement bridges were identified and evaluated [26]. From this study, it was determined that 69% of the counties were interested in designing and constructing short span bridges using their own labor forces, provided the procedures are relatively simple. Obviously costs would be greatly reduced by doing so.

Based on the questionnaire responses and the investigation described above, the research team developed one new bridge replacement concept and a modification of an existing bridge replacement system. Modifications were proposed to the existing beam-in-slab bridge (BISB) shown in Fig. 1.1a. This system consists of closely spaced steel beams and unreinforced concrete. The beam top flanges aid in the screeding process and the beam bottom flanges resist tension and support the stay-in-place plywood forms. Steel straps are welded to the beam bottom flanges at third points to eliminate transverse movement of the beams during placement of the concrete.

Three modifications to this system have been proposed in this study. These modifications are shown in Fig. 1.1b. The first modification involved using inverted T-beams, which can be cut from used I-beams to obtain the desired beam depth. If a used I-beam is deep enough, it can be cut in half to obtain two T-beams. This modification would reduce costs significantly; the skid resistance of the riding surface would also be improved as a result of eliminating the top flange of the beam from the deck surface.

The second proposed modification required the removal of concrete in the tension zone by changing the lower profile. One method proposed was to replace the plywood forms

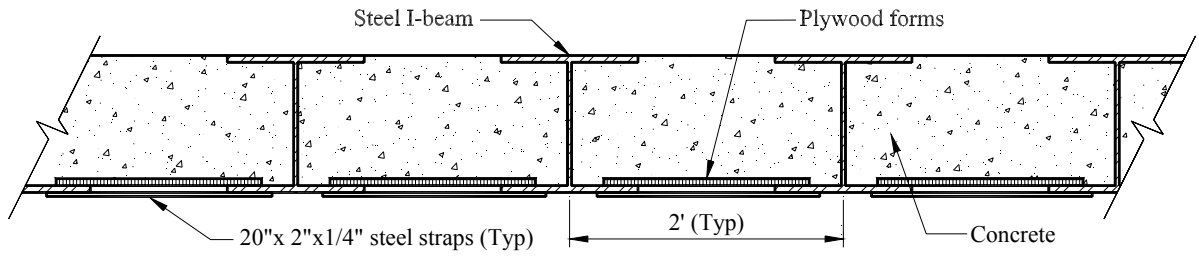

a. Existing BISB system

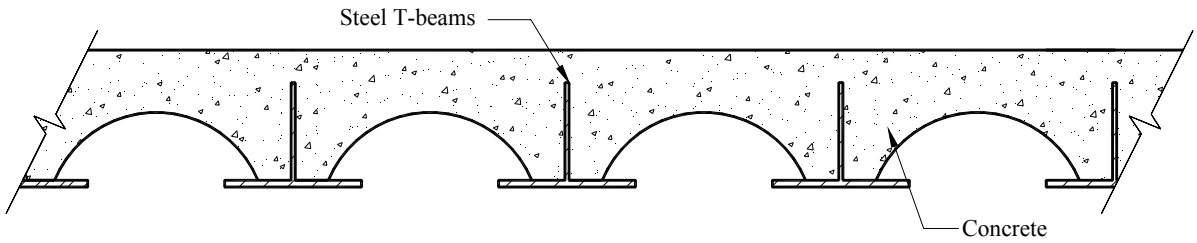

b. Modified BISB system

Figure 1.1. Existing and modified BISB systems.

with pipe sections between the beams. This reduces the self-weight and subsequently allows the system to span longer distances.

Finally, the third modification was to utilize composite action between the steel beams and the concrete. By taking advantage of this composite system, a weight savings in steel of 20 to 30% can be expected [20], thus allowing the system to span longer distances while reducing costs at the same time.

One of the objectives of the Iowa State University (ISU) investigation entitled "Investigation of Two Bridge Alternatives for Low Volume Roads, Volume 2, Concept 2: Beam-in-Slab Bridge" [10] was to evaluate and determine an effective method of developing composite action between the steel beams and concrete. Since there was not a top flange for welding shear studs, and since most counties do not have shear stud welding capabilities, an

alternate shear connector (ASC) was developed to create composite action. The ASC developed in that study consisted of drilled or torched holes in the top of the beam web and placement of transverse reinforcement through some of the holes. This concept is similar to the "Perfobond Rib" shear connector concept developed by German researchers [12].

A total of 36 push-out tests were performed in the ISU study to determine the ultimate strength and slip characteristics of the ASC. Eleven different hole patterns were used to evaluate five variables: hole size, hole spacing, hole alignment, inclusion of reinforcing steel in holes, and effects of sloppy workmanship in torching the ASC holes. The results of this testing were used to develop a strength equation to be used for design purposes.

In addition, three full-scale composite beams each utilizing the ASC and one with standard shear studs were tested. The intent of the composite beam tests was to determine the effectiveness of the ASC in providing composite action, the behavior of each composite beam under service loads, and the ultimate strength and failure mode of each composite beam.

In that study, tests were also performed on a two-beam specimen and a four-beam specimen, both modeled after the BISB system, to determine the strength and behavioral characteristics of the system under service and ultimate loads. A field test of an existing BISB in Benton County was also performed to obtain strength and behavior data.

1.2 Objective and Scope of Research

The objective of this research was to further investigate the static and fatigue strength of the ASC and to test the proposed modifications to the Benton County BISB system. This

was accomplished by constructing and testing composite beam specimens: three full-scale single beam specimens (two subjected to static loading and one to fatigue loading), two full-scale two-beam specimens representing potential bridge systems, and 27 push-out specimens.

1.2.1 Composite Beam Specimens

Continuing the research by Peterson [10,16], additional composite beam specimens were constructed and tested. In contrast to his work, a more efficient ASC design was used, along with a more realistic slab size. The ASC configuration Peterson used was over-designed causing the concrete slab to fail by crushing rather than at the shear connector. Thus, static tests were performed on two full-scale composite beams to obtain data on the revised ASC configuration. A fatigue test was also performed on a full-scale specimen to determine the fatigue strength of the ASC when used in composite beams.

Specimens 1 and 2 consisted of a W21x62 with its top flange and 1 in. of the top of the web removed, resulting in an inverted T-beam (see Chapter 3 for specimen details). Specimen 1 was loaded statically and Specimen 2 was the fatigue specimen. Specimen 3 was a W21x62 with its top flange embedded in the concrete slab. All three specimens employed the improved ASC design as mentioned previously and all holes were torched rather than drilled.

Each specimen was tested at the service level load and then loaded (statically or cyclically) to failure. The ultimate load of Specimen 1 was used in determining the load range used in Specimen 2. The following information was gathered during the static tests: degree of composite action at service load, strain/deflection/slip at service and ultimate loads,

ultimate load capacity, and mode of failure. The purpose of the fatigue test was to determine the number of cycles required to fail the ASC and to identify the mode of failure.

1.2.2 Two-beam Specimens

Two full-scale two-beam specimens, incorporating the ASC with other modifications to the BISB, were constructed and tested. These specimens represent two completely different bridge systems. As these two bridge systems were being developed, ease of construction was a major consideration.

Specimen 4 consisted of two W21x62 beams with the top flanges embedded in the concrete slab and was constructed in the same manner as Specimen 3, but without reinforcement in the slab. This system is more of a modification of the conventional slab-on-girder system than of the BISB system; however, its investigation was desirable due to its ease of construction and since it could also be used in the precast units proposed in project HR-382, Concept 1: Steel Beam Precast Units [9]. Specimen 5 is more directly related to the BISB and incorporates some of the proposed modifications. It consisted of two W21x62 beams fully embedded in concrete. A plastic pipe section, placed between the beams, was used to form a concrete arch section. This reduced the self-weight by removing the concrete in the tension region of the specimen. Both specimens employed the ASC design that was used in the composite beam specimens.

A static concentrated load, representing a wheel load, was applied between the beams and at several locations along the span of both specimens. The intent of the testing was to determine the potential application of both bridge systems, based on ultimate load capacity, failure mode, and strain/deflection behavior during service and ultimate loading.

1.2.3 Push-out Fatigue Specimens

Continuing the research of Ried [10,17], additional push-out specimens were constructed and tested. In contrast to the previous work, specimens were subjected to cyclic loading to develop the relationship between the fatigue load and the fatigue life of the connector and also to determine the slippage of the connector during testing. Three different shear hole arrangements were investigated to determine their effect on the fatigue strength; variables investigated were alignment of shear holes and the presences of reinforcing bars through the shear holes.

Six of the push-out specimens (see Chapter 3 for specimen details) were loaded statically to determine the ultimate static strength of the ASC used. The remaining 21 specimens were loaded cyclically between a constant minimum level of load and various levels of maximum load to determine the fatigue strength.

2. LITERATURE REVIEW

2.1 Perfobond Rib Connector

As introduced in Chapter 1, the ASC was developed based on the concept of the Perfobond Rib Connector. An in depth literature review, concerning the Perfobond Rib Connector, was conducted by Peterson [16], and Reid [17], and Klaiber et al. [10]. Therefore, only the information pertaining to this study will be summarized in this section.

The Perfobond Rib Connector – developed by a German consulting firm, Leonhardt and Partners [12] – was first used on the Third Caroni Bridge in Venezuela to overcome potential fatigue problems. Leonhardt et al. claims that the connector has superior fatigue resistance when compared with shear studs, which is the conventional form of shear connection used today.

The connector consists of a rectangular steel strip (typically 15 in. in length) perforated with a series of holes and welded to the top flange of a steel beam. Concrete dowels are formed when the steel strip is embedded into a concrete slab. These dowels resist the horizontal shear at the steel-concrete interface and prevent vertical separation of the two materials. Transverse reinforcement included in the holes is required to confine the concrete around the strip.

According to Yam [27], shear connectors are divided into two categories, rigid connectors and flexible connectors. Rigid connectors do not deform under load and they provide a connection that is almost slip-free; however, a brittle failure, such as a crushing or shearing failure of the concrete, is typical and undesirable. The failure mode of a flexible shear connector is more ductile and less catastrophic than a rigid connector [27]. Despite a

desirable failure mode, the flexible connector is not quite ideal because it deforms under load and therefore it is prone to fatigue problems. A rigid connector does not suffer from fatigue problems [19].

As explained by Leonhardt et al., the ideal shear connector is one that provides slip-free behavior at service level and ductile behavior at ultimate. Therefore, the characteristics of a rigid connector are desirable at service level and the characteristics of a flexible connector are desirable at ultimate. The shear stud offers a ductile failure, but since the shear stud is a flexible connector it deforms under load and therefore is prone to fatigue problems [19]. The Perfobond Rib Connector offers the ideal combination of a rigid and flexible connector. It provides a rigid connection at service level while exhibiting ductile behavior at ultimate [12].

Leonhardt et al. confirmed this ideal performance through a series of three push-out tests using the Perfobond Rib Connector and two push-out tests using shear studs [12]. Each specimen with the Perfobond Rib Connector was subjected to a static service load before 2 million load cycles at approximately 40% of ultimate strength was applied. Finally, the specimens were loaded statically to failure. Only fatigue tests were performed on the specimens with shear studs. The following summarizes the performance of the Perfobond Rib Connector:

- Very little slip occurred between the concrete and steel during the static service load tests (approximately 0.004 in.).
- Essentially no increase in slip occurred due to the cyclic loading.
- After 500,000 cycles, slips of between 0.004 in. and 0.008 in. were measured.

- After 2 million cycles, slips of between 0.006 in. and 0.010 in. were measured (slips for the shear studs were significantly higher at 0.06 in.).
- A superior fatigue performance compared to that of the shear stud was concluded.
- Large plastic deformations were recorded at ultimate.
- After failure, load was adequately sustained.

Three possible failure modes were identified by Leonhardt et al.[12]: shearing of the concrete dowels, bearing failure of the concrete in the holes, and shearing of the steel strip between the holes. The desired failure mode is shearing of the concrete dowels and therefore the Perfobond Rib Connector is designed to ensure this mode of failure. With this in mind, the behavior of the connector, as explained by Leonhardt et al. [12], is presented. At service level, the load is transferred from the concrete slab to the steel strip, which is appropriately welded to the steel beam, by means of the concrete dowels in the holes. With increased loading, greater shearing stresses occur in the dowels and slip between the concrete and steel begins. Once shearing begins, the load transfer changes to that of friction between the concrete inside the holes and the surrounding concrete. Splitting between these two surfaces is prevented by the transverse reinforcement in the holes. Once the dowels completely fail in shear, confinement from the transverse reinforcement and aggregate interlock maintain the level of friction, therefore preventing a brittle failure.

Additional research has also established the Perfobond Rib Connector as a viable means of shear connection. Roberts and Heywood [18,19] incorporated the Perfobond Rib Connector into a composite section that eliminates the top flange. As pointed out by Roberts and Heywood, the top flange contributes little to the strength of a composite section and its

primary function is to provide lateral stability during construction and a location for welding shear studs. Therefore, a shear connector that does not require a top flange is desirable.

Their investigation was aimed at evaluating the performance of the Perfobond Rib Connector (i.e. holes through beam web) without the top flange. A series of push-out tests, consisting of Perfobond Rib Connector specimens with and without a top flange, were performed. From these tests the following conclusions were made:

- Using the Perfobond Rib Connector (i.e. holes through beam web) without a top flange is feasible.
- The strength of the concrete to steel bond (at the concrete slab and beam web interface) contributes to the strength of the shear connection.
- The initial stiffness was similar when comparing the behavior of the connector with and without a top flange. However, a reduction in the ultimate strength was experienced without the top flange, because the concrete was not tightly confined around the holes by the flange.
- As holes are spaced closer, the load decreases.
- Cracking and spalling of the concrete at the interface of the concrete and steel was a typical failure for the specimens without a top flange.

A full-scale bridge was also constructed and tested to reproduce the behavior exhibited by the push-out test specimens and to verify the claimed fatigue performance of the Perfobond Rib Connector [18]. The conclusions of the test results are as follows:

- No measurable signs of deterioration was observed after 500,000 cycles.
- The section performed satisfactorily under ultimate loads.

- No relative displacement between the slab and girder occurred during the ultimate load test.
- The innovative bridge cross-section is feasible, which will lead to more economically competitive composite designs.

Roberts and Heywood noted that despite economical advantages of the steel T-beam cross-section, the section has its disadvantages. Special handling and construction techniques are required because the T-beam is unstable before the concrete deck is in place. Erecting the section with the concrete deck precast onto the steel T-beam was investigated and found to be feasible. In doing so, the steel beams would not be required to support construction loads without a top flange. Another disadvantage is that deck replacement would be more difficult. However, in places where climatic conditions are not severe, deck replacement is unusual [18].

2.2 Fatigue Tests

Currently, studies on the static behavior of the ASC are fairly well established. However, data on the fatigue strength and behavior of this type of shear connector when subjected to cyclic loading is limited.

Fatigue problems with shear connectors are always a concern in composite structures subjected to cyclic loading. Considerable research has been conducted on the fatigue of shear connectors in steel - concrete composite structures, especially stud shear connectors. Previous studies consisted of two approaches: fatigue tests of push-out specimens and of composite beams [8,24].

Although direct shear stress in the concrete slab of a push-out specimen is not really comparable to the flexural stress in a composite beam concrete slab, the use of push-out tests is commonly used for several reasons [11,21,23]. In beam specimens, the failure of one or two connectors can not always be detected, and does not significantly affect the beam behavior as the shear is redistributed to other connectors. On the other hand, in push-out specimens, the loads on the connectors can be evaluated more easily because redistribution is not significant. In addition, early investigations indicated that the fatigue strength of shear connectors obtained from push-out tests was lower than that obtained from beam tests [11,23]. In the beam tests, after loss of interaction between the shear connector and the concrete, load on the connector was redistributed, which resulted in a less severe stress condition than computed from elastic theory assuming complete interaction [21]. In the push-out specimens, the loading on the connectors was maintained at a reasonably constant level throughout their life. Push-out tests, therefore, represent a lower bound for connector failures. As a result, push-out tests can be used in evaluating the fatigue strength of the ASC. Also, a relatively large number of push-out specimens can be tested more economically, compared to full-scale composite beam specimens.

In previous studies of the fatigue strength of shear connectors, cyclic loading was often applied at a frequency of 250 or 500 cycles per minute. In these studies, strains were seldom recorded as the fatigue strength of connectors can not be established by measuring the local peak stresses and strains.

The relationship between fatigue stress and fatigue life (S-N curve) was used to determine the fatigue strength of shear connectors. Data were plotted either logarithmically or semi-logarithmically.

2.3 Arching Action and Steel-free Decks

The reinforcing system used in Specimen 4 of this study was based on the steel-free deck concept. Extensive research on steel-free decks has been conducted in Canada and is briefly summarized in this section.

It is now recognized, based on extensive research on the behavior of reinforced concrete deck slabs, that an internal arching action is developed when the concrete deck is subjected to a concentrated load. In-plane compressive stresses generated by the arching action cause the slab to fail by punching shear, rather than flexure [13]. Furthermore, a higher failure load is attained with a punching shear failure than with a flexural one. Unfortunately, concrete deck slabs are designed for failure by flexure, which leads to unnecessary amounts of reinforcing steel. Research findings have proved that only a minimal amount of reinforcement is required to develop arching action. Therefore, by taking advantage of this enhanced behavior of the slab smaller amounts of reinforcement are required. Less reinforcing steel would increase the durability of the concrete against the effects of steel corrosion. The elimination of all reinforcing steel would be ideal for a most durable concrete deck slab.

AASHTO's LRFD Bridge Design Specifications [1] permit an empirical deck design that recognizes the arching action behavior. This empirical design is similar to the one specified by the Ontario Highway Bridge Design Code (OHBDC) [15] since its first edition in 1979. Although prototype tests indicated that 0.2% steel in each direction of a reinforcement layer was sufficient for strength, a conservative value of 0.3% of the gross area is specified in both codes [5].

Research has found that arching action can be fully developed if the slab is confined adequately in both the transverse and longitudinal directions [6]. Restraining the relative lateral displacements of the beams provides the transverse confinement. Longitudinal confinement of the slab is provided by connecting the slab to the beams with shear connectors and by providing adequate edge stiffening. Tests conducted by Bakht and Agarwal [4] have shown that for a deck slab to maintain the compressive forces developed by the arching action near a transverse free edge, the edge must be appropriately stiffened to provide restraint in the plane of the slab. As suggested by Mufti et al. [13], a channel placed with its major flexural rigidity in the horizontal plane and connected to the concrete slab by some form of mechanical connector can provide the necessary edge stiffening.

It was realized by Mufti et al. [13] that in a conventionally reinforced deck slab, the bottom transverse reinforcement provides the confinement in the transverse direction. This was later confirmed by Bakht [3]; Bakht stated that the bottom transverse reinforcing bars act as ties to the transverse internal arch within the slab thickness. In addition, the reinforcement in a conventional slab provides the in-plane restraint necessary to develop the arching action near a transverse free edge. Recall, however, that the amount of reinforcement provided in a conventional slab is more than what is needed for the confinement of the slab; only 0.2% of the gross concrete area is required.

As stated earlier, eliminating all reinforcing steel would be ideal. In light of this, Mufti et al. [13] developed a deck slab in which transverse confinement was provided by an external means and the control of cracking due to temperature and shrinkage was provided by low-modulus fibers in the concrete. Therefore, no steel reinforcement was required in the slab. The purpose of the research was to develop a steel-free deck slab that has the same

load-carrying characteristics as conventionally reinforced deck slabs. Four specimens were tested primarily to determine an effective means of restraining lateral displacements of the beams.

In the first specimen, there were only three intermediate diaphragms for lateral restraint. End diaphragms were added to the second specimen. In both specimens it was realized that the arching action could not be developed because the diaphragms could not effectively restrain the lateral movement of the beams above their connection points at the webs of the beams. Therefore, steel straps were welded to the top flanges in the third specimen. Due to the localized failure at midspan, a second and third test was performed 3 ft and 1.5 ft from the ends of the model, respectively. Conclusions from the testing of the third model are as follows:

- Punching shear failures indicate that the arching action was developed.
- The steel straps provide transverse confinement (lateral restraint of the top flange) in the same manner as the bottom transverse reinforcement. The only difference being the steel straps provide an external means of restraint while the reinforcement restrains internally.
- As the load was placed closer to the unstiffened transverse free edge, the ultimate load decreased and the failure mode degenerated towards a flexural one, which suggested a decline in longitudinal restraint (due to the unstiffened edge).
- Punch failure areas at the top of the slab were slightly larger near the ends than at midspan, also due to a reduced in-plane restrain caused by an unstiffened edge.

The fourth specimen was the same as the third except a third girder was added to study the behavior of the system subjected to a pair of concentrated loads straddling the

interior girder. Tests confirmed that arching action could be developed under this loading scenario.

It should be noted that additional research by Bakht and Selvadurai [7] concluded that the low-modulus fibers in the steel-free decks have no influence on the strength of the deck slab and that cracks have no effect on the performance of a deck slab that is suitably confined.

3. SPECIMEN DETAILS

3.1 Composite Beam Specimens

Three full-scale composite beam specimens were constructed and tested to evaluate the ultimate strength and fatigue strength of the ASC. Two of the specimens consisted of inverted T-beams and the other was constructed with an I-beam. All three specimens utilized the improved ASC configuration, as mentioned in Chapter 1, and all of the ASC holes were torched. Each specimen was 34 ft in length.

The ASC was designed to develop the full capacity of either the steel beam or concrete slab whichever was lower (in this case the steel beam controlled). The nominal shear resistance was determined from ultimate strength results obtained from previous push out tests of various hole configurations [22]. The method used to design the ASC was according to the one described in the AASHTO LRFD Bridge Design Specifications [1].

The slab width for all three specimens was chosen to be 3 ft – 9 in., which was based on a typical beam spacing for a 30 ft wide bridge. Reinforcement for the slab was based on conventional bridge deck design [1]. The longitudinal reinforcement consisted of two layers of #3 bars spaced on 11 in. centers. The transverse reinforcement consisted of two layers of #4 bars spaced on 18 in. centers. The design required a spacing of 7 in., but since in these beam tests the transverse reinforcement was structurally unnecessary, the maximum spacing permitted for shrinkage requirements (i.e., 18 in.) was used.

3.1.1 Inverted T-beams

Specimens 1 and 2, shown in Fig. 3.1, each consisted of a W21x62 with its top flange and 1 in. of the web removed, resulting in an inverted T-beam with a depth of 19 1/2 in. The

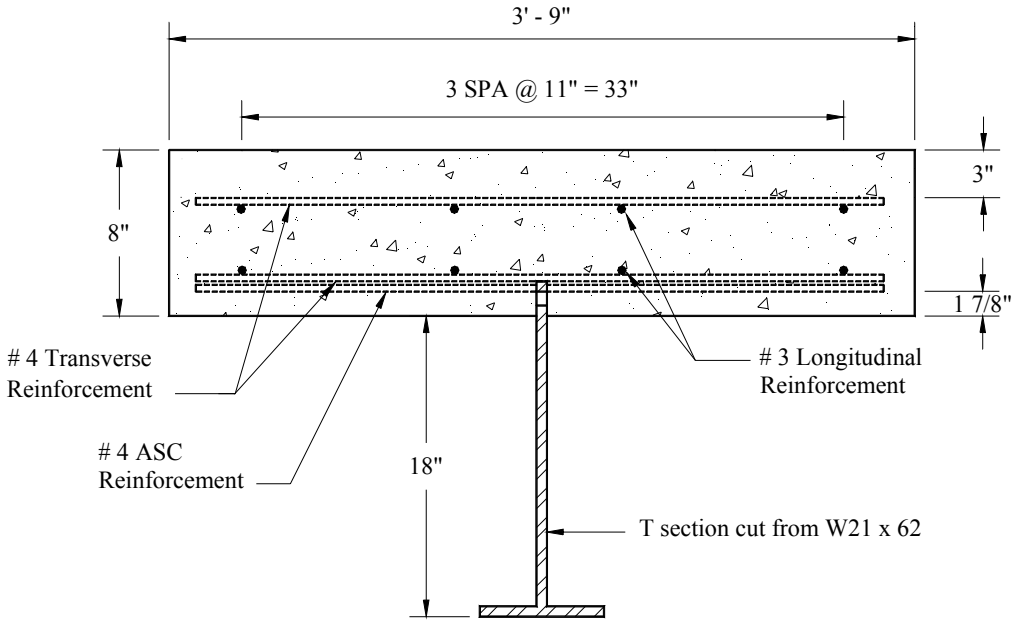

a. Cross-section view

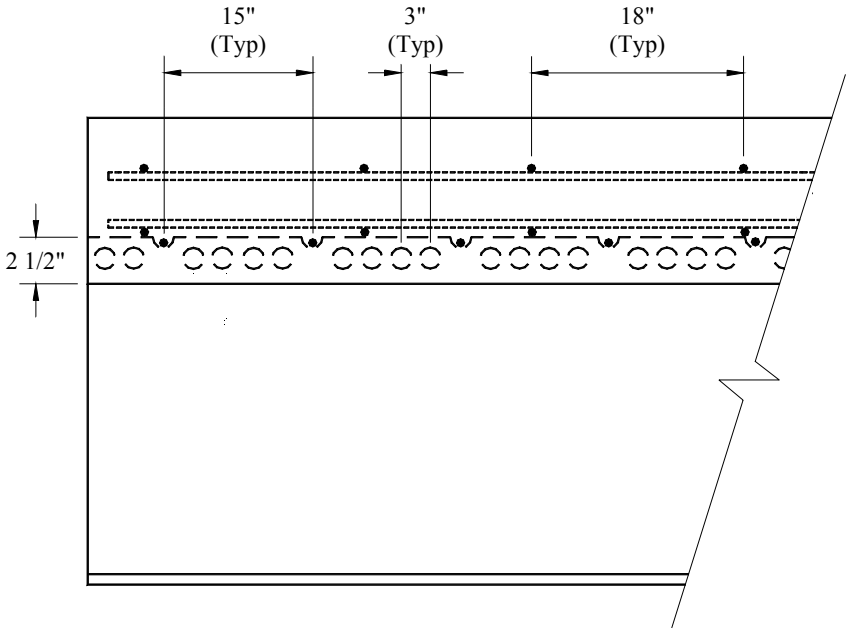

b. Side view

Figure 3.1. Details of Specimens 1 and 2.

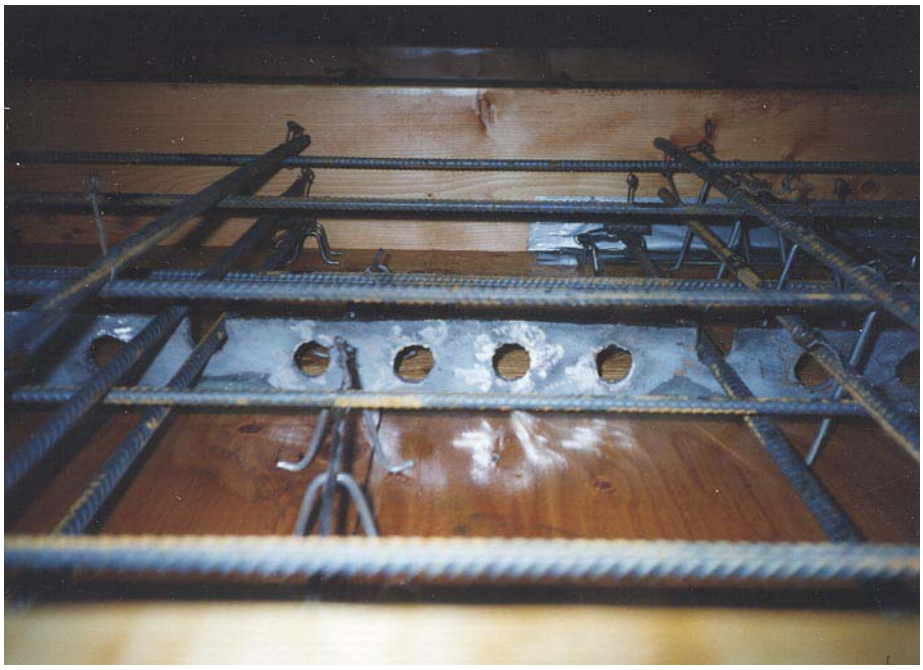

c. Photograph of ASC and slab reinforcement

Figure 3.1. Continued.

top 2 1/2 in. of the remaining web was embedded into the bottom of the 8 in. concrete slab, giving a total specimen depth of 25 in. The ASC consisted of 1 1/4 in. diameter torched holes spaced on 3 in. centers and vertically centered within the 2 1/2 in. embedment of the web; the exception to this was a half hole every 15 in. located at the top of the inverted T-beam. To resist transverse tension forces developed during horizontal shear transfer, #4 reinforcing bars were placed in the half holes.

The beams and formwork were fully supported during placement of the concrete. To remove the formwork it was necessary to lift the specimens, allowing access to the forms. For this reason, formwork removal did not begin until the concrete obtained an adequate compressive strength.

3.1.2 I-beam

Specimen 3, illustrated in Fig. 3.2, was a W21x62 with its top flange embedded in the concrete slab. The depth of embedment was 3 1/4 in. resulting in a specimen depth of 25 3/4 in. Since the top flange was not removed, the ASC was modified from that used in Specimens 1 and 2. It consisted of a continuous line of 1 1/4 in. diameter holes spaced on 3 in. centers. Due to the absence of the half holes, the #4 reinforcing bars were placed through every fifth hole (15 in. spacing), as illustrated by Figs. 3.2b and 3.2c. These bars simply rested on the bottoms of the holes and were kept firmly in place by attaching the ends of the bars to the formwork, which prevented movement during concrete placement. The center of each hole was located midway between the bottom of the slab and the bottom of the top flange (1 3/8 in. from both).

The top flange was not removed in Specimen 3 to obtain information on the behavior of the ASC in conjunction with a top flange. Recall from Chapter 1, one reason to remove the top flange from a used I-beam is to reduce the beam depth to the desired depth. However, it is possible that the used I-beam is already at the desired depth so removal of the top flange would not be necessary. Therefore, Specimen 3 was tested to represent this scenario.

Once again, the beams and formwork were fully supported during placement of the concrete, and the formwork was removed once the concrete obtained an adequate compressive strength. After the removal of the forms, a small void was found under the top flange at one end of the beam; however, it would not have an effect on the shear transfer since the void was located beyond the centerline of the end support and was relatively small. It was then realized that due to the embedment of the top flange, special attention during the

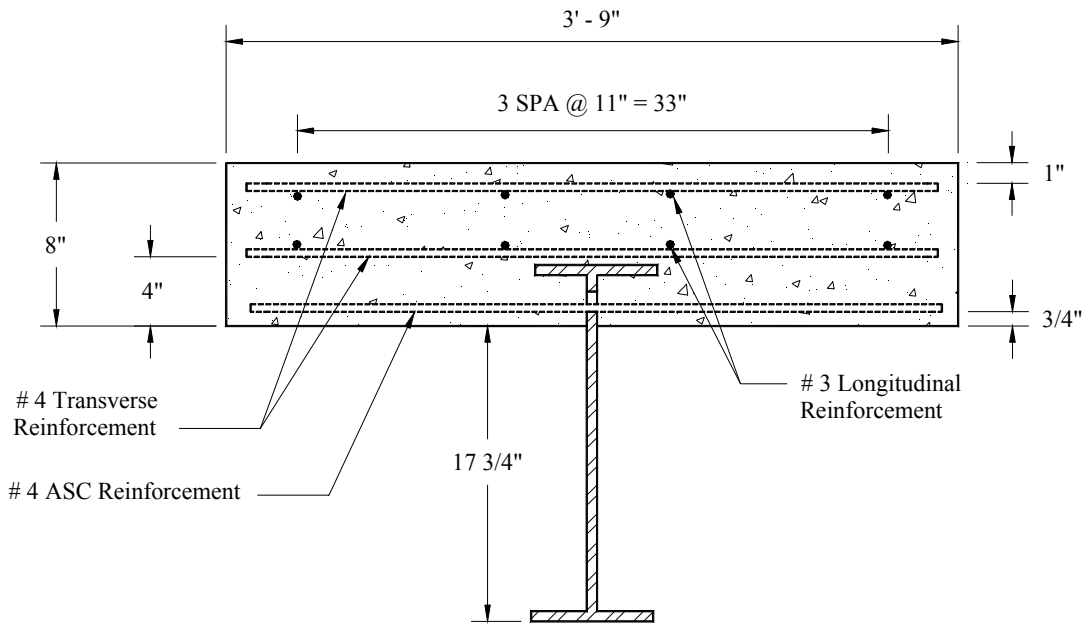

a. Cross-section view

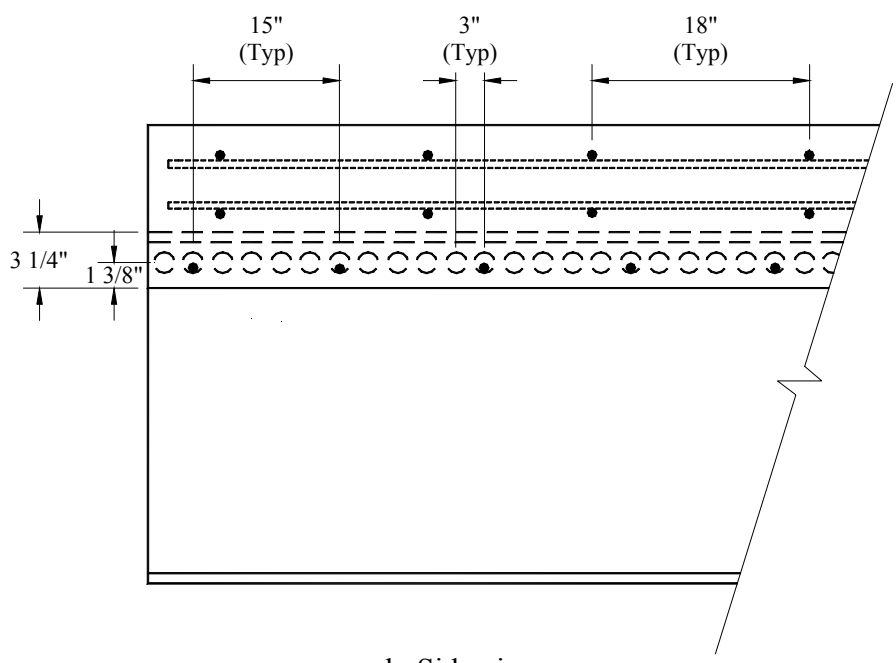

b. Side view

Figure 3.2. Details of Specimen 3.

c. Photograph of the embedded top flange and the ASC

Figure 3.2. Continued.

placement and vibration of the concrete was necessary to ensure minimal voids at the web-flange intersection.

3.2 Two-beam Specimens

Two full-scale two-beam specimens, representing possible bridge systems, were constructed and tested to determine the potential of each. Both specimens utilized the ASC configuration used in Specimen 3. In developing these systems to incorporate the ASC with other modifications to the BISB, certain constructibility requirements had to be met. As previously noted, one way of increasing the span length was to reduce the self-weight – that is remove concrete on the tension side of the specimen. Minimum reinforcement shall be used except for that used in the ASC (easier to construct and lowers construction and

maintenance costs). To keep costs minimal, no manufactured stay-in-place forms shall be used. The following two systems were chosen over other innovative concepts due to their compliance with these requirements.

3.2.1 Steel-free Deck System

As shown by Fig 3.3, Specimen 4 consisted of two W21x62s with their top flanges embedded into an 8 in. concrete slab. A beam spacing of 3 ft – 9 in. was used, which was again based on a typical beam spacing for a 30 ft wide bridge. Specimen 4 was constructed similar to Specimen 3 except the slab was unreinforced. The only reinforcement in the slab was #5 bars placed every 15 in. through the holes of both beams.

The reinforcing system used in Specimen 4 is based on the Canadian research on steel-free decks. As explained in Chapter 2, a steel-free deck obtains its strength through an arching action type behavior of the concrete slab, with the beams acting as the supports and the reinforcing steel as tension ties (lateral restraint). This contradicts the philosophy currently in use for designing slabs, which is based on a flexural behavior and requires more steel.

The transverse reinforcement previously noted (i.e., #5's on 15 in. centers) has a dual purpose; it acts as a tension tie between the beams and it contributes to the strength of the ASC just as it did in previous specimens. Due to the minimum reinforcement ratio required to develop the arching action, #5 bars were used instead of #4 bars. As illustrated in Fig. 3.3b, four bars spaced on 3 in. centers were used at both ends in an effort to provide edge stiffening, which is necessary in developing arching action near a transverse free edge (see

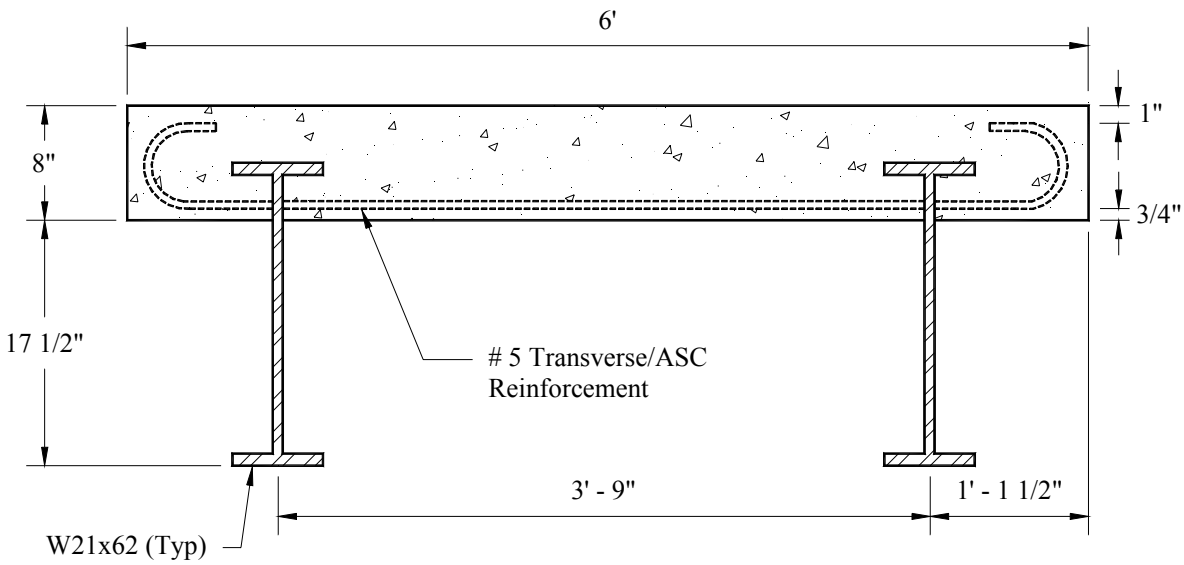

a. Cross-section view

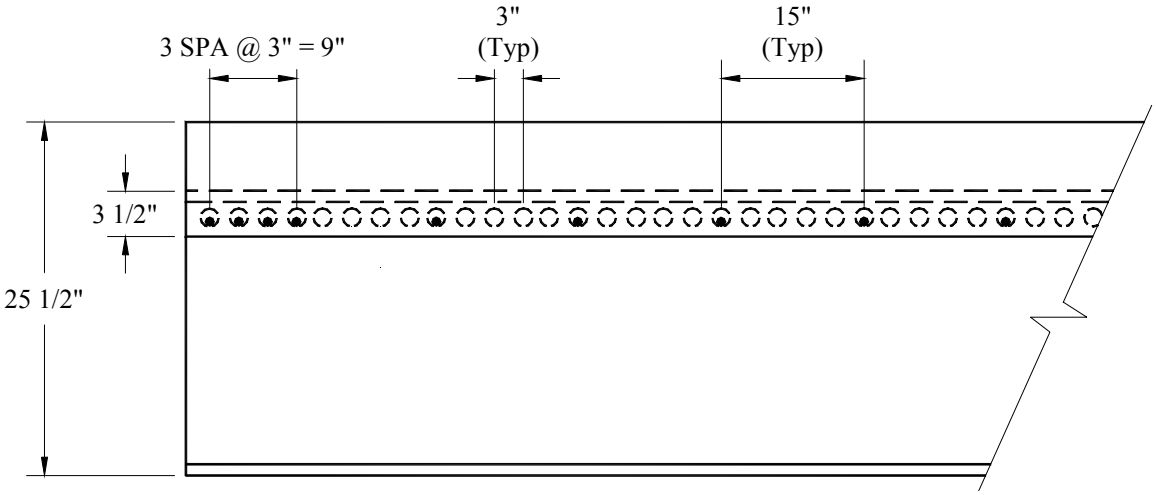

b. Side view

Figure 3.3. Details of Specimen 4.

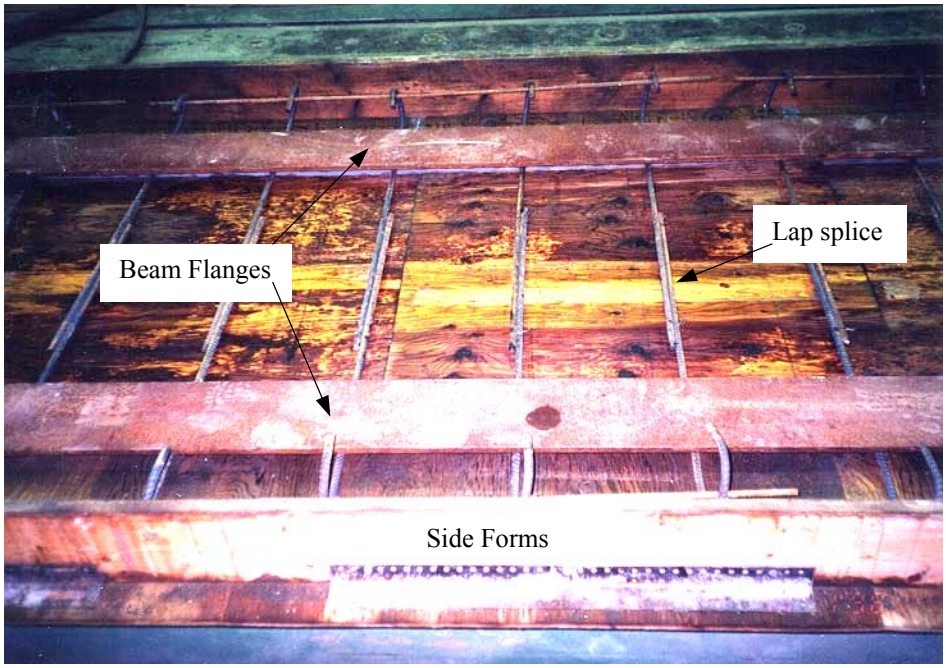

c. Photograph of transverse/ASC reinforcement

Figure 3.3. Continued.

Chapter 2). In Specimen 4, the ends of the reinforcing bars were bent to obtain proper anchorage; however, in a full width bridge these bars would be continuous. Because of these bends and the fact that these bars needed to be placed through the holes of both beams, bars with one bent end and one straight end were fabricated. Once the straight ends were placed through the holes, they were tied together at the proper lap splice length (see Fig. 3.3c).

Once again, the beams and formwork were fully supported during placement of the concrete, and the formwork was removed once the concrete obtained an adequate compressive strength. After the forms were removed, a void was found again under the top flange at the end of one of the beams. Due to the size of the void, it was filled with high strength grout. To help ensure proper confinement of the concrete under the top flange, it is

suggested that the concrete be poured between the beams allowing the concrete to flow under the flanges, rather than pouring it directly over the flanges as was done in the construction of Specimen 3.

3.2.2 Concrete Arch System

Illustrated in Fig. 3.4 is Specimen 5; this specimen consisted of two W21x62s fully embedded in a concrete arch system with the arch spanning between the beams. Again, a beam spacing of 3 ft – 9 in. was used. This specimen is more directly related to the BISB than Specimen 4 and incorporates the proposed modifications, stated in Chapter 1. Such modifications include removing some of the concrete on the tension side of the specimen by using pipe sections in between the beams and utilizing composite action by connecting the steel beams and the concrete.

The modification that consisted of removing the top flange was not included in Specimen 5. A practical case could be made for not removing the top flange because the flange aids in the screeding process for the system represented by Specimen 5. In addition, the top flange can provide lateral stability to the steel beam during construction. If, however, skid resistance is a primary concern, the top flange could be fully encased by concrete (4 in. of additional concrete on top) or it could be removed as it was in Specimens 1 and 2. Additional concrete would increase the self-weight and removal of the top flange would decrease the ultimate capacity of the composite section.

In the design of Specimen 5, a minimum concrete thickness at the top of the arch was conservatively chosen to be 8 in., which is consistent with the thickness of the slabs in the previous specimens. A pipe section, cut from a 42 in. diameter plastic pipe, was used to form

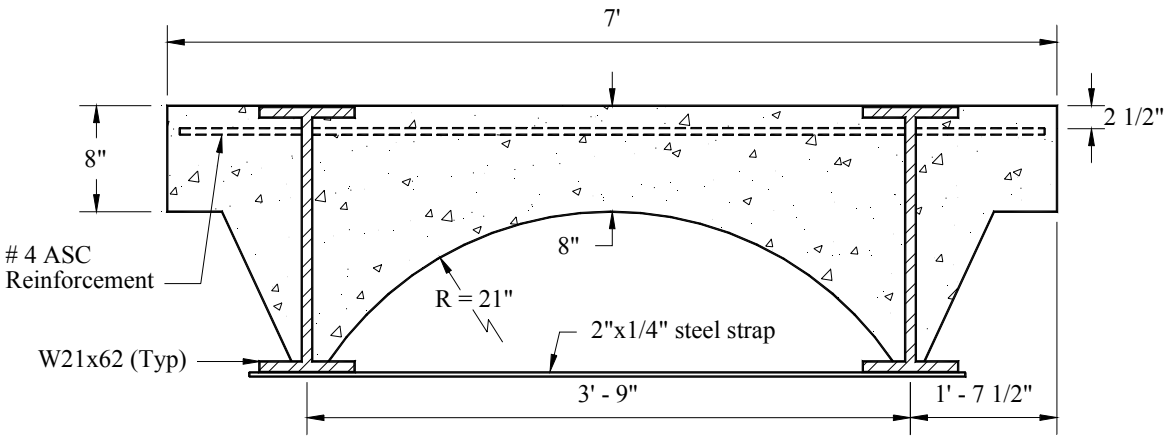

a. Cross-section view

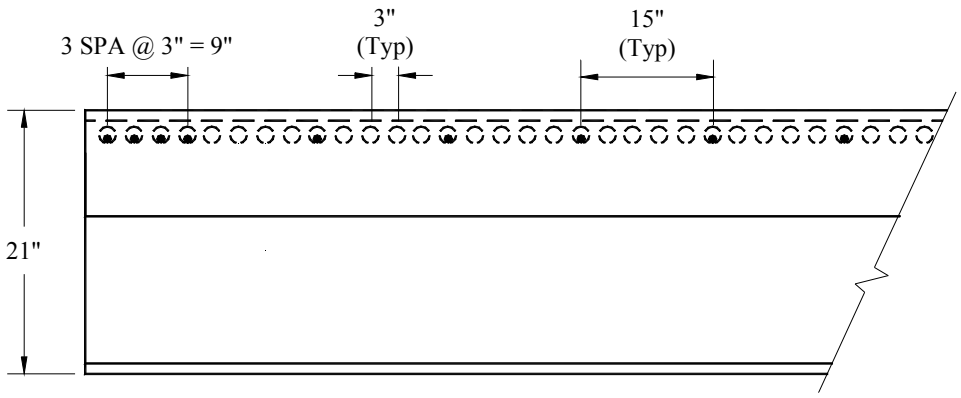

b. Side view

Figure 3.4. Details of Specimen 5.

c. Photograph of formwork and reinforcement

d. Photograph of end with concrete

Figure 3.4. Continued.

the arch and reduced the amount of concrete between the beams by 36%. The use of a 42 in. diameter pipe was necessary to obtain a pipe section that satisfied the geometric conditions (i.e., beam spacing and depth, and minimum concrete thickness). The sides of the specimen were formed with plywood to simulate a half arch shape.

Number four bars on 15 in. centers were again used for part of the shear connection. Due to the increase in specimen width (84 in.), the reinforcement did not require hooks for anchorage. To restrain movement of the beams during placement of the concrete, 2 in. x 1/4 in. steel straps were welded to the bottom flanges at the third points, an idea originating from the Benton County BISB system.

Most likely the concrete arch system would not be used as a pre-cast unit. Thus, it was decided to not provide continuous support of the beams and formwork, as was done in the previous specimens. This would simulate actual field conditions assuming unshored construction. Concrete was placed in three lifts due to the depth of Specimen 5; each lift was vibrated separately. The second lift ended just below the bottom of the ASC holes (see Fig. 3.5a). The third lift was first placed between the beams and vibrated until concrete flowed through the holes as illustrated by Fig. 3.5b. Once this was accomplished for all the holes, concrete was placed along the sides to complete the third and final lift. This method ensured proper placement of the concrete through the ASC holes. The forms were removed after one week, and no voids were visible.

3.3 Push-out Specimens

In this investigation, 27 push-out specimens were tested. These specimens were grouped into three series. The first series (SH1) consisted of 12 specimens. SH2, the second.

a. Photograph after first two lifts

b. Photograph after vibration of third lift in between the beams

Figure 3.5. Placement of concrete for Specimen 5.

series, consisted of nine specimens, and the last series, SH3, had three specimens. Each specimen consisted of a stiffened, steel shear plate 3/8 in. x 20 in. x 15 in. partially encased in two concrete slabs 8 1/4 in. x 21 in. x 20 in. Overall dimensions of each test specimen are presented in Fig. 3.6

The contact area in each slab -17 in. x 2 1/2 in. - between the concrete and steel was held constant in each series. Details of the shear hole arrangements are given in Fig. 3.7. The diameter and the center-to-center spacing of the shear holes were kept constant while the alignment of the shear holes was varied (SH1 vs. SH2). In addition to studying the effects of the alignment of the shear holes, the influence of placing reinforcing bars through the shear holes was also investigated (SH1 vs. SH3). All of the ASC were made from 3/8 in. thick steel plate, which was chosen to simulate beam web thicknesses that might be encountered in the field.

The concrete for these specimens was an Iowa DOT Class C-4 mix purchased from a ready-mix company. The cement content for Iowa Class C-4 concrete is 624 lb/yd^3 with a water cement ratio of 0.429.

Transverse slab reinforcement in each of the concrete slabs was kept constant. For each specimen, two #4 reinforcing bars were used per specimen (i.e. one bar for each ASC). The amount of transverse slab reinforcement used was based on previous research [3] for consistency.

An initial concern was that large loads applied on the 3/8 in. thick steel shear plate might induce lateral buckling. To prevent such buckling, C8 x 11.5 channel stiffeners were bolted on each side of the steel shear plate; as illustrated in Fig. 3.6, one stiffener was cut shorter than the other to facilitate the instrumentation.

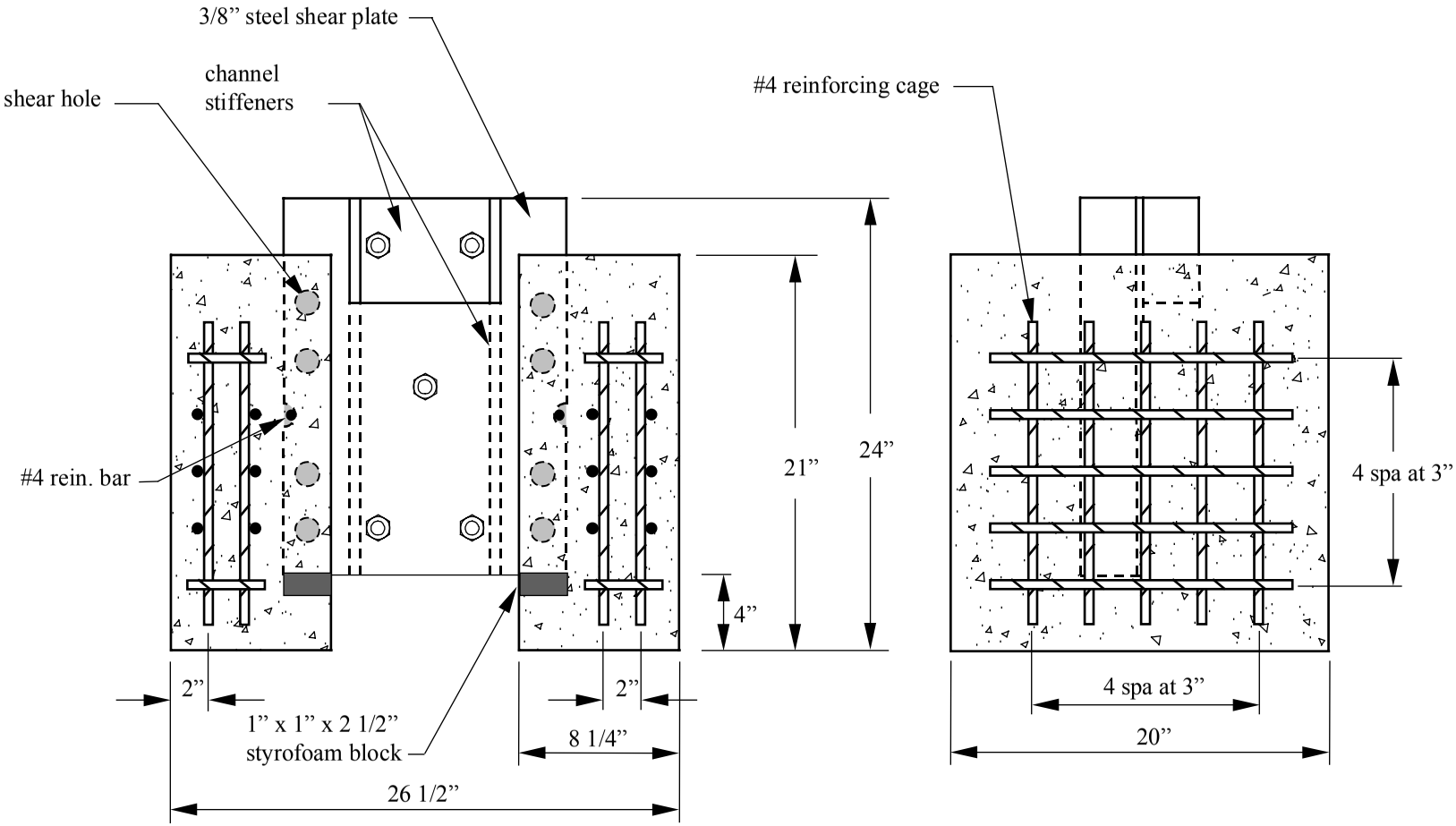

Figure 3.6. Push-out specimen for SH1.

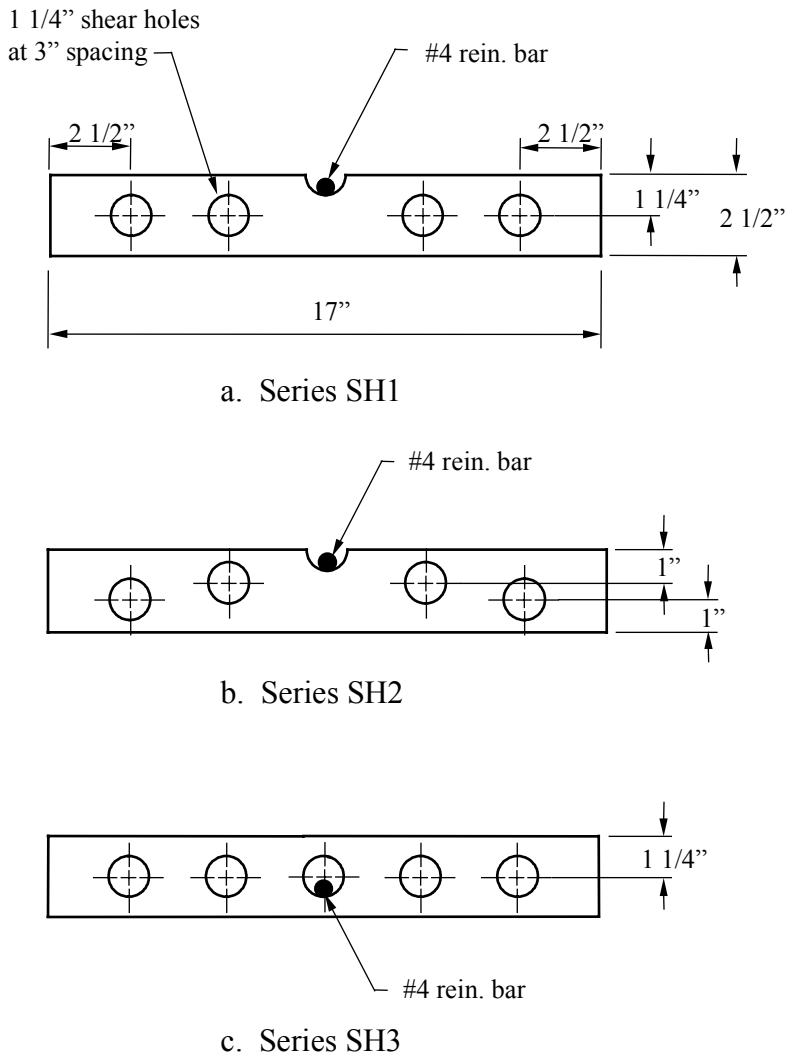

Figure 3.7. Shear hole arrangements used in the push-out tests.

Fabrication of the push-out specimens involved torching shear holes in the 3/8 in. shear plate. The shear holes were torched instead of drilled because torching is more suitable for available county bridge equipment. To fasten the lateral stiffeners, five 3/4 in. diameter holes were drilled in the shear plate. An unrestricted slip path for the shear plate was created by attaching styrofoam to the bottom edge of the shear plate (Fig. 3.6). Reinforcing steel cages illustrated in this figure were fabricated to provide transverse slab reinforcement. Steel forms were constructed so that three specimens could be cast simultaneously (see Fig. 3.8). Once the plywood dividers were placed in the steel form, form oil was applied to the interior surfaces of the forms to facilitate removal. Figure 3.9 illustrates how the 16 in. long #4 reinforcing bars were placed through the shear holes. Each reinforcing bar was held in place against the shear plate by wire through the plywood portion of the forms. Once the pre-fabricated reinforcing steel cages were placed in the forms, the forms were sealed.

Both sides of the push-out specimens were cast at the same time, ensuring consistent concrete strength. Specimens SH1 were cast from the first batch of concrete; specimens SH2 and SH3 were cast from the second batch. The concrete was placed in three lifts. Each lift was thoroughly vibrated to eliminate air voids in the specimens. Concrete samples were taken during the casting to determine the slump and air content of the concrete.

In addition to the push-out specimens, 24 - 6 in. diameter x 12 in. high - standard ASTM concrete test cylinders and four 6 in. x 6 in. x 5 ft modulus of rupture beams were cast from each batch of concrete. Table 3.1 and Fig. 3.10 show the concrete properties and cylinder strength curves of the concrete, respectively.

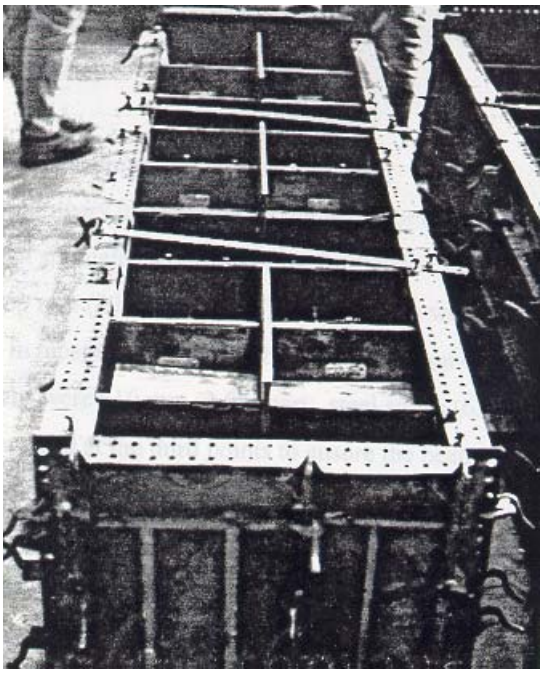

Figure 3.8. Photograph of formwork.

Figure 3.9. Reinforcing bar placed through the shear hole.

Although the same type and strength of concrete was ordered each time, the concrete strength differed from series SH1 to series SH2 and SH3 (series SH2 and SH3 were cast from same batch of concrete). The higher slump in series SH1 indicated a high water content which resulted in the lower concrete strength in series SH1.

After completion of each pour, the exposed surfaces of the specimens were finished and covered with polyethylene to prevent moisture evaporation. Forms were removed after seven days and the specimens were allowed to air cure until tested. All of the specimens were tested after the 28-day curing period.

Table 3.1. Push-out specimens concrete properties.

Series	Air content (%)	Slump (in.)	Modulus of Rupture (psi)	Compressive Strength 28-day (psi)
SH1	5.5	7	408	3,700
SH2, SH3	7.5	3	621	6,130

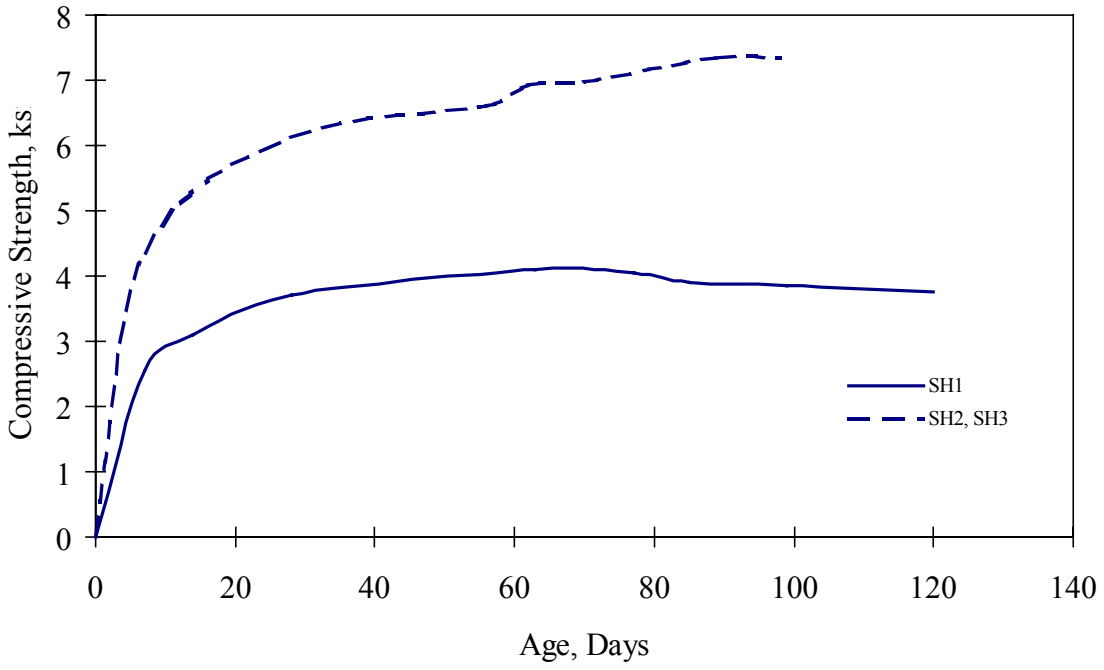

Figure 3.10. Push-out specimen cylinder strength curves.

4. TESTING PROGRAM

As previously noted, tests were performed on three full-scale composite beam specimens (two loaded statically and one loaded in fatigue), two full-scale two-beam specimens (both loaded statically) and on 27 push-out specimens. This chapter presents the load setup, instrumentation, and testing procedures used for these specimens.

Instrumentation for all of the beam tests included three different types of measuring devices. Direct current displacement transducers (DCDTs) were typically used to measure slip between the concrete slabs and steel beams. Celesco string potentiometers (Celescos) were used to measure vertical deflection of the specimens. Electrical-resistance strain gages (strain gages) were used to measure strain in the concrete and steel.

The strain gages were applied and protected according to recommended procedures. A three-lead-wire system was employed for all strain gages to minimize the effects of long lead wires and temperature changes. The lead wires, including those for the DCDTs and Celescos, were connected to a computer controlled data acquisition system (DAS), where the output from the measuring devices was collected and stored in a report-ready format.

Instrumentation for the push-out specimens consisted of DCDTs to measure the relative slip between the concrete slabs and the steel shear plate. The transducers were positioned to measure the slip relative to the centerline of the shear connectors.

4.1 Composite Beam Tests

The purpose of the composite beam tests was to further investigate the static and fatigue strength of the ASC. The investigation involved gathering the following information

during the static tests: degree of composite action at service load, strains/deflections/slip at service and ultimate loads, ultimate load capacity, and mode of failure. The following information was obtained during the fatigue test: slip, deflections, the number of loading cycles applied to the specimen, and the mode of failure.

4.1.1 Load Setup

As illustrated in Fig. 4.1, the load setup used during the composite beam tests consisted of two line loads across the slab width, each located 4 ft – 6 in. from midspan. The load was applied using two, 55 kip capacity, hydraulic actuators. These actuators were used for both static loading and cyclic loading. It was necessary to use two actuators to obtain the force needed to fail the specimens. The actuators were controlled by two Materials Testing System (MTS) 443 controllers.

The load applied by the actuators was transferred through 10 in. x 10 in. steel plates onto a W12x79 spreader beam. The spreader beam was simply supported on two W10x39s, each located 4 ft – 6 in. from midspan and resting on 1 in. thick neoprene pads across the width of the specimen. The W10x39s transferred the reaction forces from the spreader beam, through the neoprene pads, onto the specimen as line loads.

Each specimen was situated so that the two actuators were centered at midspan to ensure symmetrical loading. To ensure in-plane loading, each specimen was positioned so that the actuators were directly above the specimen's steel beam web. This alignment is illustrated in Fig. 4.1c; also shown in this photograph are the steel frames used at the ends of the specimen to prevent it from tipping.

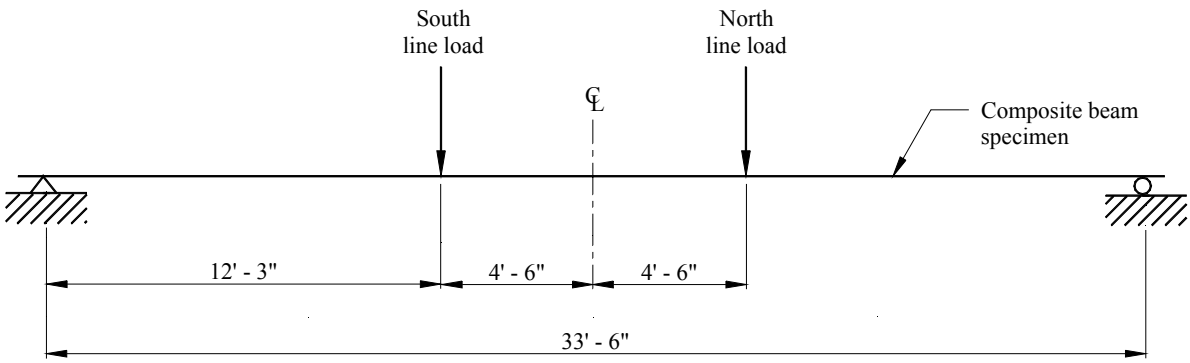

a. Location of line loads on span

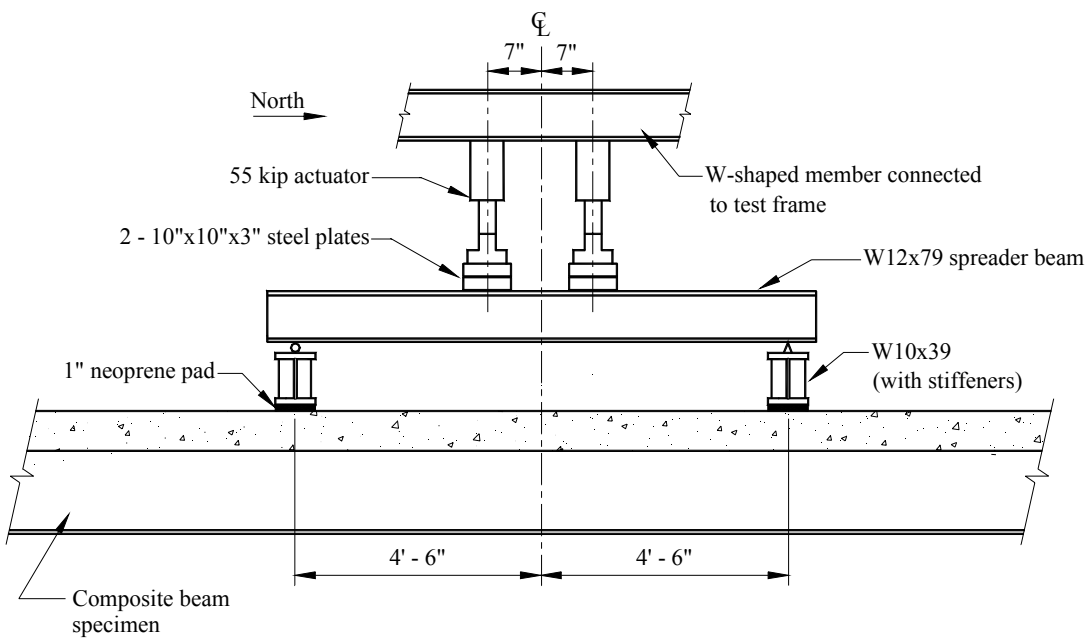

b. Side view of load setup

Figure 4.1. Load setup for composite beam tests.

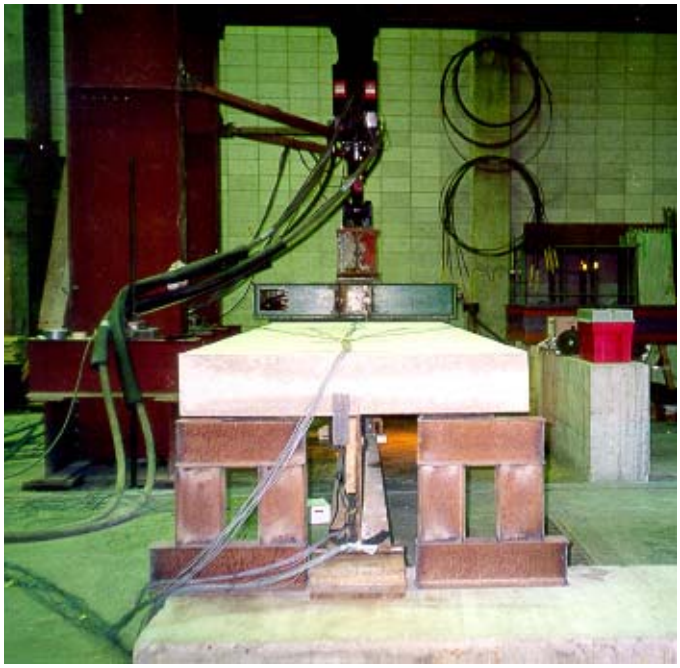

c. Photograph of end view of load setup

Figure 4.1. Continued.

Two internal load cells, one located within each actuator, measured the total applied load. Since the actuators were properly centered, it can be assumed that the total applied load was distributed equally to the two spreader beams. Based on this assumption and the fact that the spreader beams were also properly centered, the loading for each specimen was symmetrical about midspan.

4.1.2 Instrumentation

The location of the various instruments used during the composite beam tests are shown in Figs. 4.2 through 4.5. Strain gages were placed at the quarter point, midspan (see Fig. 4.2), and the three-quarter point in all three specimens. A minimal number of gages were installed at the quarter point, primarily to check for symmetry about midspan. Since a

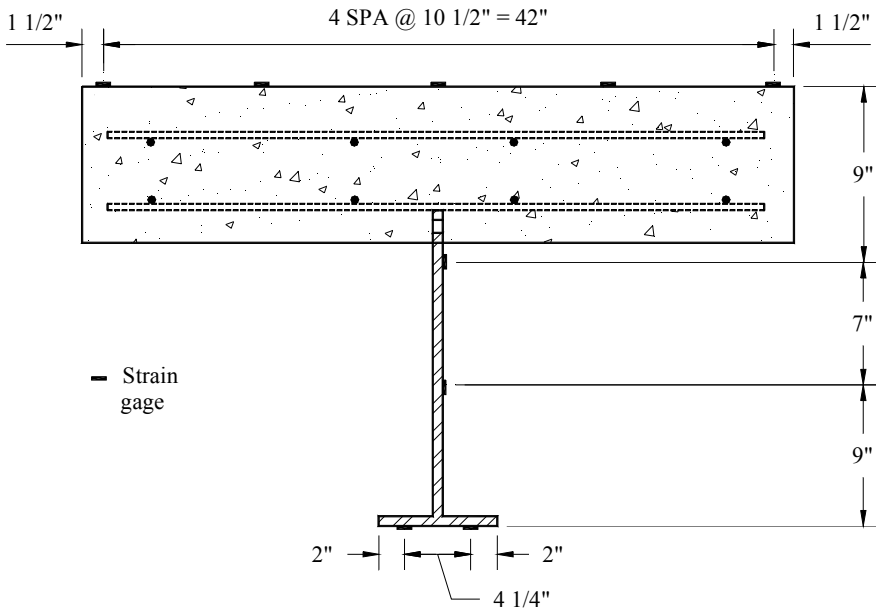

a. Specimens 1 and 2

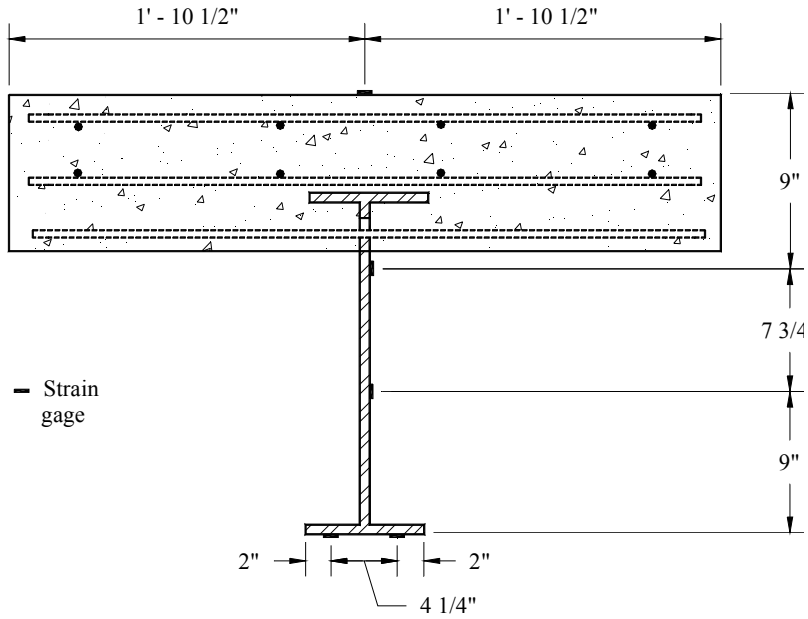

b. Specimen 3

Figure 4.2. Location of strain gages at midspan.

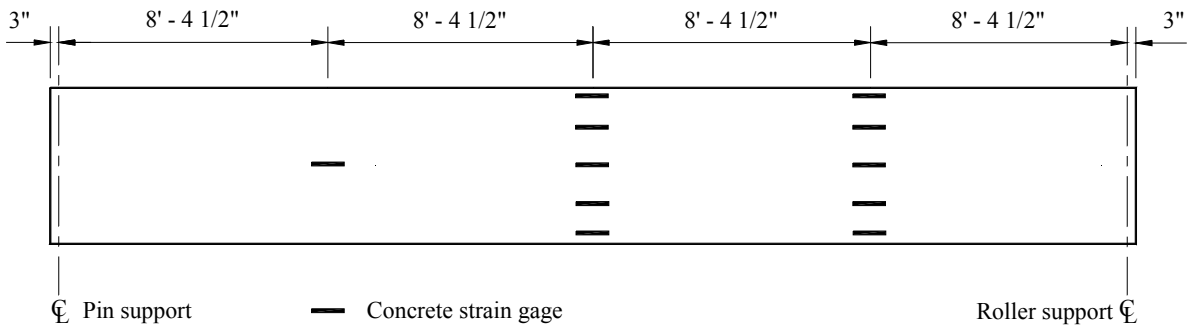

a. Specimens 1 and 2

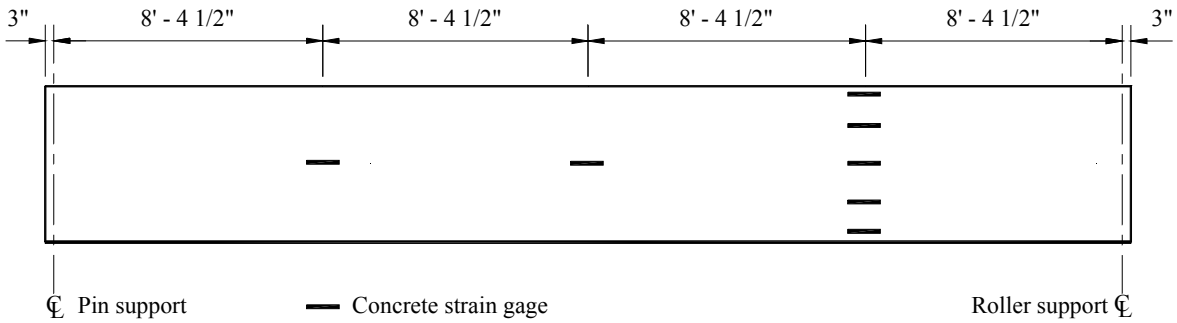

b. Specimen 3

Figure 4.3. Location of concrete strain gages on top of slab.

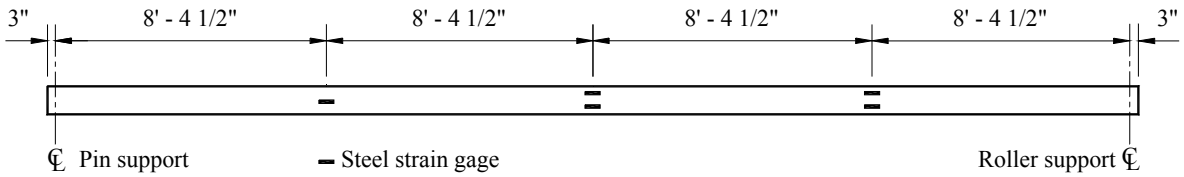

Figure 4.4. Location of steel strain gages on underside of bottom flange.

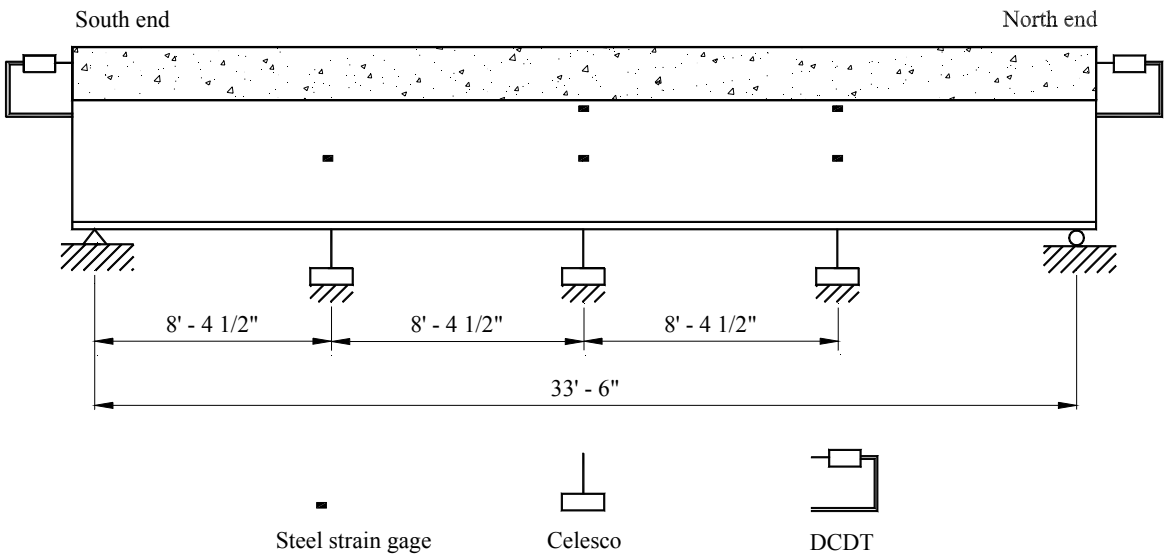

Figure 4.5. Side view of instrumentation.

uniform distribution of strain across the width of the slab at midspan was determined in the testing Specimens 1 and 2, only one concrete strain gage was applied at midspan for Specimen 3 (see Figs. 4.2b and 4.3b). The locations of steel strain gages on the bottom surface of the bottom flange are shown in Fig. 4.4; the locations were the same for all three specimens. All gages were oriented to measure longitudinal strains in the steel beams and concrete slabs.

Instrumentation used for measuring deflections and slip was the same in each composite beam specimen. Celescos were placed at the quarter point, midspan, and three-quarter point and a DCDT was placed at each end. Figure 4.5 shows the locations of these instruments and the steel strain gages on the steel beam web.

4.1.3 Testing Procedures

Three service load tests were performed on each specimen to obtain strains, deflections, and slip and to check the reproducibility of the response. A total applied load of

40 kips (20 kips from each actuator) was chosen as the service load, which is 50% of the load required to initiate yielding in the bottom flange. Strains, deflections, and slip were measured and recorded at 1,000 lb increments (500 lb per line load) using the DAS.

After completing the service load tests, the specimens were loaded to failure. Specimens 1 and 3 were loaded statically and Specimen 2 was loaded cyclically. The purpose of the failure tests was to determine the ultimate load capacity, strains and deflections/slip at the ultimate load, and the failure mode. Strains, deflections, and slip were again measured at 1,000 lb increments of total load. Measurements were taken more often as failure became evident.

For Specimen 2, a cyclic load was applied until failure. The total load range was 73 kips (i.e.,, from a minimum of 2 kips to a maximum of 75 kips). The 75 kip load represented approximately 75% of the ultimate load of Specimen 1. The minimum load was required to maintain stability of the specimen in the load frame. The determination of the maximum load was based on the results of Siow's research [22] and the ultimate load of Specimen 1. The test started at a load frequency of 0.75 cycles/sec, but the actuators could not maintain this rate with the amount of deflection that was occurring. Thus, the load frequency was lowered to 0.65 cycles/sec. Deflections and slip were recorded every hour for two seconds (i.e., every 2,340 cycles for 1.3 cycles). The DAS obtained 40 readings from each instrument during the two second interval. The MTS kept a continuous count of the loading cycles applied to the specimen, and occasionally a qualitative check was made by multiplying the testing time by the load frequency.

4.2 Two-beam Tests

In contrast to the composite beam tests, the two-beam tests involved an investigation of a slab and beam system, rather than just a single composite beam. The purpose of the tests was to investigate the static behavior of the two-beam systems. The data collected included strain/deflection behavior during service and ultimate loading, ultimate load capacity, and failure mode.

4.2.1 Load Setup

The load setup for Specimens 4 and 5, shown in Fig. 4.6, consisted of a single concentrated load applied to the specimens by a 400 kip capacity hydraulic cylinder. A spreader beam connected to the tie-down floor by two high strength threaded rods provided the necessary resistance to the hydraulic cylinder. Two W12x79s, welded side-by-side, were used as the spreader beam.

The load supplied by the hydraulic cylinder was transferred through a 1 in. thick steel plate to two 6 in. x 6 in. structural steel tubes. The bottoms of the steel tubes were welded to a 1/2 in. thick steel plate, which rested on a 1 in. thick neoprene pad. Steel tubes were necessary to ensure a uniform load distribution over the contact area.

The concentrated load represented a wheel load with a footprint as specified by the AASHTO LRFD Bridge Design Specifications [1]. Width of the wheel footprint was specified as 20 in.; the code only recognizes the width of a dual truck tire. Assuming a uniform contact pressure of 125 psi, the length of the footprint was determined to be 16 in. Orientation and size of the footprint are illustrated by Fig. 4.7.

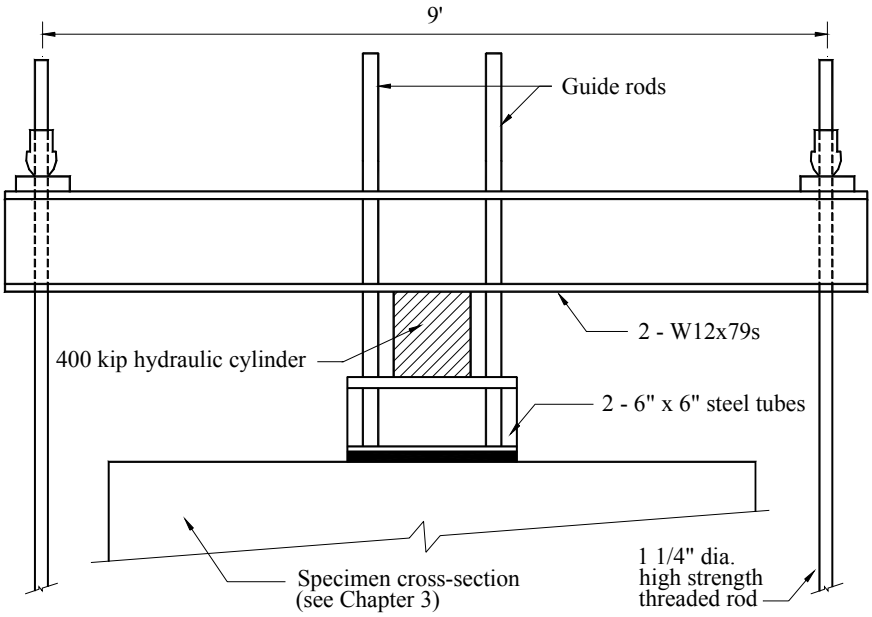

a. Side view

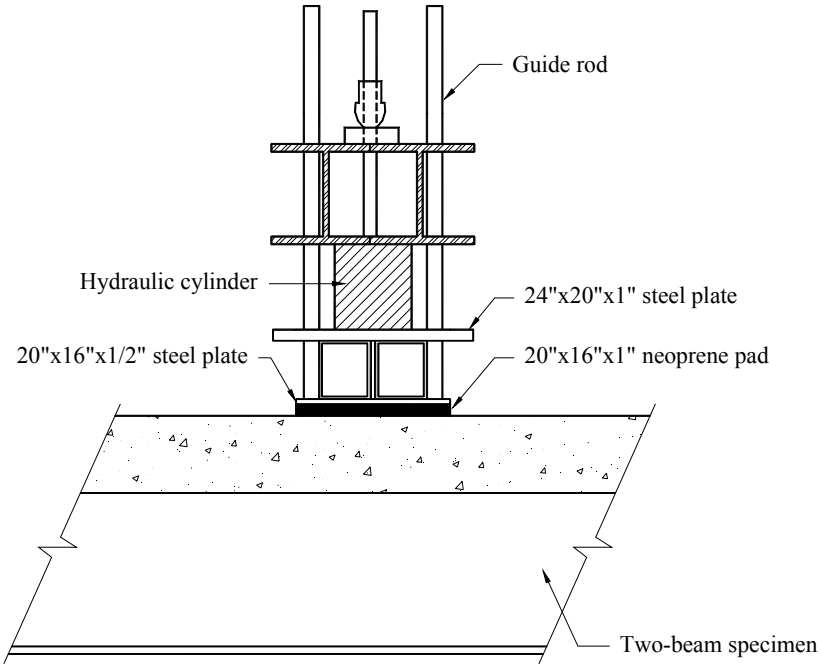

b. End view

Figure 4.6. Load setup for two-beam tests.

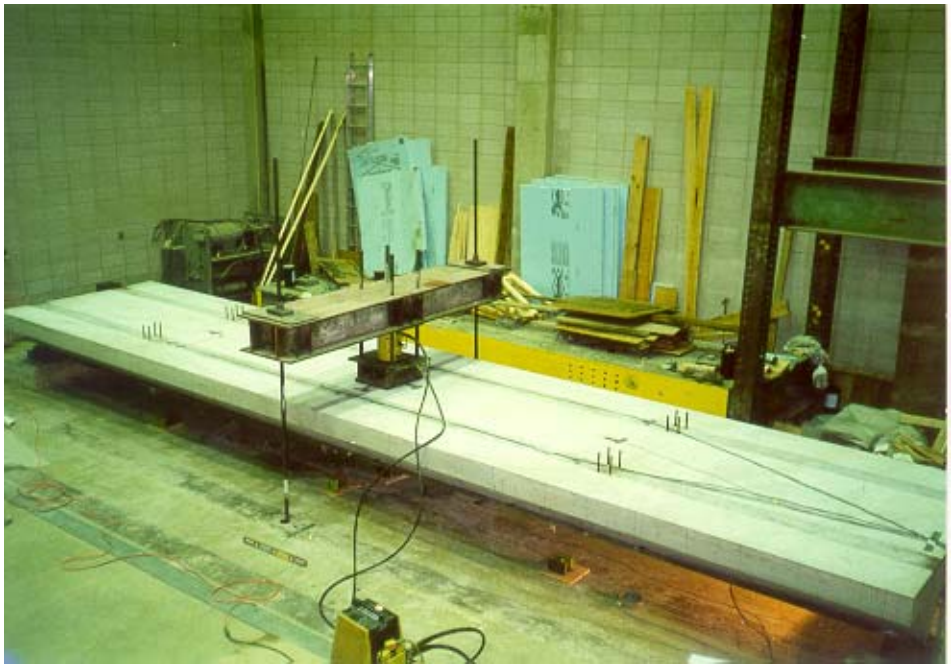

c. Photograph of typical load setup at Load Position 1

Figure 4.6. Continued.

Figure 4.7 also identifies the various load positions used in each specimen. Specimen 4 was tested at three locations (see Fig. 4.7a), which was possible because of the localized nature of each failure. Tests were performed at only two locations for Specimen 5 (see Fig. 4.7b); cracks resulting from the failure of the first test prohibited testing at a third location.

For both specimens, it was necessary to offset the center of Load Position 1, 3 1/2 in. from midspan, to position the load between transverse reinforcing bars in the slab. This was done to simulate a worst case scenario. The centers of Load Positions 2 and 3 were 2 ft from the pin support and 4 ft – 6 in. from the roller support, respectively. All load positions were centered on the longitudinal centerline of the specimen.

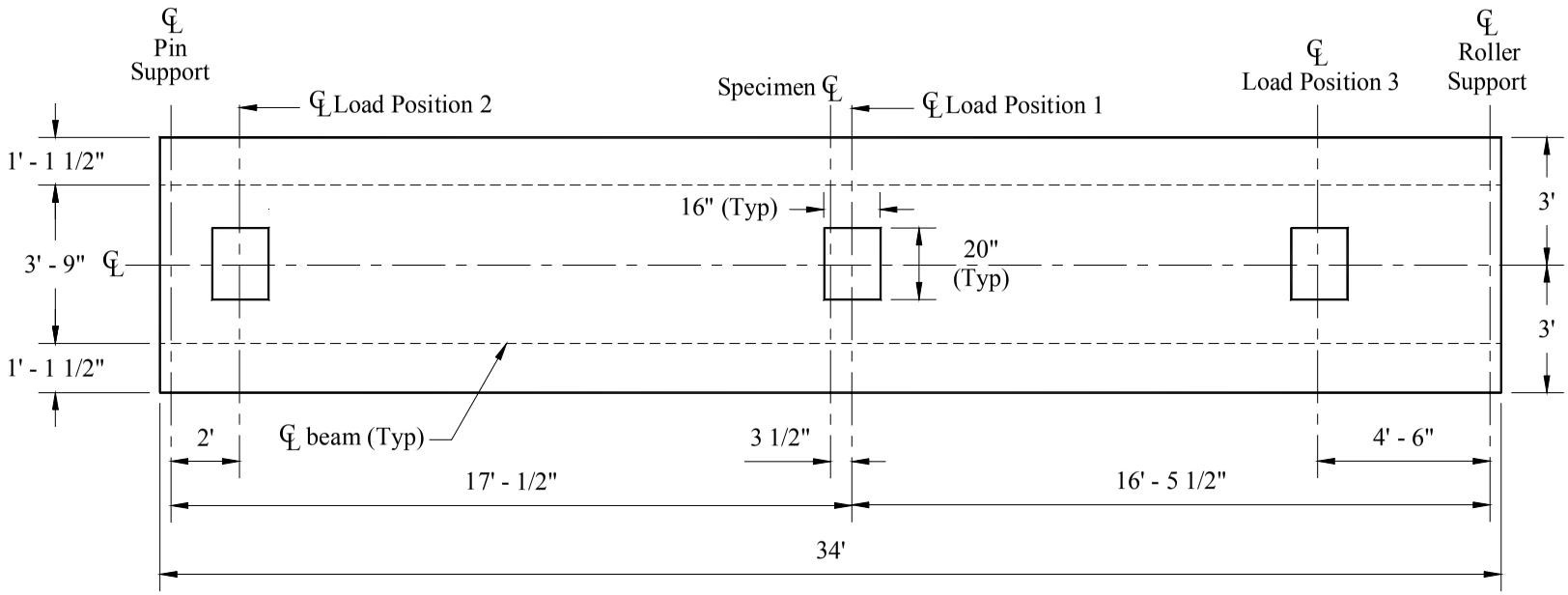

a. Specimen 4

Figure 4.7. Load Positions on Specimens 4 and 5.

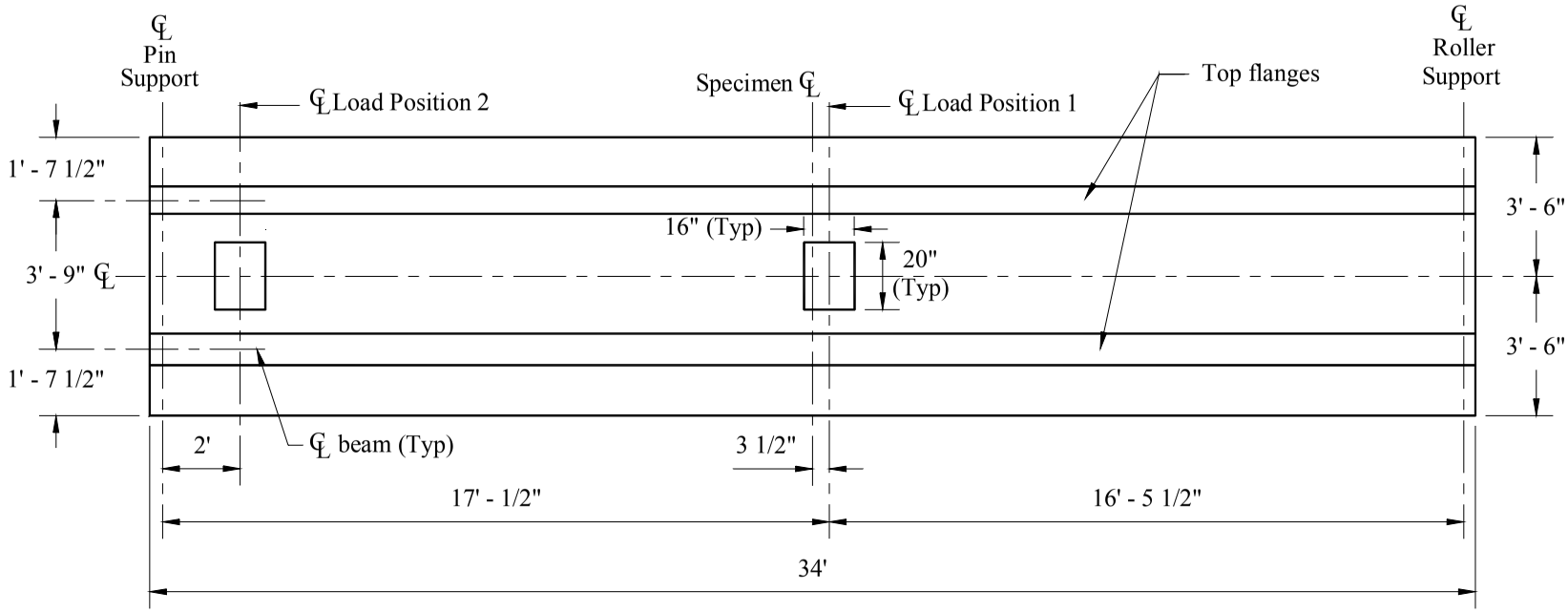

b. Specimen 5

Figure 4.7. Continued.

The applied load was measured using strain gages applied to both high strength threaded rods. Two strain gages oriented in the longitudinal direction and two in the transverse direction were applied to each rod. Four gages on each rod were necessary to complete a full-bridge configuration, which was used for added sensitivity. After calibrating both rods, the DAS was set so that the applied load could be displayed and recorded directly.

4.2.2 Instrumentation

The instrumentation used in Specimens 4 and 5 was different due to geometric differences in the slab and beam systems and also due to differences in their expected behavior. Instrumentation used and their location on the two specimens is presented in the following sections.

4.2.2.1 Specimen 4

Nineteen concrete strain gages, eight steel strain gages, nine Celescos, and one DCDT were used to determine the response of Specimen 4 during loading. Strain gages placed at the quarter point, midspan, and the three-quarter point are shown in Fig. 4.8. Concrete strain gages were placed directly above the steel beams at the quarter point and midspan. At the three-quarter point, a concrete strain gage was placed between the steel beams to compare strains at this location with concrete strains above the steel beams at the quarter point. Figure 4.8a illustrates the orientation of these concrete strain gages. Steel strain gages were placed on the bottom surface of both bottom flanges and at the top of both webs (midspan only). All steel strain gages were oriented in the longitudinal direction.

Refer to Figs. 4.8b and 4.8c for the location of the nine Celescos used. Six Celescos were placed under both steel beams and located at the quarter point, midspan, and the three-

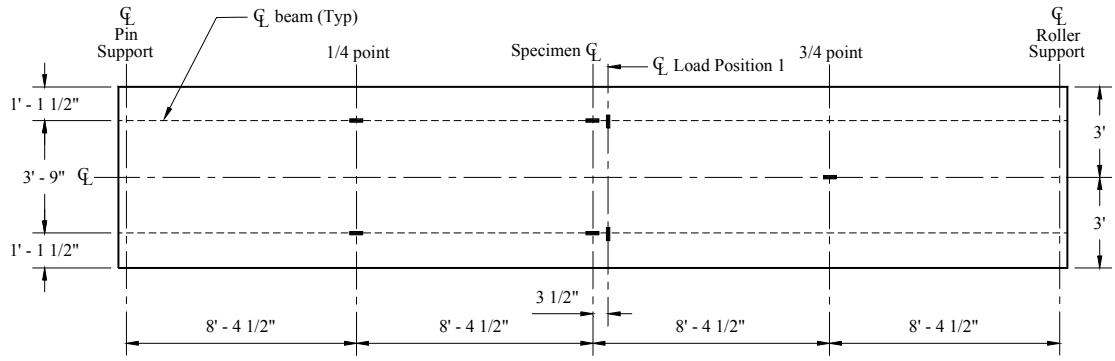

a. Top view

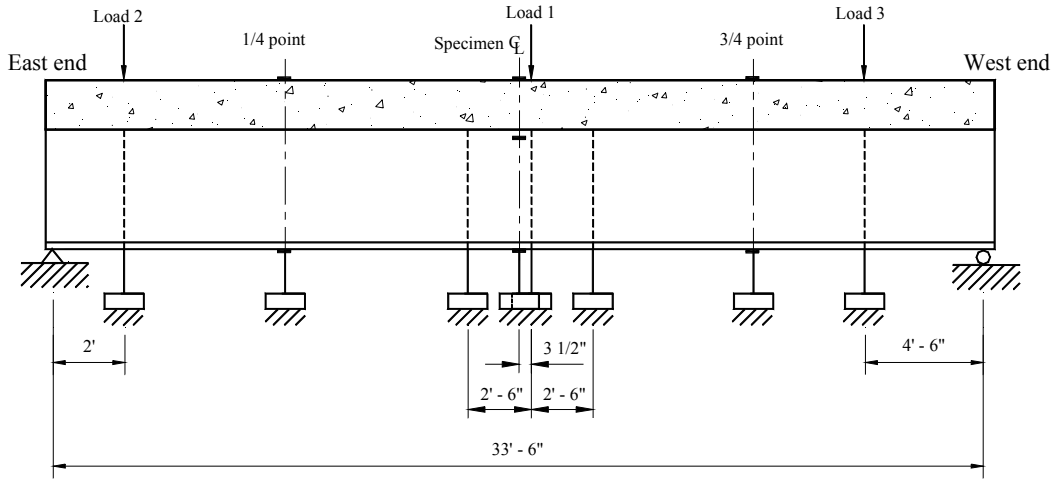

b. Side view

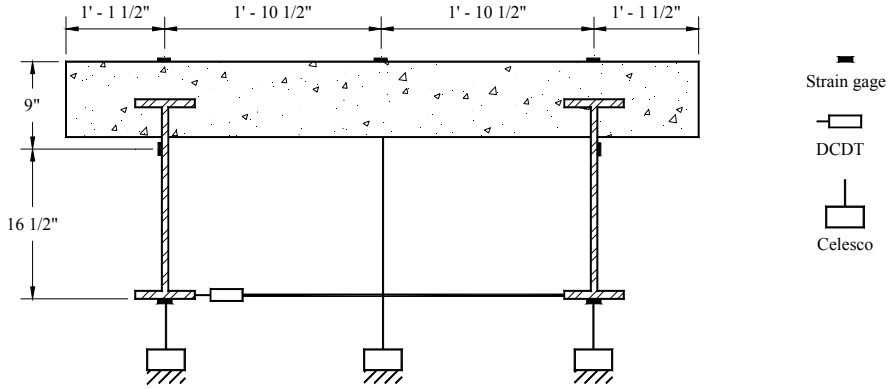

c. End view

Figure 4.8. Location of instrumentation on Specimen 4.

quarter point. Two additional Celescos, each located 2 ft – 6 in. from the center of Load Position 1 and on the longitudinal centerline of the specimen, were installed to obtain additional insight on the deflection of the slab. The ninth Celesco was positioned directly below the center of the load for each of the three tests. The DCDT shown in Fig. 4.8c was used to measure the relative out-of-plane displacement between the beams at midspan.

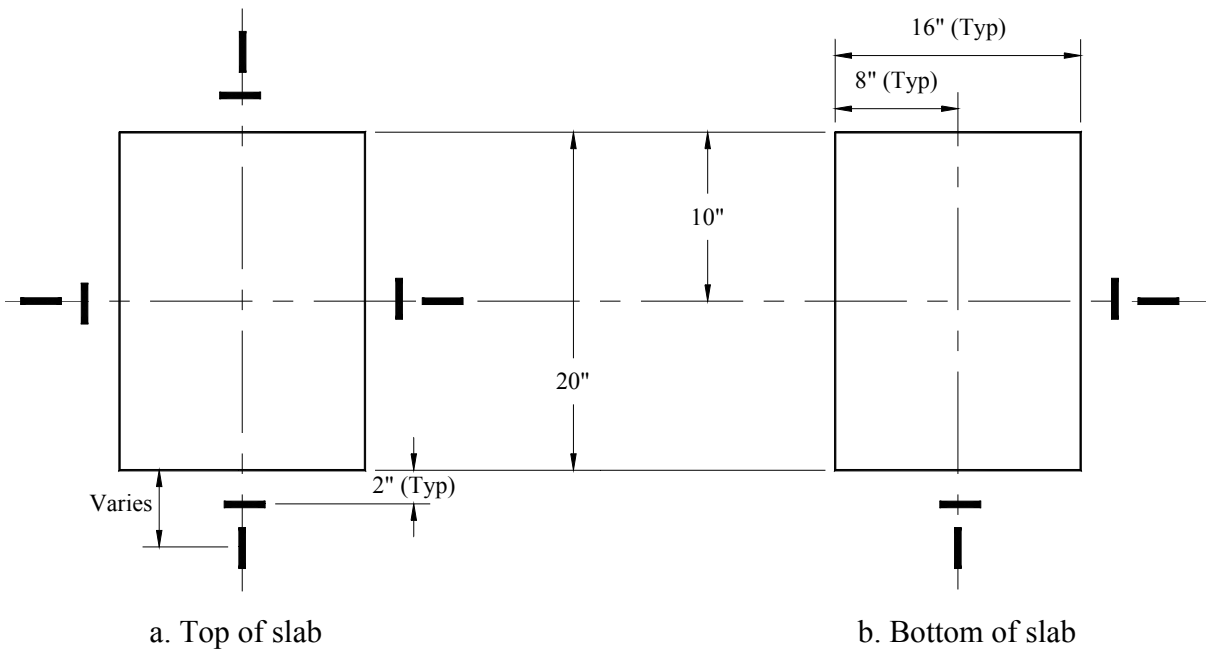

Figure 4.9. Concrete strain gages around wheel footprint at Load Position 1.

Concrete strain gages were also positioned around the perimeter of the wheel footprint (top and bottom of slab), only at Load Position 1. The locations and orientation of the strain gages are shown in Fig. 4.9. The viewing perspective for Fig. 4.9b is looking at the top surface of the slab. The strain gages were placed no closer than 2 in. to the perimeter of the footprint. For clarity, the concrete strain gages around the footprint were not included in Fig. 4.8.

4.2.2.2 Specimen 5

Six concrete strain gages, 16 steel strain gages, and seven Celescos were used to determine the response of Specimen 5 during loading. Figure 4.10 shows the location of these instruments. Strain gages were placed at the quarter point, midspan, and the three-quarter point (see Figs. 4.10a and 4.10b). The steel strain gage locations on the bottom flanges are identical to those on the top flanges. Steel strain gages were also applied to the tops and bottoms of the two steel straps welded to the bottom flanges (see Fig. 4.10c).

At Load Position 1, concrete strain gages were again placed around the perimeter of the wheel footprint, no closer than 1 in. (see Fig. 4.10a). Unlike Specimen 4, only four strain gages, each oriented perpendicular to the perimeter, were used to measure transverse and longitudinal strains on the top surface of the slab in the vicinity of the wheel footprint. The pipe section, used as a stay-in-place form, prohibited the application of strain gages on the bottom of slab. Strain gages were not placed parallel to the perimeter of the wheel footprint because strain gages in this location on Specimen 4 produced inconclusive data. All strain gages were oriented to measure longitudinal strains except for two of the four concrete strain gages placed around the perimeter of the wheel footprint.

For the location of the seven Celescos, refer to Fig. 4.10b and 4.10c. Similar to the strain gages, Celescos were also placed at the quarter point, midspan, and the three-quarter point. Six Celescos were positioned below the steel beams and one was placed directly below the center of the wheel footprint during both tests.

4.2.3 *Testing Procedures*

The load positions for Specimens 4 and 5 were previously shown in Fig. 4.7. Three service load tests were performed at each location for both specimens to check the

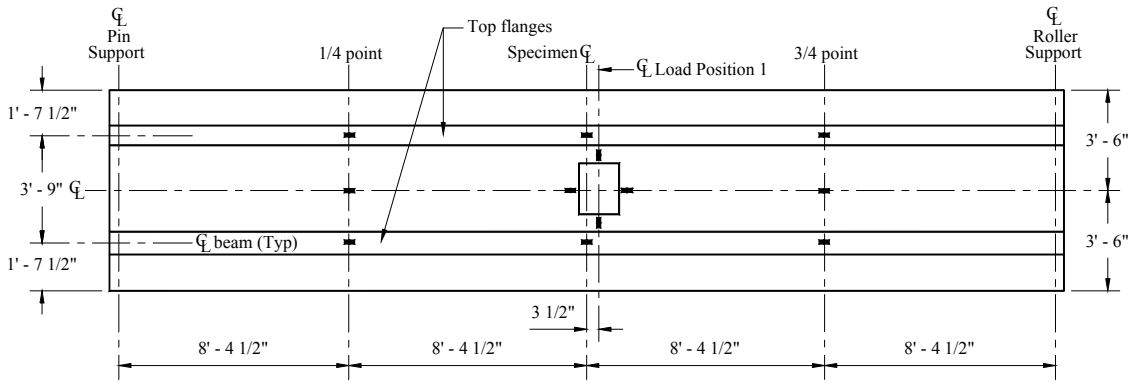

a. Top view

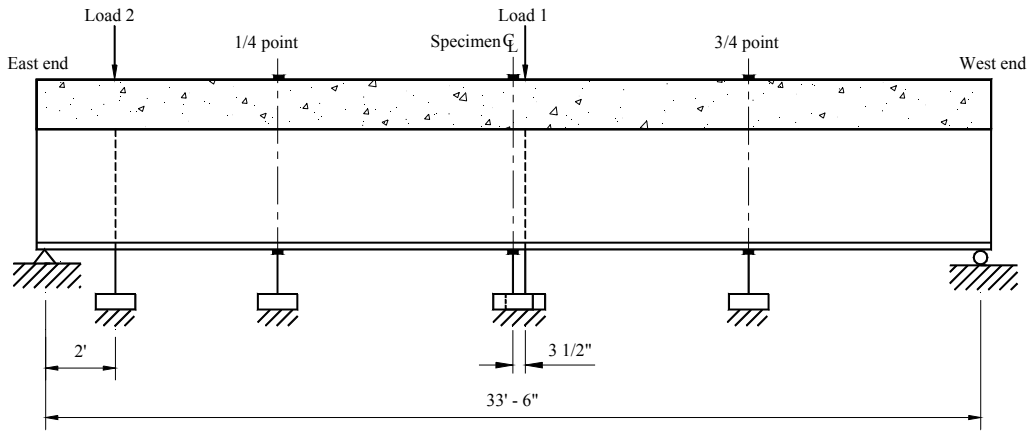

b. Side view

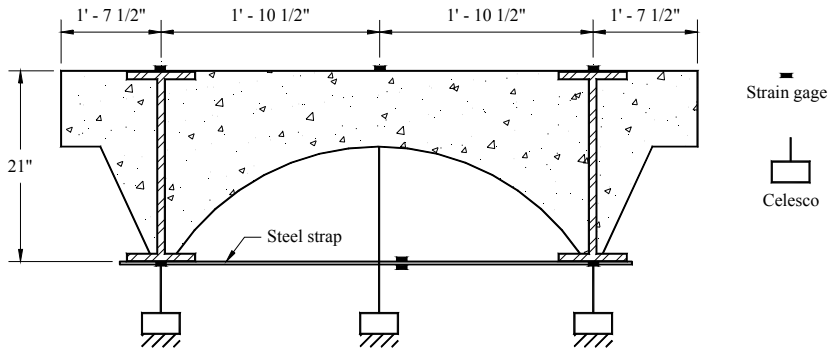

c. End view

Figure 4.10. Locations of instrumentation on Specimen 5.

reproducibility of the response. In accordance with the AASHTO LRFD Bridge Design Specifications [1], bridge decks are to be designed for a nominal wheel load of 16 kips and the following factors are used to calculate a factored wheel load:

- Multiple presence factor: 1.2
- Dynamic allowance factor: 1.33
- Limit state load factors: Fatigue: 0.80
  Service: 1.00
  Strength: 1.75

Therefore, based on the strength limit state, a maximum factored wheel load of 45 kips was calculated and chosen as the service load. Strains and deflections were measured at 5,000 lb load increments.

After completing the three service load tests, load was applied to the specimen until failure occurred. As discussed previously, Specimen 4 was loaded to failure at three locations and Specimen 5 was loaded to failure at only two locations. The purpose of the failure tests was to determine the ultimate load capacity, strains and deflections at the ultimate load, and the failure mode. In both specimens, strains and deflections were measured at 2,000 lb increments of load using the DAS. Measurements were taken more frequently as failure became evident.

4.3 Push-out Specimen Tests

4.3.1 *Test Setup*

All of the specimens were tested using a Materials Test System (MTS) fatigue machine. Because of the configurations of the machine, it was necessary to fabricate a loading table for the specimens. An overall view of the loading arrangement is shown in Fig. 4.11. Details of the loading table are presented in Reference 22.

To achieve an even load distribution under the concrete slabs, a 1/4 in. thick neoprene pad was inserted between the slab and the loading table. At the top edge of the steel shear plate, a load block arrangement was used to transmit the applied load evenly between the steel shear plate and the load cell. As previously noted, C 8 x 11.5 stiffeners were bolted to the shear plate to prevent lateral buckling of the 3/8 in. thick shear plate. Two angles, shown in Fig. 4.11, were clamped to the loading table to restrict any movement of the specimens during the fatigue test.

After installing the two DCDTs, they were connected to a computer-controlled DAS. With the use of the high speed DAS, displacements were measured and recorded without stopping the fatigue test. The number of cycles was recorded electronically by the MTS machine. A photograph of the overall test set-up and instrumentation is shown in Fig. 4.12.

4.3.2 Testing Procedures

For each series, two specimens were tested statically to determine the ultimate static strength of the connectors. Fatigue tests, cycling between a constant minimum load level and various maximum load levels, were conducted to develop the relationship between the fatigue load and the fatigue life of the ASC, and to determine the slippage of the connector

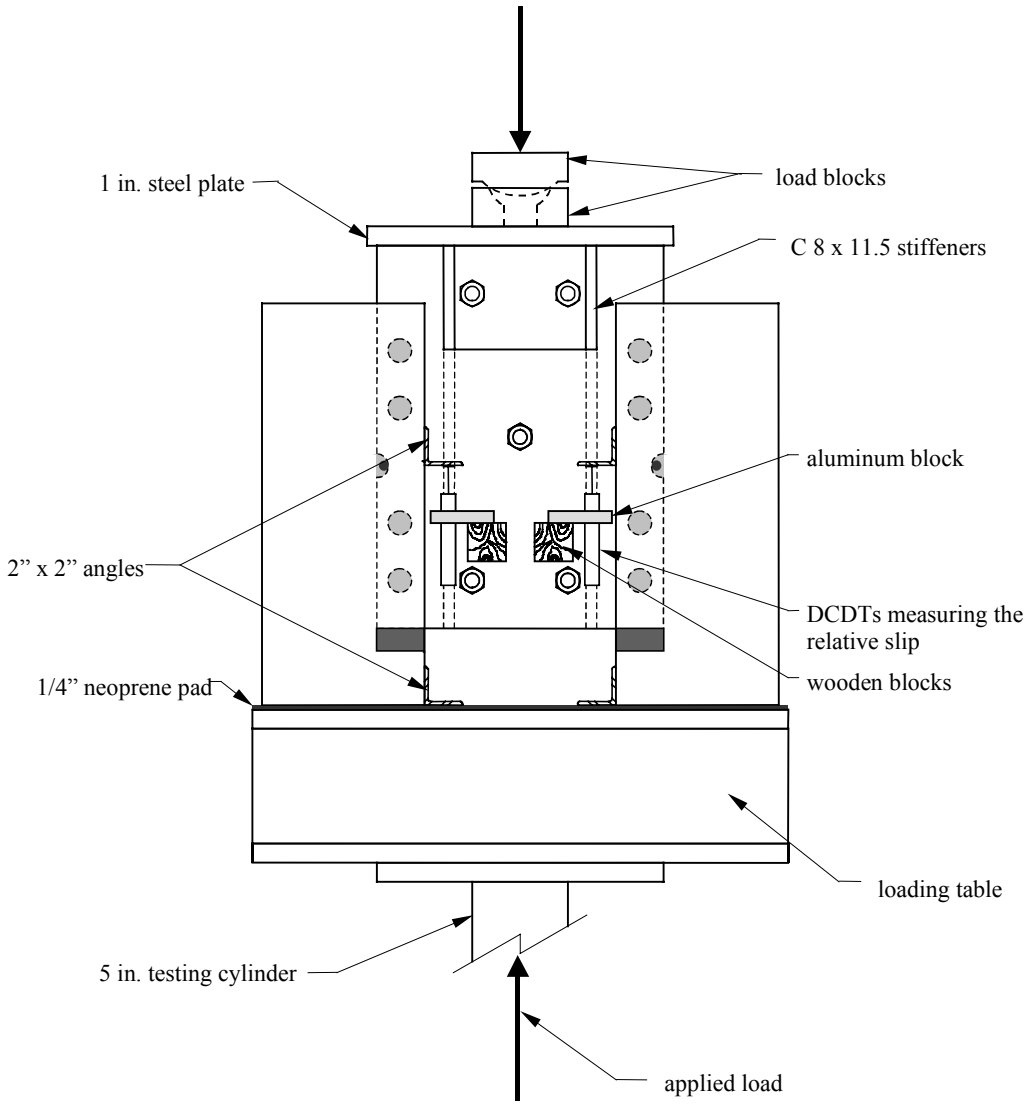

Figure 4.11. Push-out specimen loading arrangement and instrumentation.

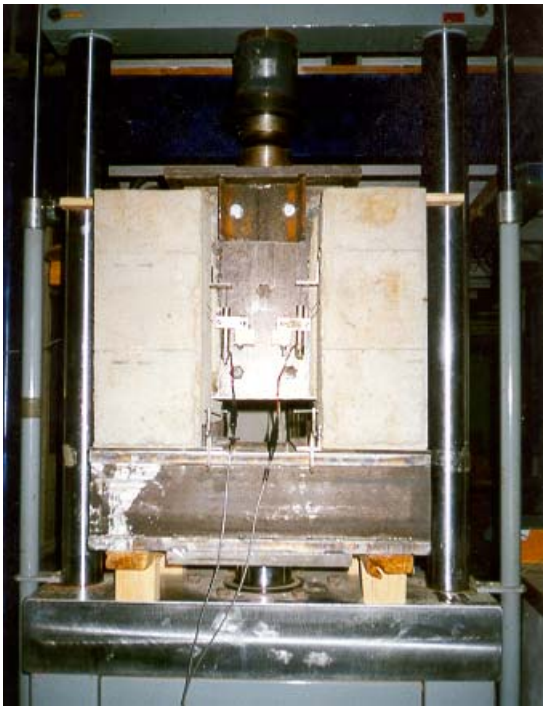

Figure 4.12. Photograph of push-out test set-up.

during testing. A minimum of two specimens was fatigue tested at each maximum level of load.

Static testing began with an initial load of approximately 1,000 lbs. The initial load was applied to make sure the slip instrumentation was operating correctly and to ensure an even distribution of load through the distribution plate on the steel shear plate. Load was then gradually increased without stopping until the specimen failed. During the testing, applied load and slippage were measured and recorded at an interval of 250 lbs.

Prior to the fatigue test, a load equal to the mid-point of the loading range was gradually applied to all specimens. Once the fatigue test started, the cyclic load was applied

to the connectors, ranging from a minimum to the predetermined maximum level of load. A minimum load of 2,000 lbs. (required to hold the specimens in place during the fatigue test) was used for all specimens. The loads were applied at a frequency of two cycles per second.

At the beginning of the fatigue test, the DCDTs were read every two minutes. The interval between DCDTs readings was then increased to twenty minutes until near failure when the rate of slip began to increase. Near failure when possible, DCDTs readings were taken as often as necessary to define the slip vs. cycle curve.

After failure, each specimen was removed from the testing machine and inspection. The concrete was carefully broken away from the steel shear plate to inspect the connectors and failure mechanism.

4.4 Theoretical Composite Beam Calculations

Theoretical calculations were made to verify some of the data measured by the instrumentation presented in the previous sections. The calculations performed are briefly described in the following sections. The support conditions for all specimens were assumed to be simply supported; each specimen had a clear span of 33 ft – 6 in.

4.4.1 Composite Beam Specimens

For each composite beam specimen, a theoretical neutral axis and a theoretical midspan deflection curve were calculated. Section properties (i.e., neutral axis, area, moment of inertia) were calculated assuming a full composite section. Because the beams are made of two materials, the concrete area was transformed to an equivalent steel area. Using the transformed steel area the theoretical neutral axis was calculated. Longitudinal reinforcement was neglected in all section property calculations.

Midspan deflections due to the loading shown in Fig. 4.1a.were calculated using the virtual work method. The moment of inertia for the transformed steel section was used, along with the modulus of elasticity for steel (29,000 ksi). To construct the deflection curve used to verify the service load deflection curves, the deflection for the service load of 20 kips at each load point was initially calculated. A linear deflection curve was assumed between zero and this point.

The theoretical ultimate moment capacity was also calculated for each specimen. Refer to the Appendix of Section 6 in the AASHTO LRFD Bridge Code [1] for the method used. It should be noted that the longitudinal reinforcement was included in this calculation, as required in Section 6.

4.4.2 Two-beam Specimens

For both specimens, theoretical deflections under each load position and theoretical ultimate moment capacities were calculated. Section properties were calculated assuming a full composite section and were based on the entire specimen cross-section (both beams and all the concrete). Shapes with known areas and centroids (i.e., rectangles and triangles) were used to approximate the concrete arch portion in Specimen 5. Concrete areas were again transformed into equivalent steel areas.

The deflections under the load were calculated using the virtual work method for a load placed at the various load positions shown in Fig. 4.7. Deflection of the slab relative to the steel beams was not taken into consideration. When calculating the deflection under Load Position 1, it was assumed that the load was located at midspan (it was actually located 3 1/2 in. from midspan).

The theoretical moment capacity for each specimen was again calculated according to the method described in the Appendix of Section 6 in the AASHTO LRFD Bridge Code [1]. No longitudinal reinforcement existed in either specimen. However, in the case of Specimen 5 the portion of the steel beams in compression was included in the calculation. The ultimate moment capacity was calculated using both steel beams and the full width of the specimen.

The theoretical punching shear failure load was calculated for Specimen 4, using Eqn. 4.1., which is the governing equation according to AASHTO [1].

$$V_c = 4(f_c')^{1/2}(b_o)(d) \qquad \text{(Eqn. 4.1)}$$

Where, f_c' = compressive strength of concrete

b_o = perimeter along the critical section

d = depth of the concrete

V_c = nominal shear strength provided by the concrete

5. EXPERIMENTAL RESULTS

The experimental results of the various tests described in Chapter 4 are presented in this chapter; results are from the three full-scale composite beam tests (two specimens loaded statically and one loaded in fatigue) the two full-scale two-beam specimens (both specimens statically loaded), and the 27 push-out specimens (21 of which were subjected to cyclic loading). Where applicable, experimental results were compared to the theoretical results. In the composite beam tests, both the experimental and theoretical results were based on the specimens being simply supported with a clear span of 33 ft – 6 in.

5.1 Composite Beam Results

The purpose of the composite beam tests was to further investigate the static and fatigue strength of the ASC. Tests consisted of three service tests and an ultimate load test for each of the three specimens. The results of the static tests and the fatigue test will be presented separately in the following two sections. Loads presented in these sections are the total loads applied to the specimen (see Fig. 4.1 for the load setup).

5.1.1 Static Tests

Static tests were performed on Specimens 1 and 3. Details of both specimens are presented in Chapter 3, Figs. 3.1 and 3.2. Both specimens utilized the ASC; however, unlike Specimen 3, the top flange was removed in Specimen 1. The following data recorded during the static tests will be presented and discussed: the degree of composite action at service load, strains/deflections/slip at service and ultimate loads, ultimate load capacity, and the mode of failure.

Service load test results for Specimen 1 are illustrated in Fig. 5.1. Note that the first three graphs (Figs. 5.1a, 5.1b and 5.1c) were plotted using data from the third service test. Cross-section strain profiles at midspan (for three separate loads) are shown in Fig. 5.1a. The theoretical neutral axis for a full composite section was calculated and is also shown. It can be seen that the experimental and theoretical neutral axes agree well (theoretical = 18 in. vs. experimental = 18.5 in.), indicating full composite behavior during service level loading. Strains at midspan and deflections along the span are shown in Fig. 5.1b and 5.1c, respectively. Figure 5.1c also illustrates, by comparing the deflections at the quarter point and the three-quarter point, that the loading was symmetric.

Figure 5.1d is a plot of the deflection at midspan for all three service tests, along with the theoretical load-deflection curve. The excellent agreement among the three service test curves indicates that the specimen's response was reproducible. The agreement between the service test curves and the theoretical curve was also excellent; however, deflections for all three service tests were slightly greater than the theoretical deflections for a given load. This slight difference could be caused by small dimension errors (i.e., span length, spacing of line loads) or possibly a slight error in the compressive strength of the concrete (determined by testing concrete cylinders), which would affect the modular ratio used in calculating the theoretical deflections. Overall, in the worst case (service test 2) experimental results deviated from theoretical values by less than 4%.

All strains and deflections plotted in Fig. 5.1 increased in a linearly fashion. This indicates full composite action throughout the entire service load test. In addition, horizontal slip of only 0.002 in. at the South end of the specimen and 0.001 in. at the North end

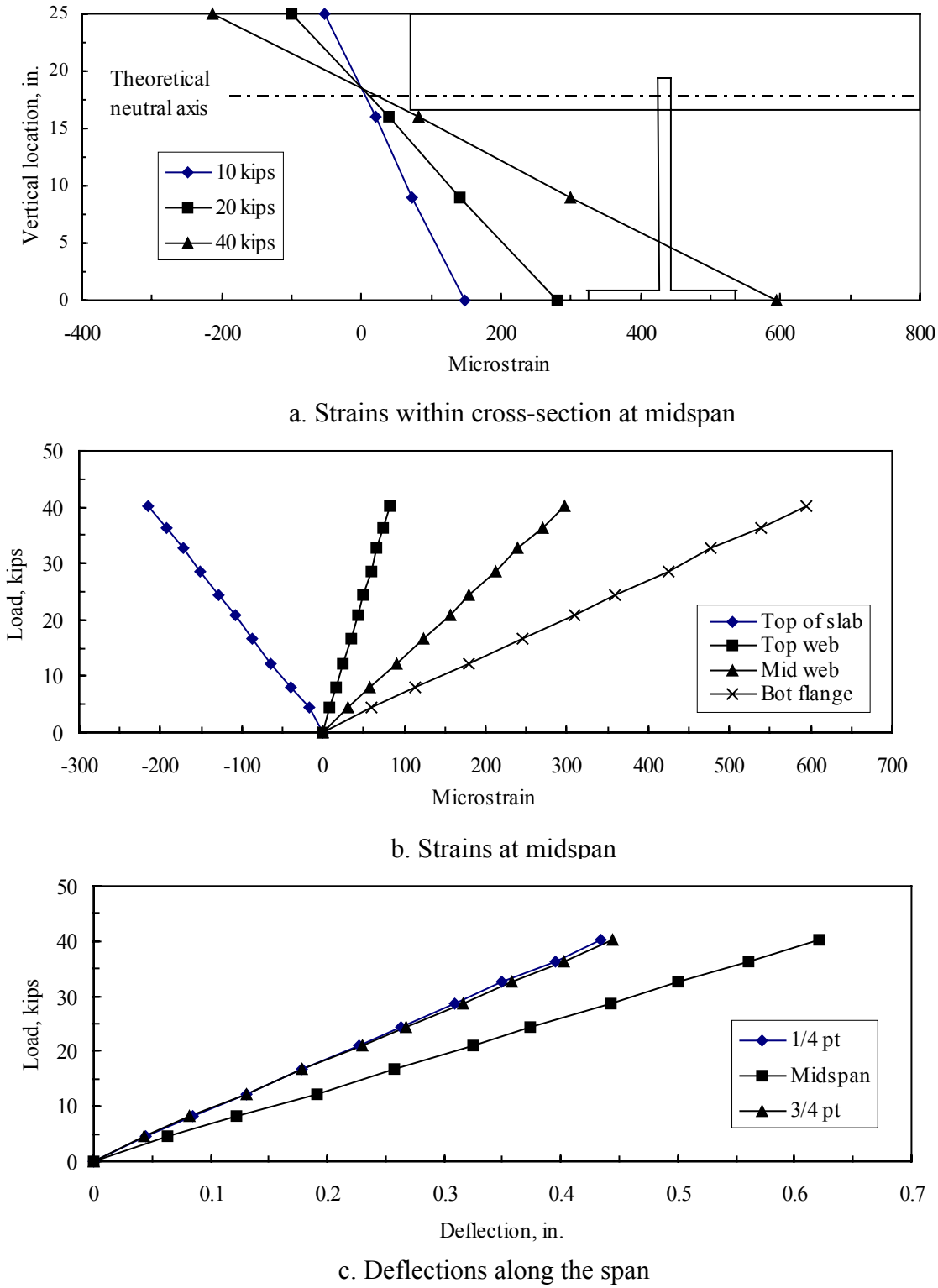

Figure 5.1. Specimen 1 service load test results.

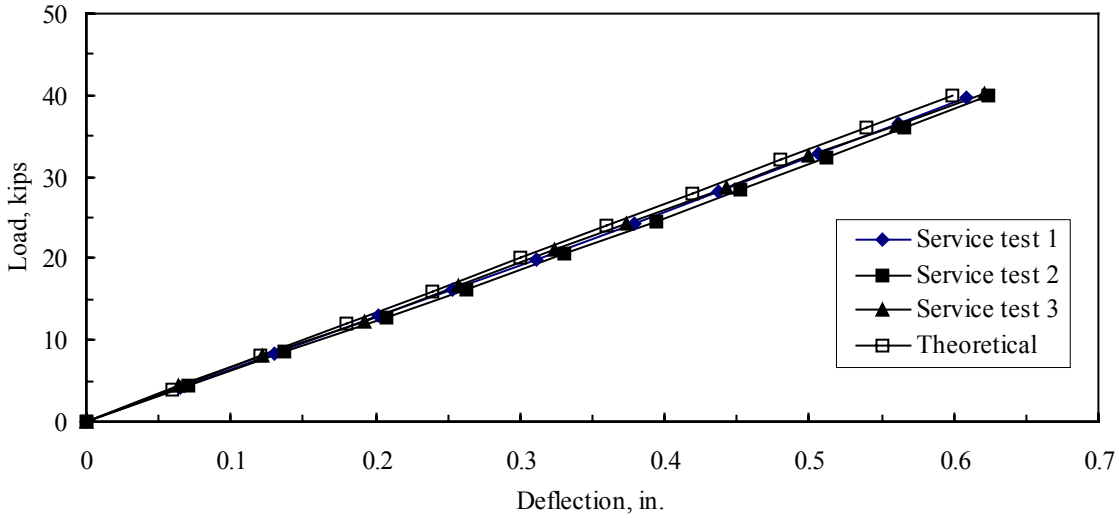

d. Deflections at midspan for all three service tests

Figure 5.1. Continued.

occurred between the steel beam and the concrete slab, which is also a strong indication of full composite behavior. An excellent correlation between the theoretical and experimental results shown in Figs. 5.1a and 5.1d verifies that the ASC used with no top beam flange is effective in creating full composite action between the concrete slab and steel beam during service level loading.

Service load test results for Specimen 3 are illustrated in Fig. 5.2. The same conclusions can be made for this specimen as were made for Specimen 1. The theoretical neutral axis agrees well with the experimental neutral axis (theoretical = 18 in. vs. experimental = 18.3 in.), as shown in Fig. 5.2a. All strains and deflections increased linearly with load. Figure 5.2c illustrates that loading was again symmetrical. The response was the same in all three service tests, as shown in Fig. 5.2d, and there was excellent agreement

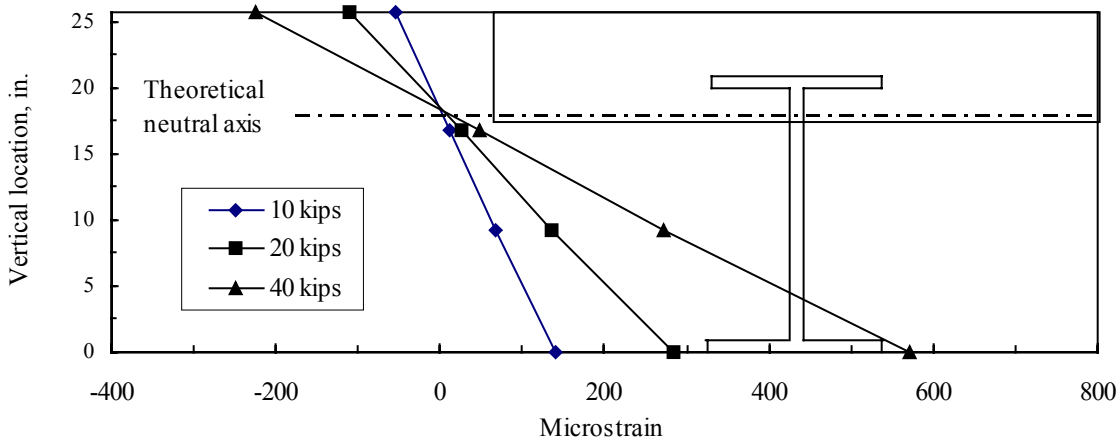

a. Strains within cross-section at midspan

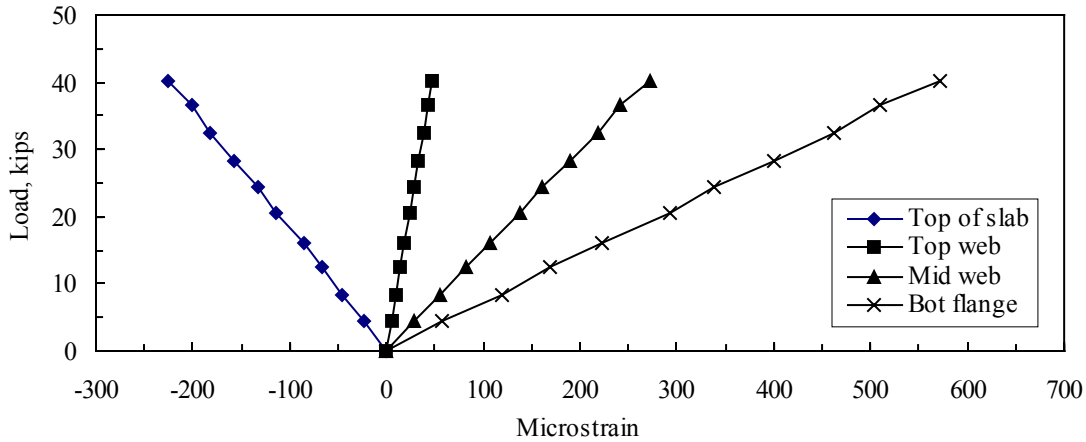

b. Strains at midspan

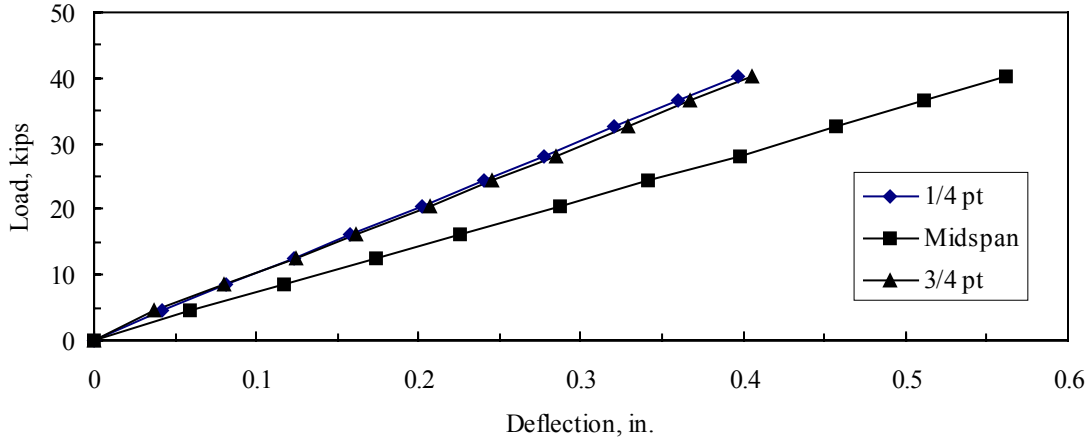

c. Deflections along the span

Figure 5.2. Specimen 3 service load test results.

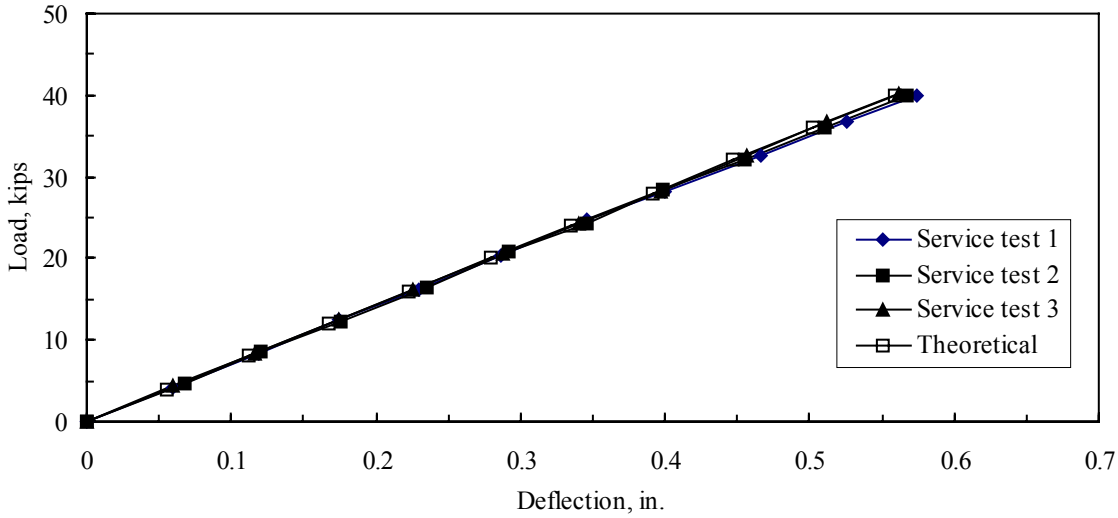

d. Deflections at midspan for all three service tests

Figure 5.2. Continued.

between the service test curves and the theoretical curve. As with Specimen 1, very little slip (0.001 in. at both ends of the specimen) occurred between the steel beam and the concrete slab. Therefore, based on the sets of data presented in Fig. 5.2, the ASC used on a beam with the top flange intact was also effective in creating full composite action during service level loading.

Since the strain data and deflection data exhibited similar behavior, only deflection data are presented for the other composite beam specimens presented in this section. The midspan deflections measured during the ultimate load testing of both specimens are shown in Fig. 5.3. As shown in Fig. 5.3a, the specimens have different flexural stiffnesses (i.e., moment of inertia). Specimen 3 had a greater stiffness due to the embedded top flange. The deflection data for Specimen 1 were adjusted by dividing each deflection value by the ratio of Specimen 3's moment of inertia to Specimen 1's moment of inertia.. As apparent in

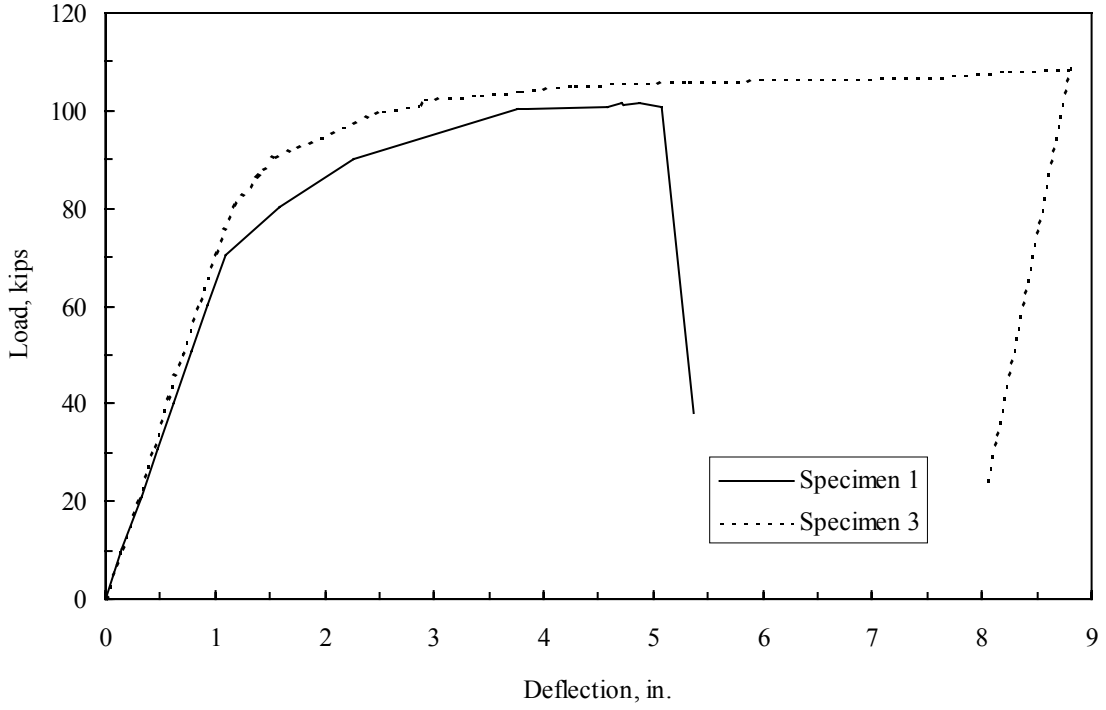

a. As tested

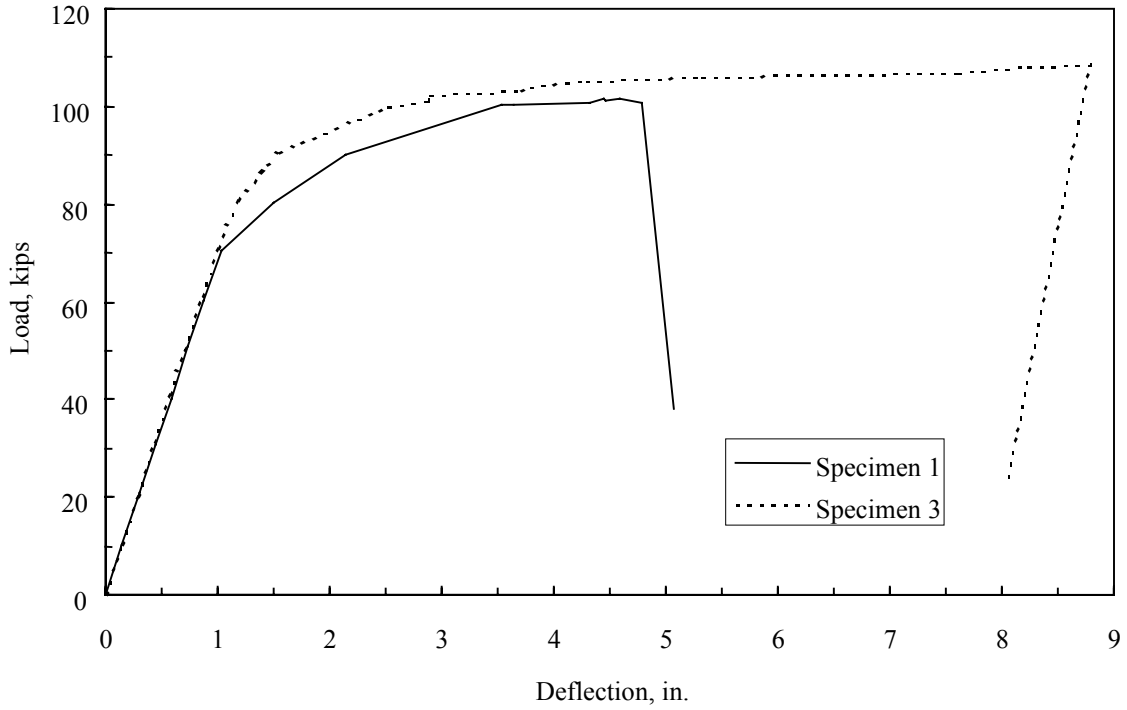

b. Adjusted for difference in flexural stiffnesses

Figure 5.3. Midspan deflections during ultimate load testing of Specimens 1 and 3.

Fig. 5.3b with this adjustment, deflections in the elastic range of these two specimens are in good agreement. Since the data were adjusted based on elastic behavior, the deflection curves diverge when the deflections begin to increase nonlinearly.

Referring to Fig. 5.3a, the ultimate loads and corresponding maximum deflections at midspan for both specimens were as follows: 101.4 kips and 5.07 in. for Specimen 1, and 108.5 kips and 8.79 in. for Specimen 3. Ultimate failure of Specimen 1 occurred when the ASC in the North shear span failed. A shear span is the portion of the clear span between the line load and its adjacent support (see Fig. 4.1 for load setup). Failure of the ASC was ductile and cracking/spalling of the concrete was observed at the slab-web interface, due to excessive slipping (see Fig. 5.4a). Transverse cracks in the bottom of the slab, in only the North shear span, initiated the failure of the ASC.

Complete failure of Specimen 3 may not have occurred because the test was terminated when the stroke limit of the actuators was reached. However, concrete crushing at the South line load and slipping of the ASC in the South shear span was occurring when the test was terminated. Based on the deflection curves in Fig. 5.3, failure of Specimen 3 was more ductile than that of Specimen 1. Flexural cracking of the concrete slab between the line loads and yielding of the steel beam also occurred in each specimen.

Figure 5.4 confirms that the ASC failed in the North shear span of Specimen 1 (see North DCDT curve in Fig. 5.4a) and started to fail in the South shear span of Specimen 3 (see South DCDT curve in Fig. 5.4b). The maximum horizontal slip that occurred in Specimens 1 and 3 was 0.155 in. and 0.008 in., respectively. The load-slip behavior illustrated in Fig. 5.4, suggests that the ASC performed like a rigid connector – little or no

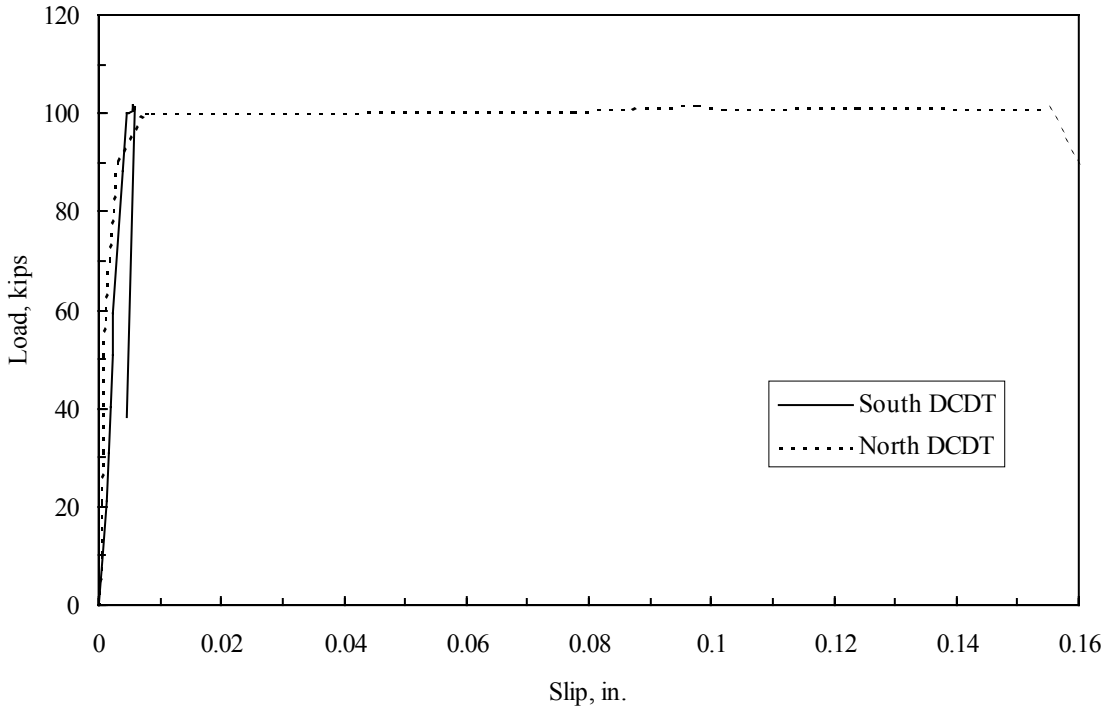

a. Specimen 1

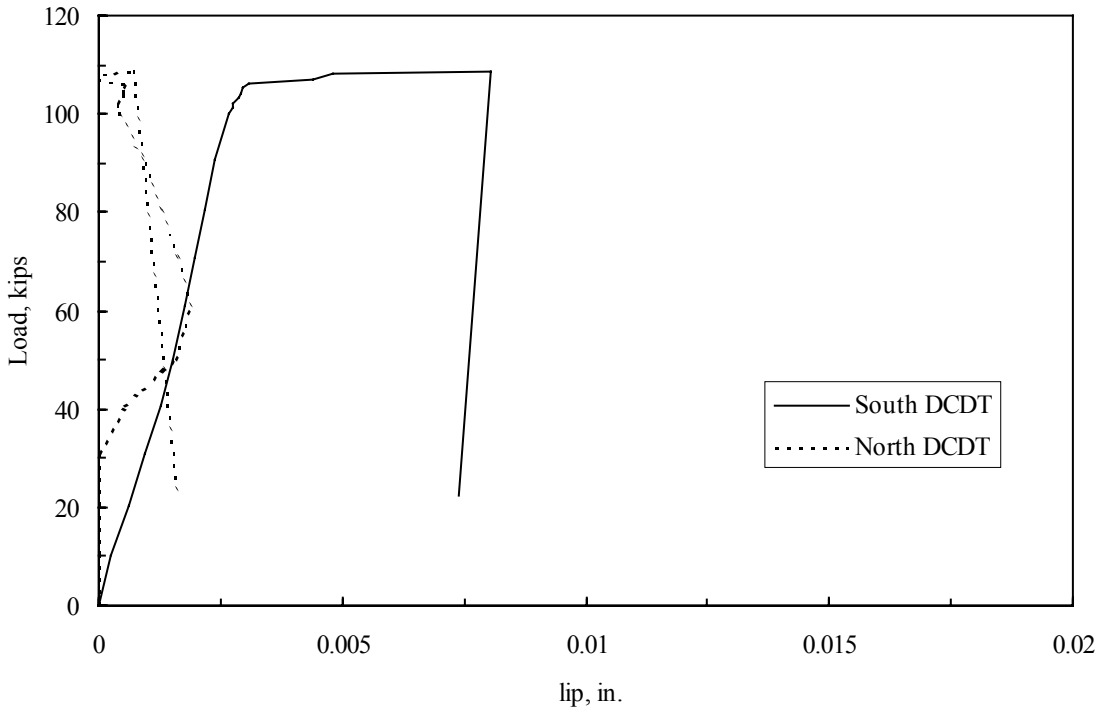

b. Specimen 3

Figure 5.4. Horizontal slip between steel beam and concrete slab in Specimens 1 and 3.

slip – at service loads while exhibiting ductile behavior at ultimate. These performance characteristics are ideal, as was explained in Chapter 2.

The experimental ultimate moment capacity, $M_{u(exp)}$, and the theoretical ultimate moment capacity, $M_{u(theo)}$ are compared in Table 5.1. The moment due to selfweight, M_{self}, was calculated and included in the experimental ultimate moment capacity. The longitudinal reinforcement was included in the determination of the theoretical ultimate moment capacity.

Table 5.1. Comparison of ultimate moment capacity for Specimens 1 and 3.

Specimen	Ultimate Load (kips)	M_{self} (ft-kips)	$M_{u(exp)}$ (ft-kips)	$M_{u(theo)}$ (ft-kips)	$M_{u(exp)}/M_{u(theo)}$
1	101.4	58.7	679.8	679.2	1.001
3	108.5	61.3	725.1	726.3	0.999

Excellent agreement between the experimental and theoretical ultimate moments indicates that both specimens failed at a load corresponding to their ultimate moment capacity.

In summary, the ASC, with and without a top flange, was effective in creating full composite action until failure and had the strength to transmit the horizontal shear force for the development of the ultimate moment capacity, as intended by design. However, with the top flange intact, the ASC was able to develop a 7% greater ultimate moment than without the flange. Furthermore, slip was considerably less at failure, despite a greater ultimate load and greater vertical deflections. This was probably due to the top flange's ability to tightly confine the concrete around the ASC holes (see Chapter 2). The performance characteristics of the ASC was excellent; it was rigid enough to prevent slipping at service level conditions, but exhibited a failure that was ductile, just as a flexible connector would.

5.1.2 Composite Beam Fatigue Test

A fatigue test was performed on Specimen 2. As shown in Fig. 3.1, the details of Specimen 2 were the same as Specimen 1. The following information obtained during the fatigue test will be presented and discussed: deflections and slip during the fatigue test, the number of loading cycles required to fail the specimen, and the mode of failure.

Before the fatigue test, three static service load tests (in which a maximum load of 40 kips was applied) were performed. Results from these tests are illustrated in Fig. 5.5. As with Specimens 1 and 3, the first three graphs were plotted using data from the third service test. Since the results are identical to those of Specimen 1, the same conclusions as previously discussed can be made.

With regard to the fatigue cycles, a failure occurring between 500,000 and 1,000,000 cycles was desired. The 500,000 is consistent with AASHTO's [1] mid-range number of stress cycles and 1,000,000 was chosen to limit the length of the test. A failure within this range would indicate that the ASC has more than sufficient fatigue strength for use in bridges on low-volume roads.

Therefore, based on the results of the push-out fatigue tests presented in Section 5.3, it was determined that a maximum load of about 75% of the ultimate static strength would be required for a failure within the desired range. Assuming the ultimate strength of Specimen 2 to be the same as Specimen 1 (101.4 kips), the maximum load was calculated to be approximately 75 kips. A minimum load of 2 kips was chosen to maintain stability of the specimen in the load system during testing which resulted in a load range of 73 kips.

As explained in Chapter 4, a load frequency of 0.75 cycles/sec was used until it was decreased to 0.65 cycles/sec after approximately 58,000 cycles. Deflections and horizontal

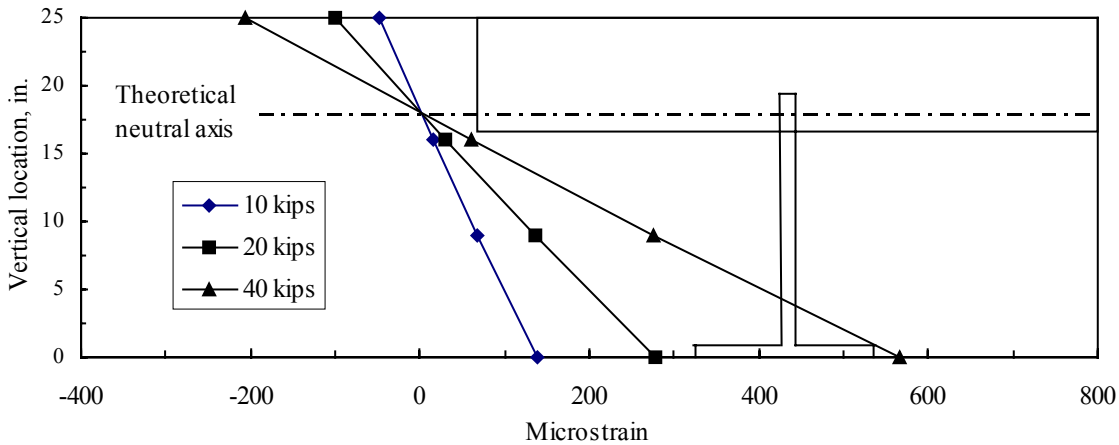

a. Strains within cross-section at midspan

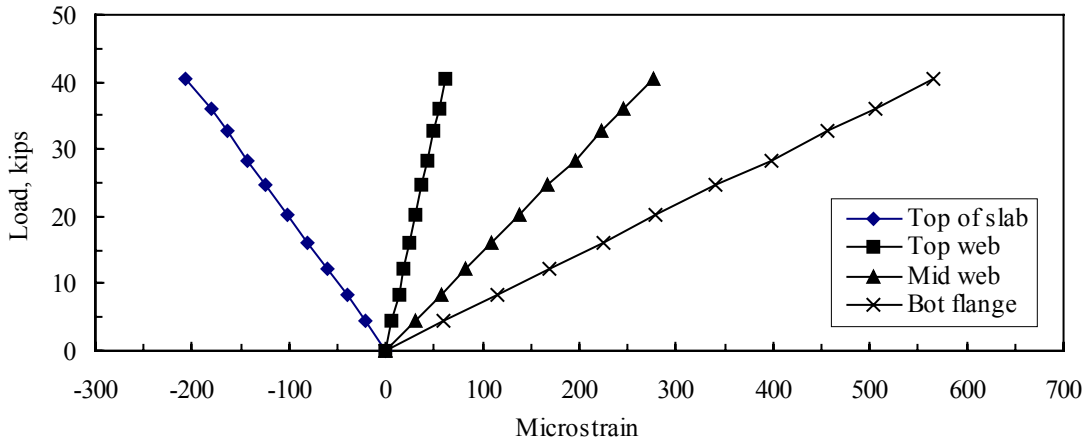

b. Strains at midspan

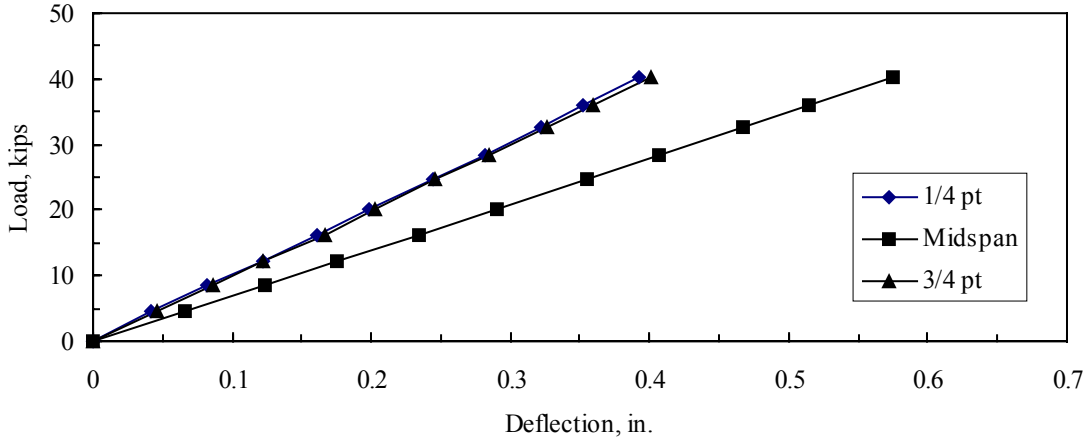

c. Deflections along the span

Figure 5.5. Specimen 2 service load test results.

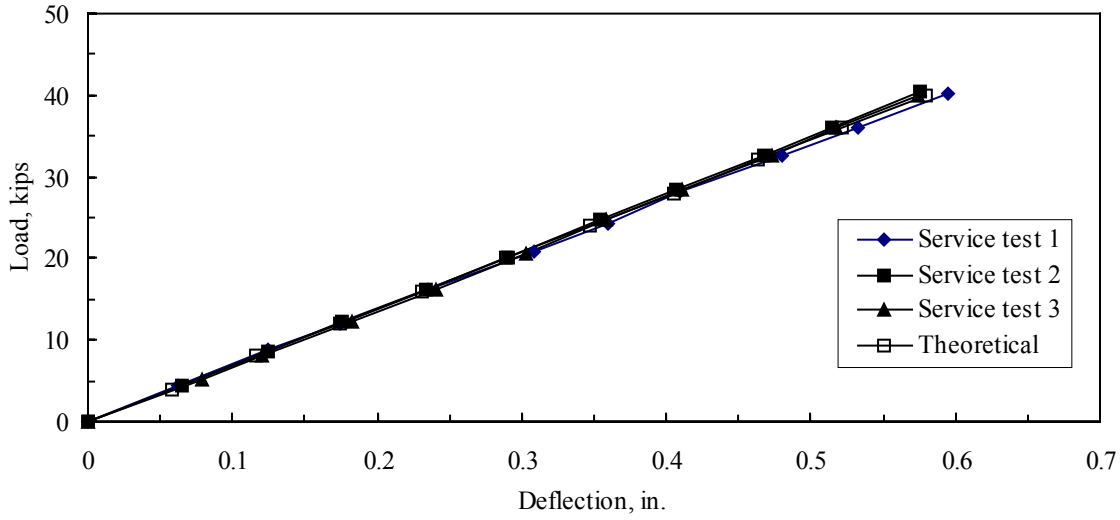

d. Deflections at midspan for all three service tests

Figure 5.5. Continued.

slip were recorded every hour over a two second period (every 2,340 cycles over a 1.3 cycle period). Figures 5.6 and 5.7 illustrate the midspan deflection and horizontal slip recorded during the first time interval (first hour) and the last time interval (194th hour), respectively. The first time interval occurred after 2,700 cycles (during 0.75 cycles/sec) and the last time interval was after approximately 462,800 cycles (during 0.65 cycles/sec), shortly before failure. The maximum and minimum values are labeled on each plot.

The specimen failed after 464,000 cycles, which is less than the desired 500,000 ycles. However, it was the steel beam that failed and not the shear connector. The steel beam failed due to a fatigue crack that initiated at a set of holes in the beam web that had been used for a diaphragm connection when the beam was in service (see Fig. 5.8). The set of holes was located approximately 1ft – 7 in. North of the North line load (see Fig. 4.1 for the load setup). Note that the maximum midspan deflection increased from 1.11 in. to

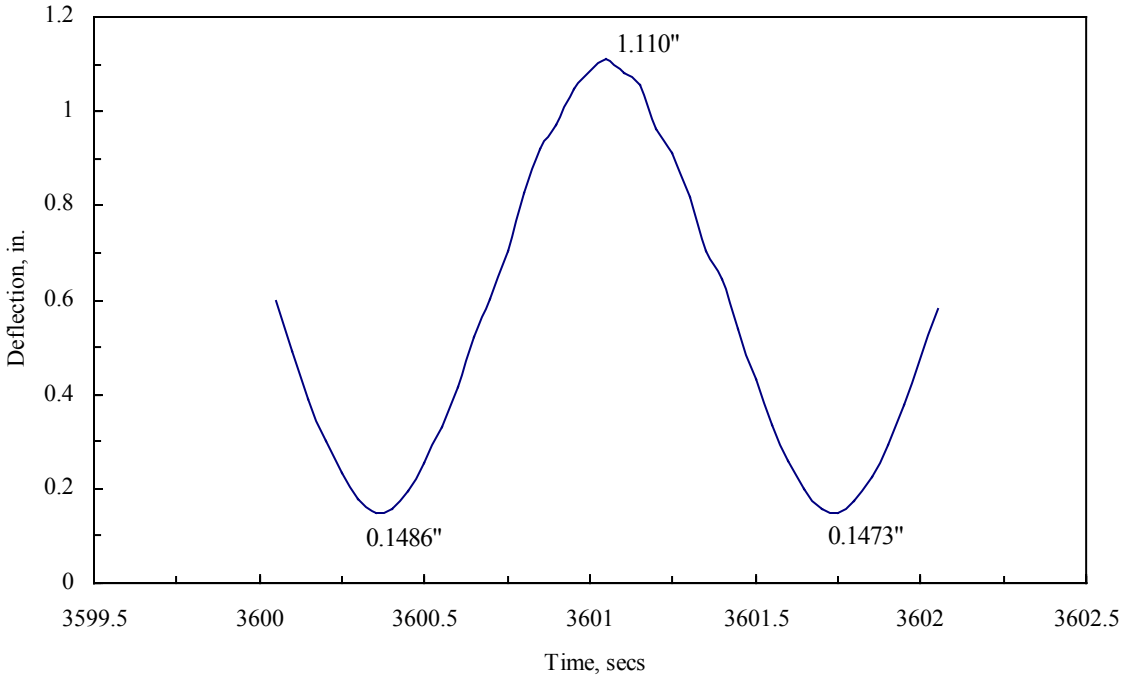

a. After 2,700 cycles (1.5 cycles shown)

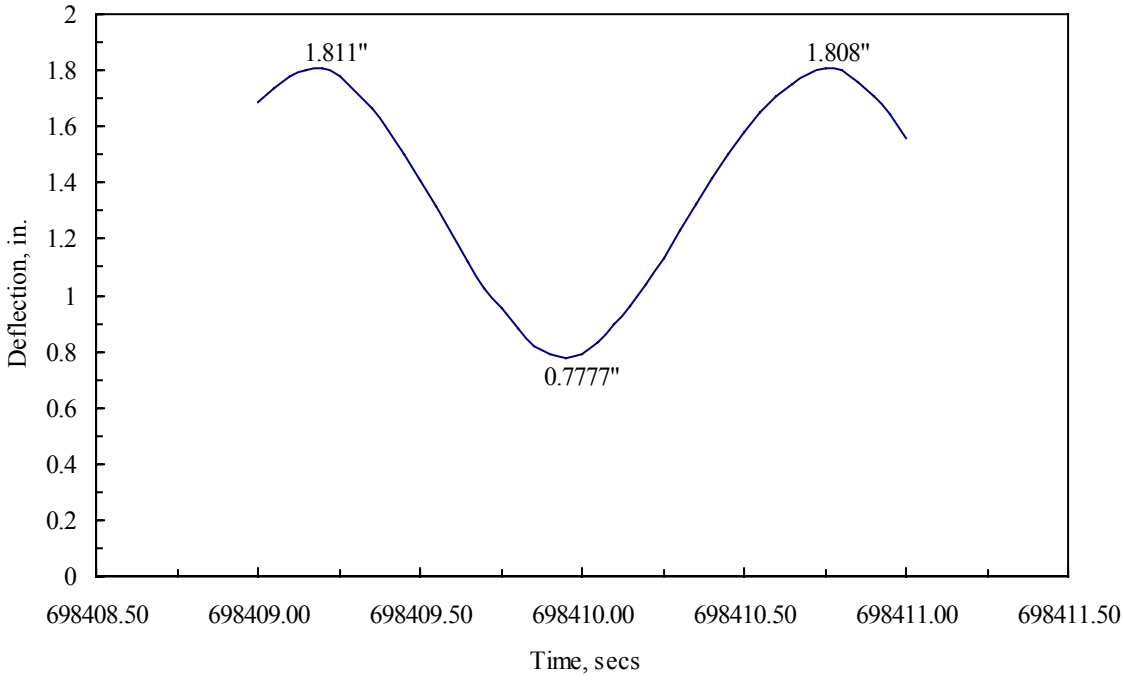

b. After 462,800 cycles (1.3 cycles shown)

Figure 5.6. Midspan deflections during fatigue testing of Specimen 2.

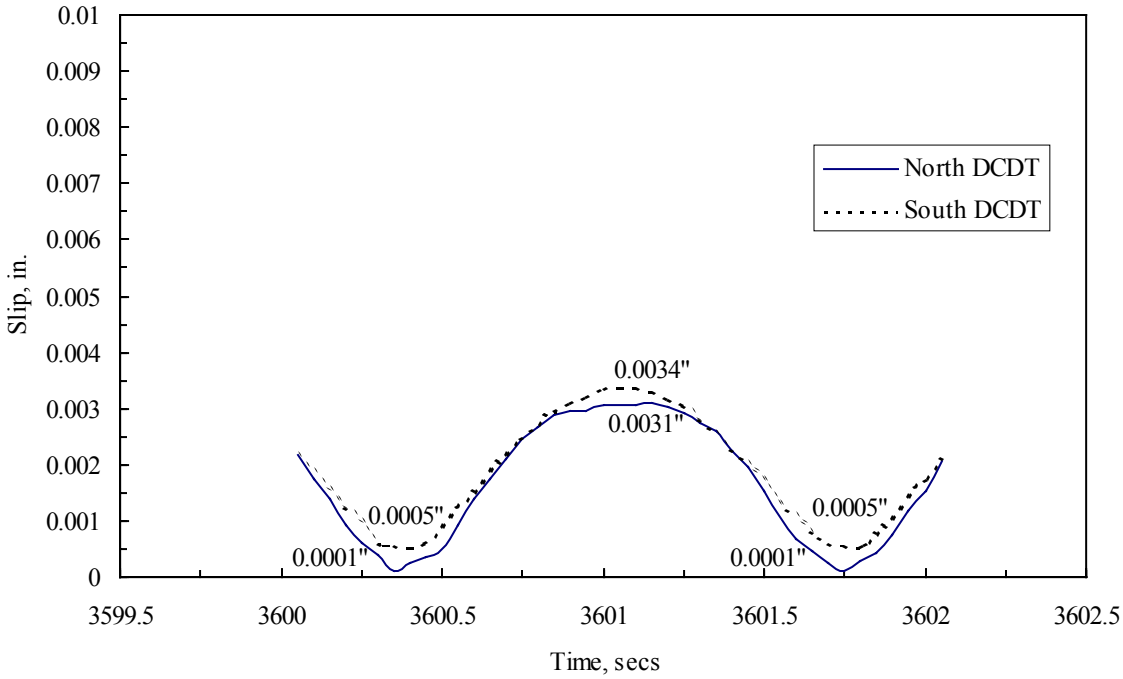

a. After 2,700 cycles (1.5 cycles shown)

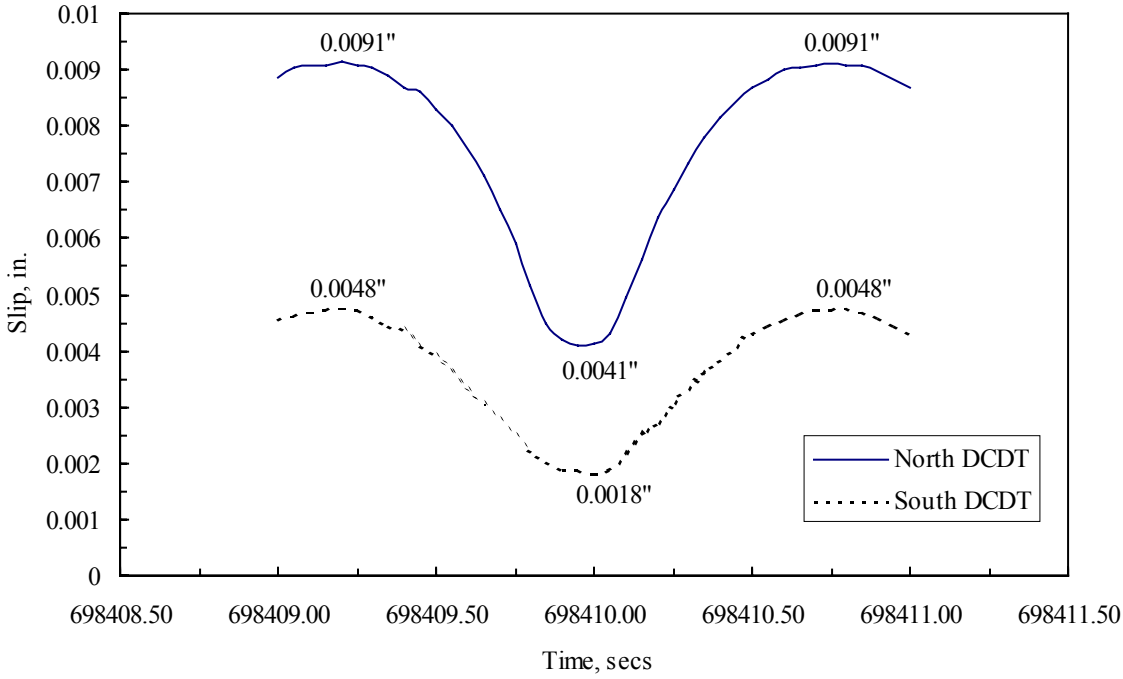

b. After 462,800 cycles (1.3 cycles shown)

Figure 5.7. Horizontal slip during fatigue testing of Specimen 2.

Figure 5.8. Fatigue failure of the steel beam in Specimen 2.

1.81 in., as illustrated in Fig. 5.6. This increase is mostly due to the fatigue crack in the steel beam.

The presence of the crack can also be noticed by comparing the slip curves in Fig. 5.7b. It is hypothesized that if the fatigue crack had not formed in the steel beam, the slip at the North end would have been comparable to the slip at the South end. A maximum slip of only 0.0048 in. at the South end signifies that composite action was still being developed after 464,000 cycles. The slip measured at the South end compares well with Leonhardt's research, which involved fatigue testing of push-out specimens [12] (presented in Chapter 2). Leonhardt measured slips between 0.004 in. and 0.008 in. after 500,000 cycles.

More than likely the ASC would have lasted beyond the number of cycles recommended by AASHTO (500,000). Furthermore, like the Perfobond Rib Connector

discussed in Chapter 2, the ASC is not prone to fatigue problems since it provides a rigid connection at service level. Therefore, it was concluded that the ASC has adequate fatigue strength for use in bridge systems on low volume roads.

5.2 Two-beam Results

The two-beam tests involved an investigation of the behavior of a slab and beam system, as a whole, rather than just the ASC. The two systems that were tested were the Steel-free Deck System (Specimen 4) and the Concrete Arch System (Specimen 5); specimen details were presented in Chapter 3. Both specimens utilized the ASC configuration used in Specimen 3 and incorporated the ASC with other modifications to the BISB. The top flange was not removed in either specimens for reasons stated in Chapter 3 and the results presented in the previous sections. The purpose of the testing was to determine the potential application of the bridge systems (represented by Specimens 4 and 5) based on the strain/deflection behavior during service and ultimate loading, the ultimate load capacity, and the mode of failure.

5.2.1 Steel-free Deck System

Specimen 4 was developed based on the Canadian research on steel-free decks (see Chapter 2). A steel free deck obtains its strength through arch action in the concrete slab. As shown in Fig. 3.3, the slab in Specimen 4 is 'steel-free' except for one layer of transverse reinforcement, which serves as a tension tie for the internal arching action of the slab and confinement of the concrete around the ASC holes. The steel tension ties provide the lateral restraint needed to develop the arching action; the mode of failure determines if proper

restraint was provided. A punching shear failure signifies that arching action was developed and the means of providing lateral restraint was sufficient.

As explained in Chapter 4, Specimen 4 was tested with the loading at three different locations (see Fig. 4.7a for load positions). Tests were performed with the load at Load Positions 2 and 3 to determine the behavior of the slab when loaded near a transverse free-edge. Limited results are presented for tests with the loading at Load Positions 2 and 3 since the deflection under the load was the only measurement recorded. Before loading to failure, a service load of 45 kips was applied three times at each load position to obtain strains and deflections and to check the reproducibility of the responses capita.

Service load test results for the load at Load Position 1 are presented in Fig. 5.9. The graphs in Figs. 5.9b, 5.9d, and 5.9e were plotted using data from the second service test. Average beam deflections and strains were plotted in Figs. 5.9b and 5.9e for clarity. Average beam deflection is used in the remaining sections to describe the average deflection measured under the two steel beams, as shown in Fig. 4.8c. Theoretical deflections were calculated using the section properties of the entire specimen cross-section (both beams).

The deflections under the load (beam deflections plus deflections of the slab relative to the beams) for the three service tests at Load Position 1 are plotted in Fig. 5.9a. It is suspected that some initial seating occurred in the specimen during the first service test since the slope of its deflection curve is not identical to that of service tests 2 and 3. Included with the experimental deflection curves is a theoretical deflection curve. It can be seen that there is a slight difference between the theoretical and experimental curves. However, the theoretical curve shown in Fig. 5.9b is identical to the average beam deflection at midspan.

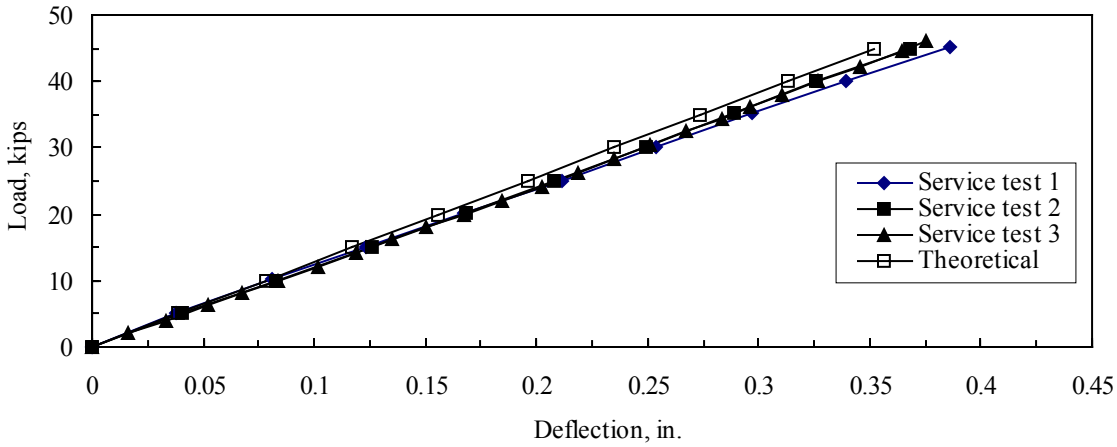

a. Deflections under load

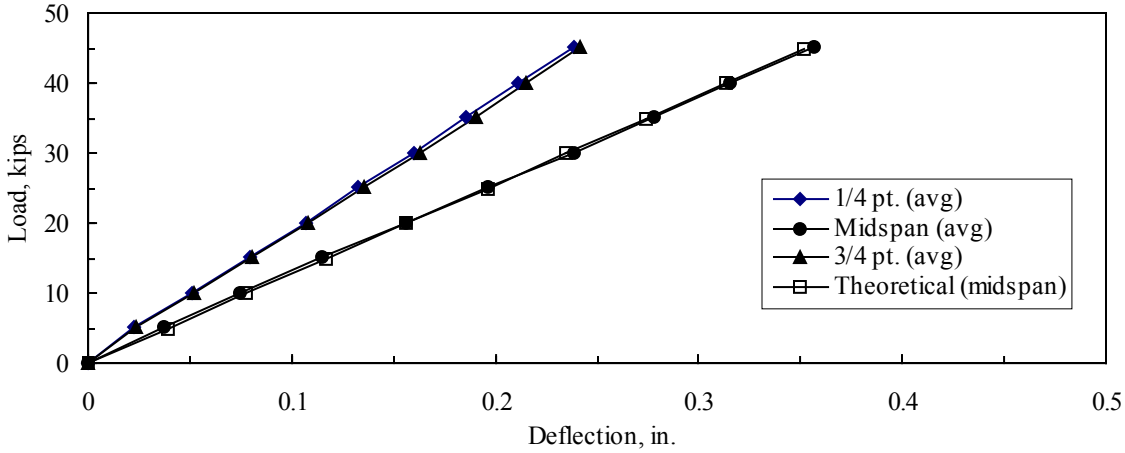

b. Beam deflections

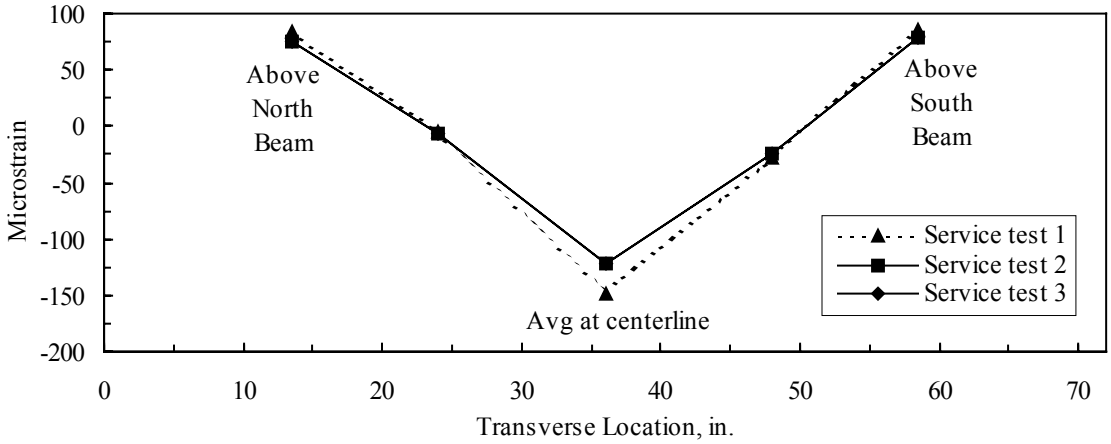

c. Transverse concrete strains at center of load

Figure 5.9. Service load test results for the load at Load Position 1 on Specimen 4.

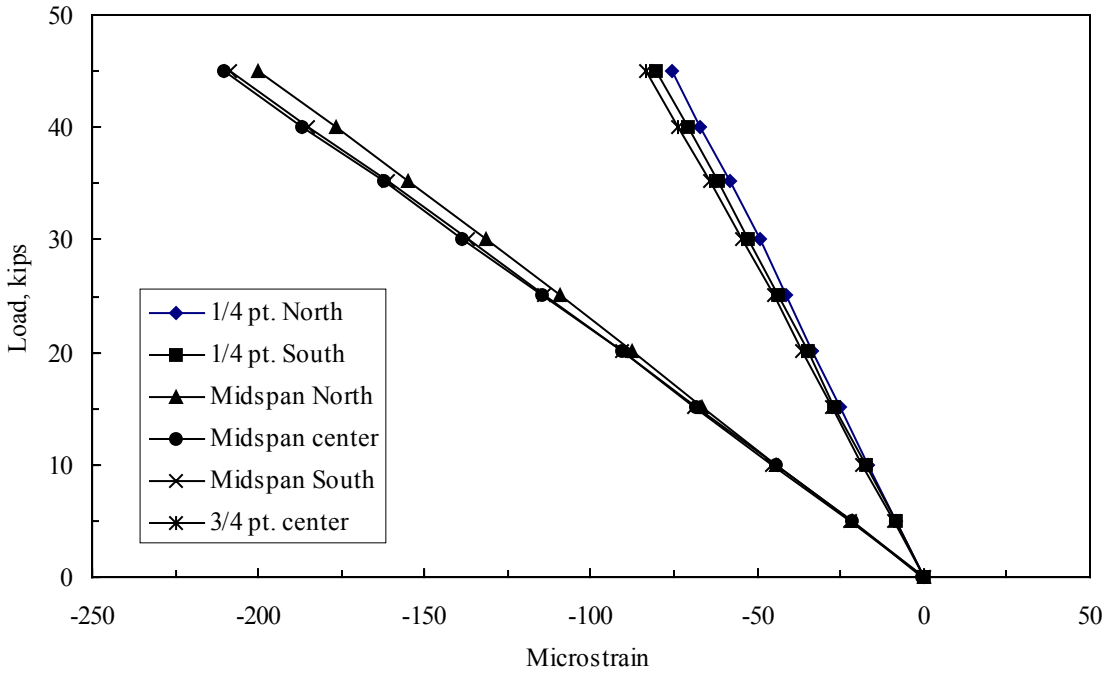

d. Longitudinal concrete strains

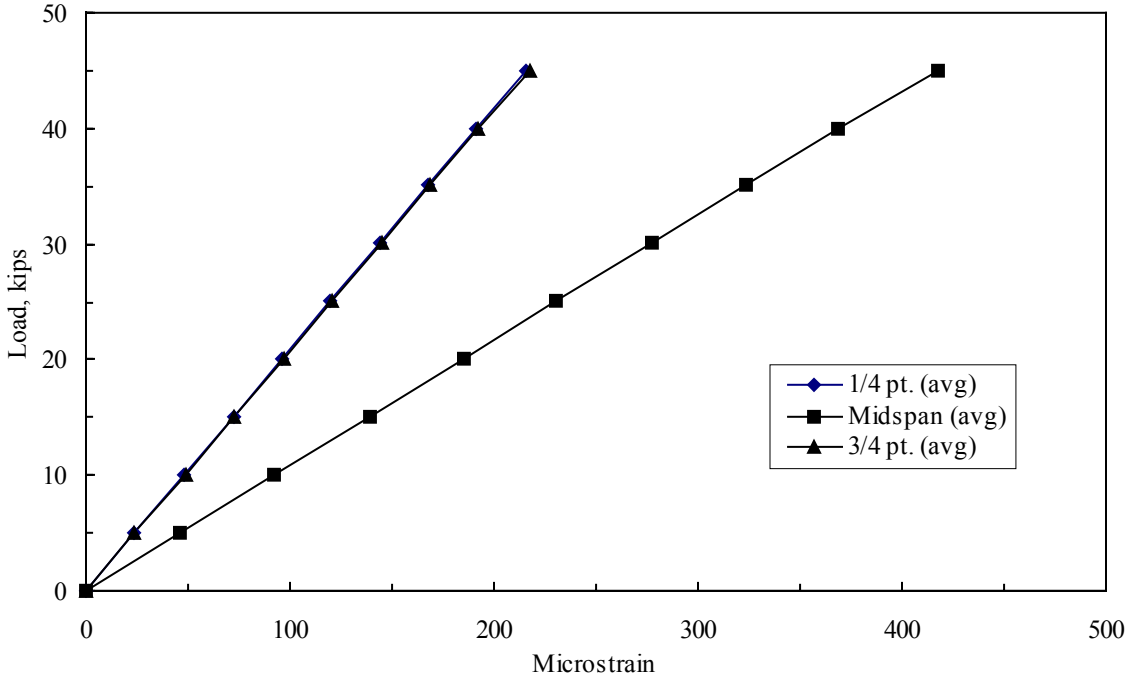

e. Bottom flange strains

Figure 5.9. Continued.

This suggests that the concrete slab was deflecting relative to the beams; relative deflection of the slab was not taken into consideration when calculating the theoretical curve. Accepting this as the reason for the difference between the theoretical and experimental curves in Fig. 5.9a, it can be assumed that the concrete slab deflected approximately 0.021 in. relative to the steel beams.

The transverse strains in the top of the concrete slab, measured by gages located longitudinally along the transverse centerline of Load Position 1, are shown in Fig. 5.9c. Refer to Figs. 4.8a and 4.9 for locations of concrete strain gages oriented in the transverse direction. A dashed line was used to represent service test 1 since initial seating affected the results as explained earlier. Positive strain above each beam indicates a negative moment in the slab. But even at a factored wheel load of 45 kips, the tensile strains were low (75 MII to 85 MII or in terms of stress 0.32 ksi to 0.36 ksi) at these negative moment locations.

Figures 5.9d and 5.9e show the longitudinal strains in the top of the concrete slab and the bottom steel flanges, respectively. Refer to Figs. 4.8 and 4.9 for the location of the strain gages. Longitudinal concrete strains, plotted in Fig. 5.9d, were measured by gages located above the centerline of the beams, which are identified by either North or South, and by gages located along the longitudinal centerline of the specimen, identified as center. Midspan center concrete strains are an average of the strains measured by two of the gages around the wheel footprint (both at the longitudinal centerline and in the longitudinal direction). Close agreement of the strains measured above the beams with the strains measured at the centerline suggests a uniform strain distribution in the top of the slab between the beams. Note the strain behavior in Fig. 5.9e is very similar to the deflection behavior in Fig. 5.9b.

The deflections under the load during service load testing with the loading at Load Positions 2 and 3 are shown in Fig. 5.10. It is obvious that the experimental curves differ from the theoretical curve for both load positions. The experimental deflection behavior at both load positions was affected by the failure at Load Position 1. Even though damage to the slab was local, significant yielding occurred in the steel beams at midspan (permanent deflection was approximately 1 in.). Details of the failure are discussed later, but it should be noted that deflections at Load Positions 2 and 3 would have been significantly less during service and ultimate load testing, if a previous failure at Load Position 1 had not occurred.

Figures 5.9 and 5.10 confirm that strain and deflection data were reproducible at all load positions. Also, all strains and deflections increased in a linear fashion and exhibited similar behavior. Thus, only deflection data will be presented in the remainder of this section.

The deflections under the load during ultimate load testing at all three load positions are shown in Fig. 5.11. The ultimate loads and corresponding deflections were as follows: 147.5 kips and 2.66 in. at Load Position 1, 123.2 kips and 0.29 in. at Load Position 2, and 136.8 kips and 0.50 in. at Load Position 3. The ultimate loads at Load Positions 2 and 3 were respectively 0.84 and 0.93 times the ultimate load at Load Position 1.

The decrease in ultimate load when the load was located closer to the end of the specimen (transverse free-edge) could be an indication that the transverse free-edges required more stiffening than the four #5 bars provided (see specimen details in Fig. 3.3b). However, the failure patterns shown in Fig. 5.12 do not confirm this because all were punching shear failures. If the edge required more stiffening, the failure mode of the slab would have been a combination of punching shear and transverse flexural failure modes, especially at Load

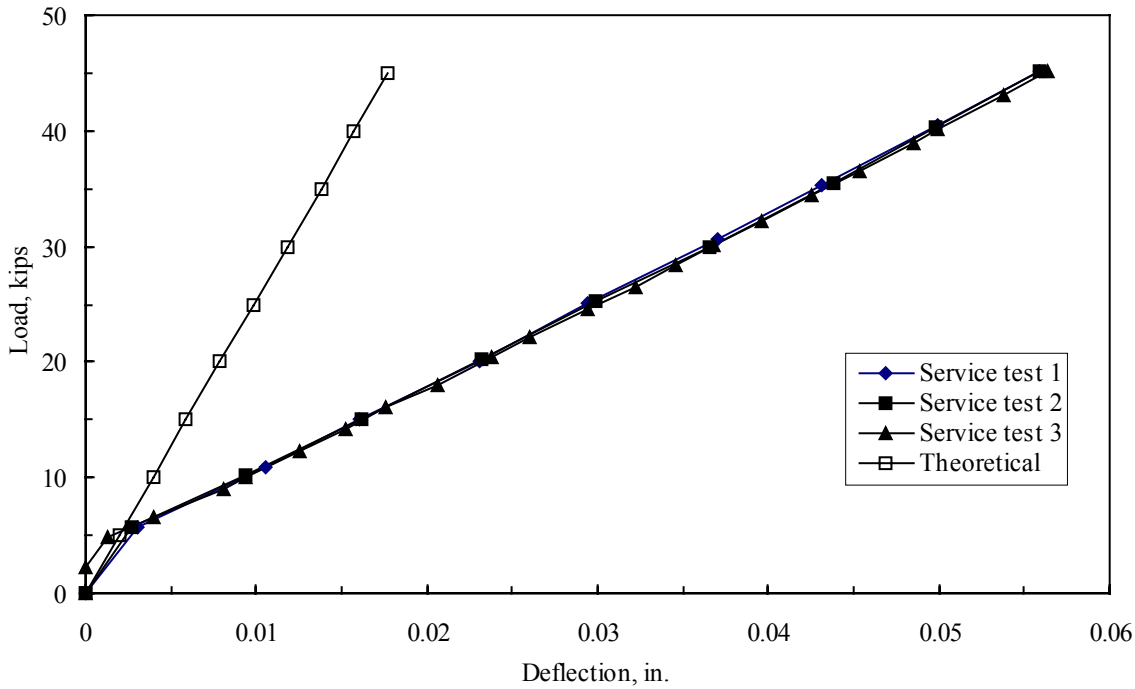

a. Load Position 2

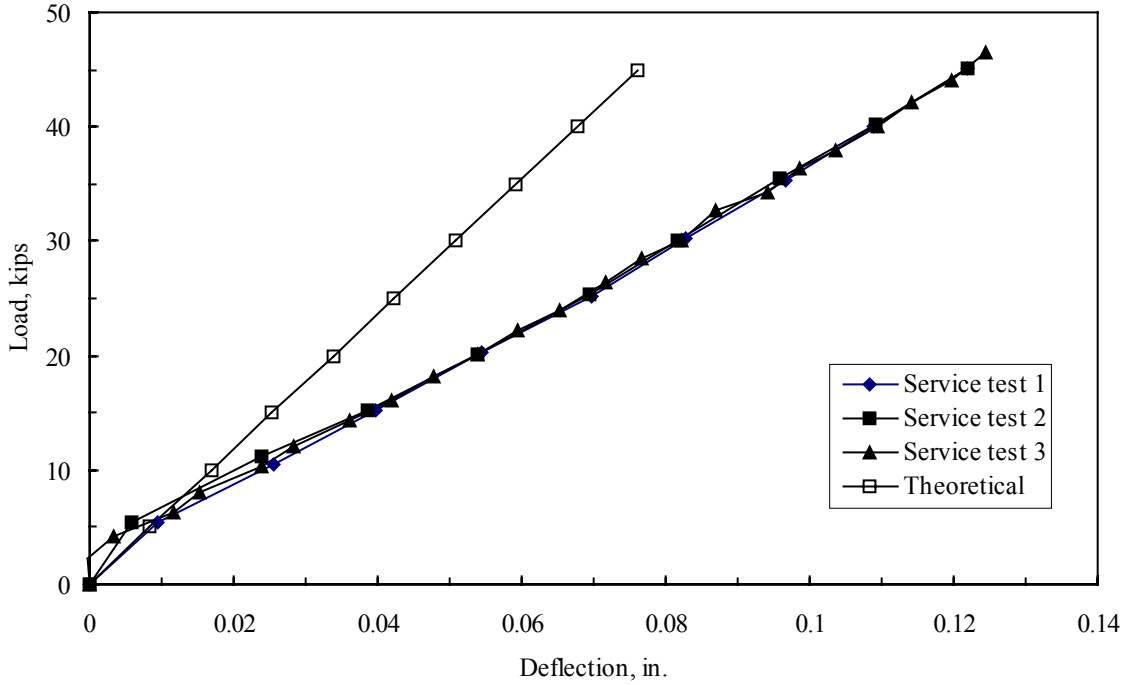

b. Load Position 3

Figure 5.10. Deflection under load during service load testing at Load Positions 2 and 3 on Specimen 4.

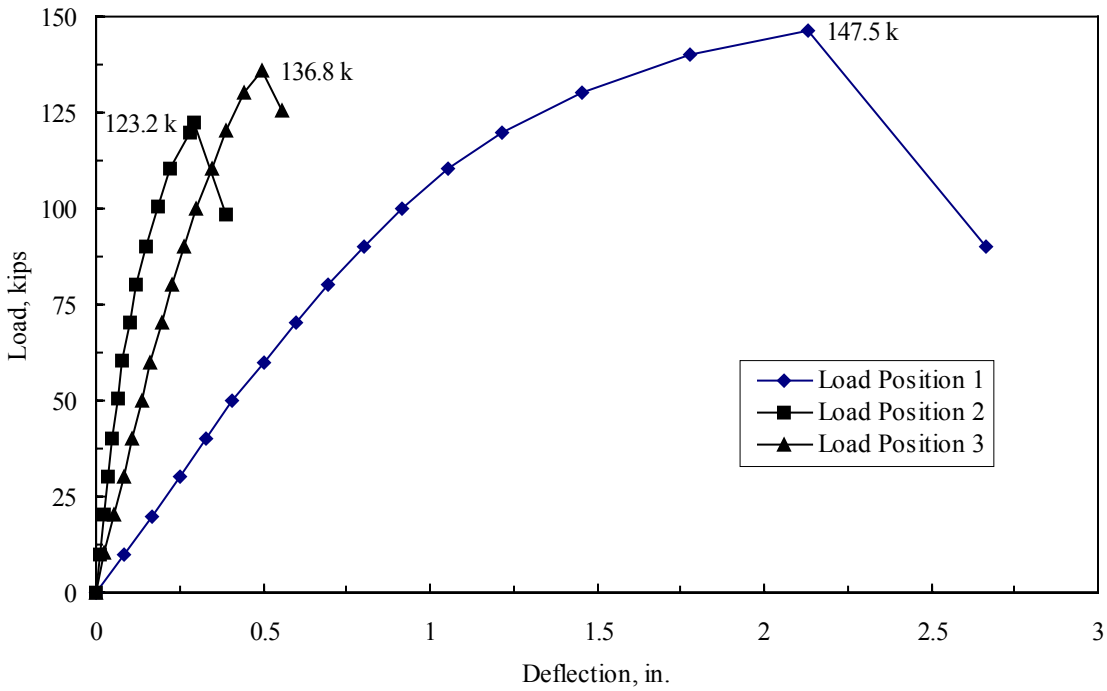

Figure 5.11. Deflections under load during ultimate load testing of Specimen 4.

Position 2. Therefore, a more likely explanation is that a greater load was required to punch through the concrete slab at Load Position 1 because of more flexibility at midspan than near the ends of the specimen. Likewise, this flexibility would explain the larger punched out regions at Load Positions 1 and 3 in comparison to that at Load Position 2, which was located closest to the end of the specimen.

As previously noted, the failures at all the load positions were punching shear failures (see Fig. 5.12) indicating that adequate lateral restraint was provided by the #5 reinforcement bars spaced on 15 in. centers and the four #5 bars at each end provided for edge stiffening. Therefore, the Steel-free Deck System exhibited the same load-carrying characteristics as a

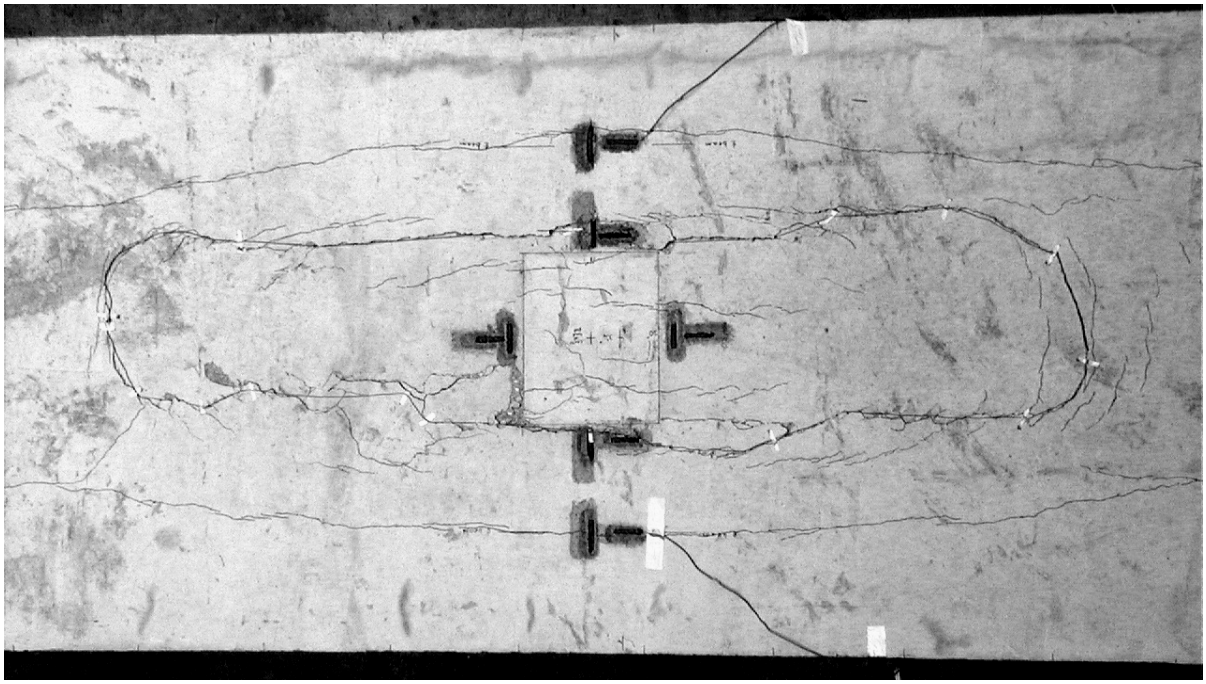

a. Failure pattern at Load Position 1

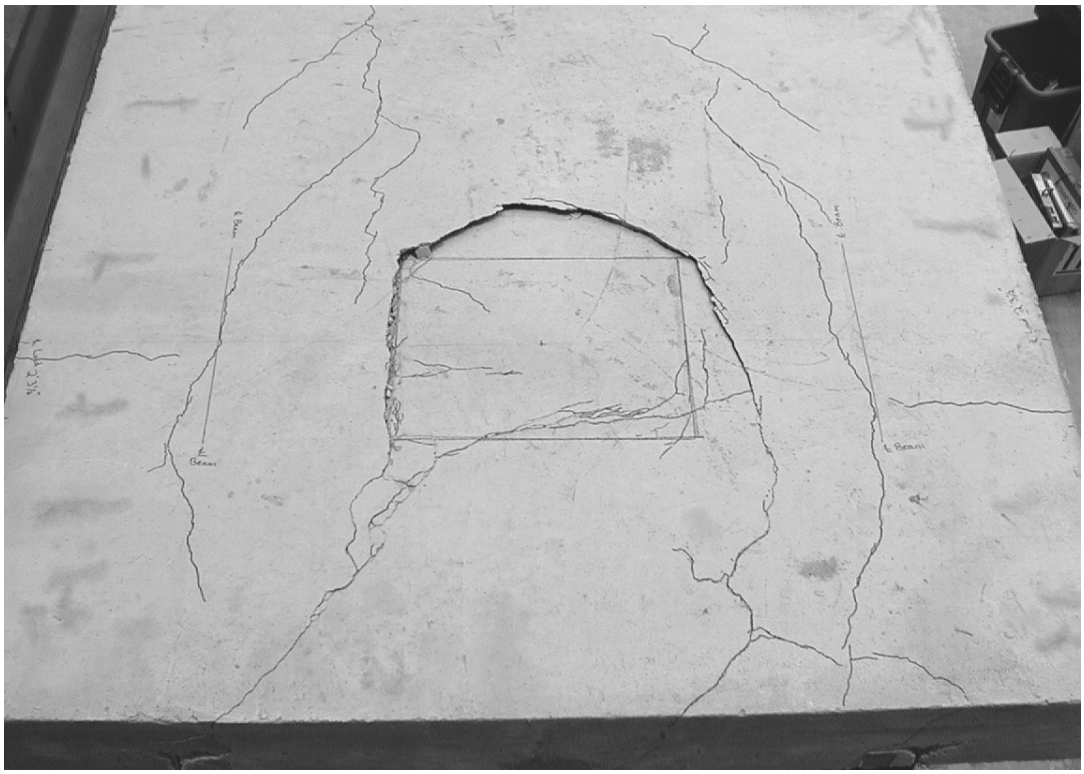

b. Failure pattern at Load Position 2

Figure 5.12. Photographs of Specimen 4 failure patterns on top surface of slab.

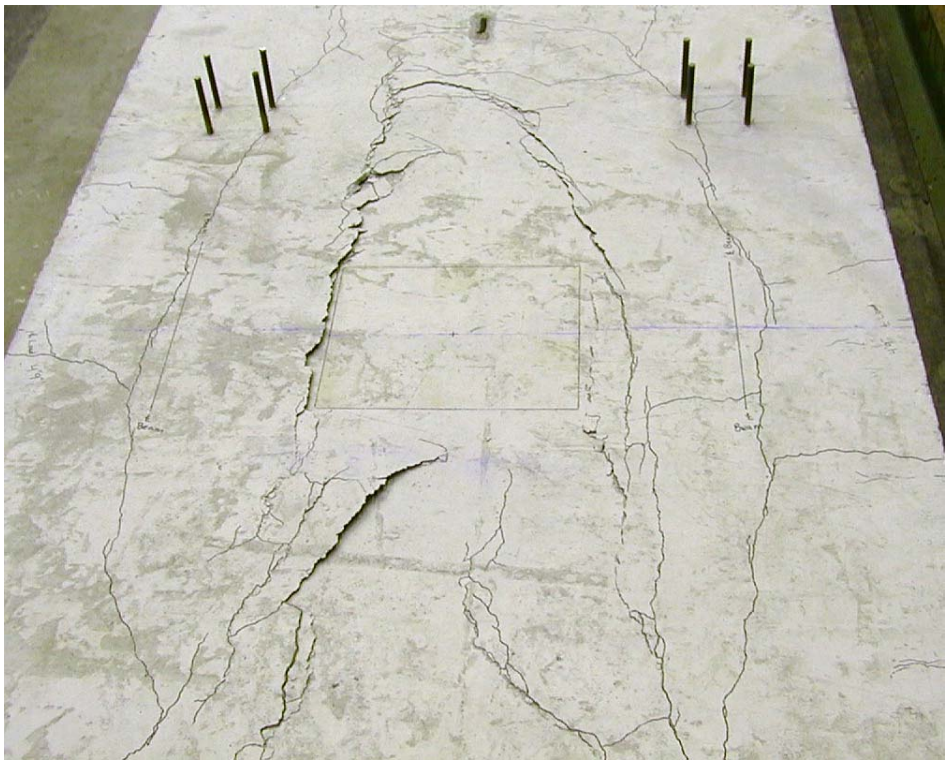

c. Failure pattern at Load Position 3

Figure 5.12. continued.

conventionally reinforced slab since there were punching shear failures rather than flexural failures. For more details on the failure patterns refer to Reference 14.

In Table 5.2 the experimental ultimate moment capacity, $M_{u(exp)}$, is compared to the theoretical ultimate moment capacity, $M_{u(theo)}$. The moment due to selfweight, M_{self}, was calculated and included in the experimental ultimate moment capacity. The theoretical moment capacity was calculated using both beams and an effective slab width equal to the full width of the specimen.

It is obvious that the punching shear failure occurred before the specimen reached its ultimate moment capacity. However, the ultimate moment ratio of 0.934 indicates that flexural and punching shear failures almost occurred simultaneously, which could be another reason for the large punched out region at Load Position 1. Theoretically the punching shear

Table 5.2. Comparison of ultimate moment capacity for Specimen 4.

Load Position	Ultimate Load (kips)	M_{self} (ft-kips)	$M_{u(exp)}$ (ft-kips)	$M_{u(theo)}$ (ft-kips)	$M_{u(exp)}/M_{u(theo)}$
1	147.5	101.6	1336.9	1432.1	0.934

failure should have occurred at approximately 242 kips. However, theoretically 157.9 kips would result in the ultimate moment capacity of the specimen; therefore, a punching shear failure was not possible. The reason why the failure load did not reach 157.9 kips was probably due to the flexure – punching shear combination.

To check the serviceability of the Steel-free Deck System, the deflections under the load, at each load position, is compared to the maximum allowable live load deflection (L/800) as specified by AASHTO [1] in Table 5.3. The deflections at the various loads were measured during the ultimate load test. It is shown that all service load deflections, including those for a factored wheel load, are less than the allowable.

Table 5.3. Comparison of Specimen 4 deflections to the maximum allowable.

Load Position	Deflections under the load (in.)			
	Nominal wheel load (16 kips)	Factored wheel load (45 kips)	Ultimate load (see Fig. 5.11)	Allowable (L/800)
1	0.135	0.365	2.660	0.503
2	0.018	0.056	0.292	0.503
3	0.042	0.120	0.499	0.503

Based on the results presented in this section, it can be concluded that the Steel-free Deck System, (i.e., Specimen 4), could be used in bridges on low-volume roads. It met serviceability requirements and the failure loads were much greater than the factored wheel load. The punching shear failures indicated the presence of sufficient lateral restraint to develop the arching action; therefore, additional reinforcement is not needed for strength

requirements. A potential application of this system is the precast units in the bridge system proposed in project HR-382, Concept 1: Steel Beam Precast Units [9].

5.2.2 Concrete Arch System

Specimen 5 was more directly related to the BISB system than Specimen 4 was; the steel beams were fully encased in concrete. The most significant modifications to the BISB was the removal of some of the concrete on the tension side to reduce the self-weight and the addition of the ASC to create composite action. As discussed in Chapter 3, this was accomplished by using a section of pipe to form a concrete arch between the beams (see Fig. 3.4). Steel straps welded to the bottom flanges provided the lateral restraint in Specimen 5. However, in a system with more than two beams, the adjacent concrete arches would provide most of the lateral restraint. The steel straps are primarily installed to restrain movement of the beams during placement of the concrete. Since Specimen 5 relies on only the steel straps for lateral restraint a worst case scenario is represented.

In contrast to the testing of Specimen 4, tests were performed at only two locations on Specimen 5 (see Fig. 4.7b for load positions). Again, limited results are presented for tests with load at Load Position 2. As mentioned in Chapter 4, the same testing procedures were used on Specimen 5 as were used on Specimen 4.

Specimen 5 service load test results with the load at Load Position 1 are presented in Fig. 5.13. The graphs in Figs. 5.13b, 5.13c, and 5.13d were plotted using data from the second service test. Average beam deflections were plotted in Fig. 5.13b for clarity. Theoretical deflections were calculated using the section properties of the entire specimen cross-section (both beams and all the concrete).

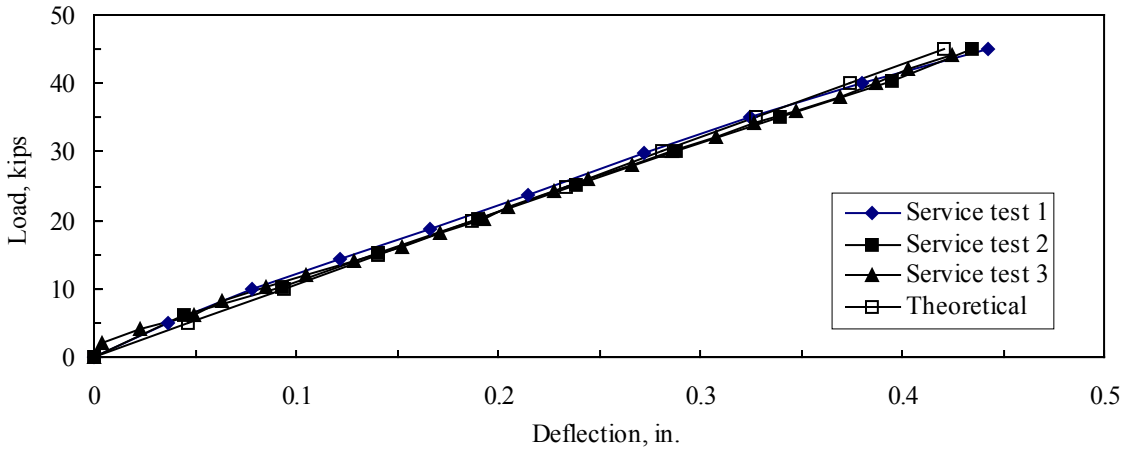

a. Deflections under load

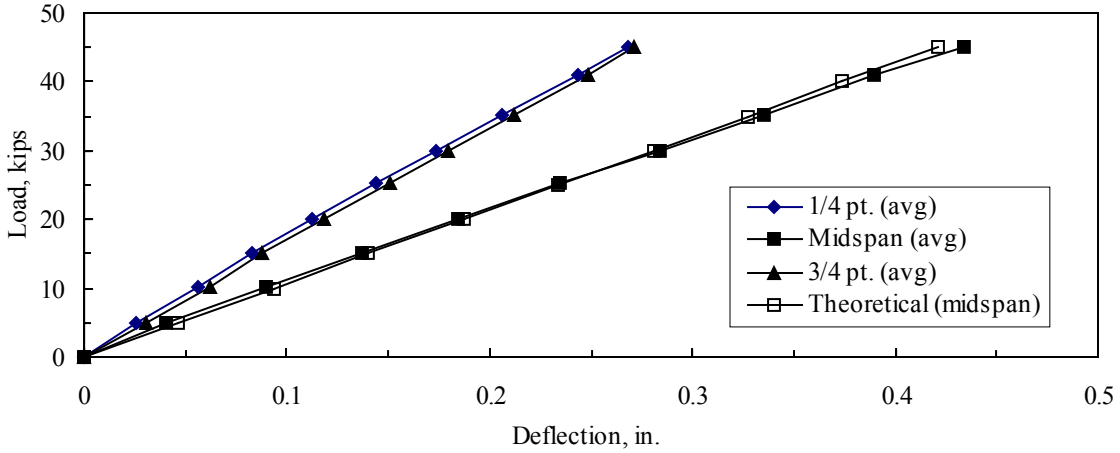

b. Beam deflections

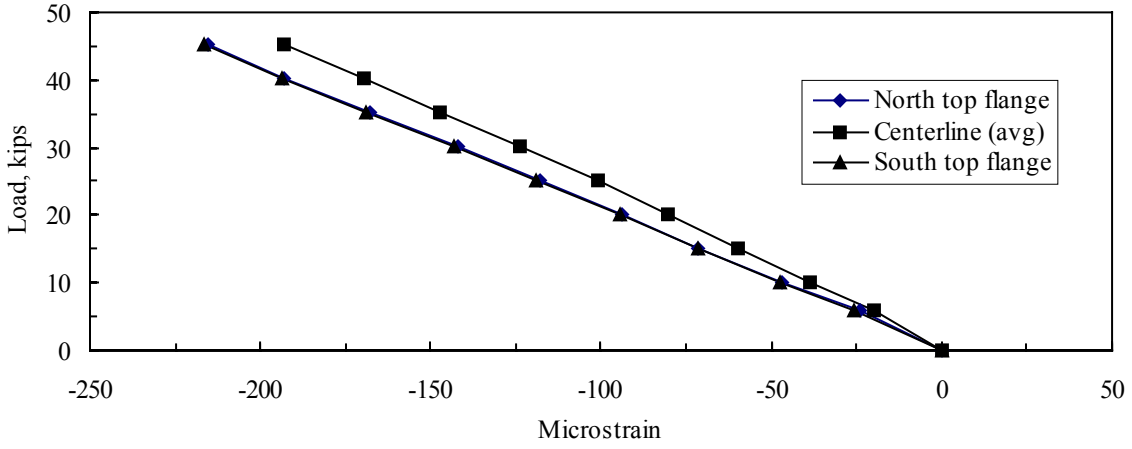

c. Longitudinal strains at midspan

Figure 5.13. Service load test results for the load at Load Position 1 on Specimen 5.

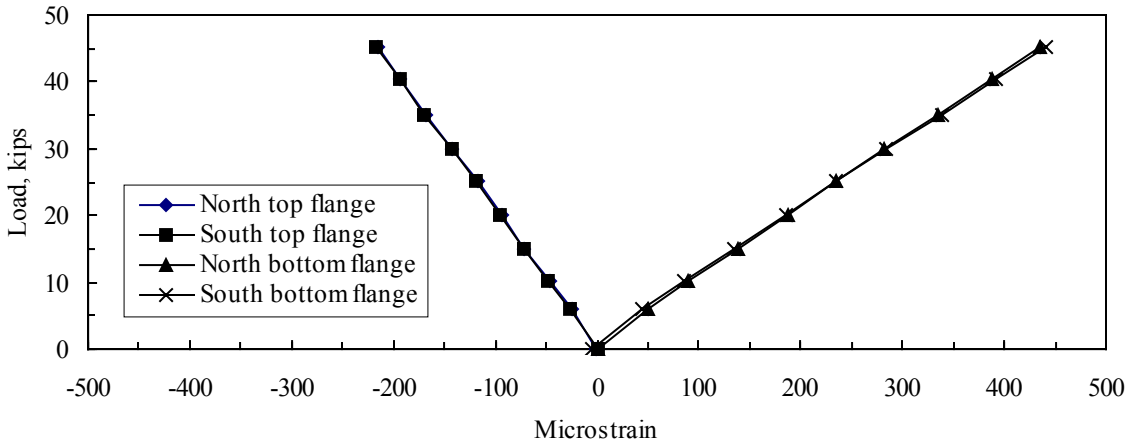

d. Top and bottom flange strains at midspan

Figure 5.13. Continued.

The deflections under the applied load for the three service load tests (in which a maximum load of 45 kips was applied) at Load Position 1 are plotted in Fig. 5.13a, along with the theoretical deflection curve. The same theoretical curve is plotted in Fig. 5.13b. The theoretical curve agrees well with both the deflection under the load and the average beam deflection at midspan. Therefore, unlike Specimen 4, deflection of the slab relative to the beams did not occur during service load testing. Relative deflection also did not occur during ultimate load testing.

Figure 5.13c presents the steel and concrete longitudinal strains at midspan. Steel strains were measured in the top flanges of the two beams. The concrete strains were measured by two strain gages placed at the longitudinal centerline of the specimen, one on each side of the wheel footprint (see Fig. 4.10a for strain gage locations). The average strain measured by these two concrete strain gages is plotted in Fig. 5.13c. Although the strain in the top flanges were slightly greater than the strain in the concrete at centerline, the strains were close enough to be considered a uniform strain distribution across the top of the

specimen. This confirms the beams were acting compositely with the concrete, despite the top flange not being fully embedded in the concrete as it was in Specimens 3 and 4.

Shown in Fig. 5.13d, is a plot of the top and bottom flange strains at midspan. Excellent agreement between the North and South flanges suggests an equal load distributed to the two beams. Note that the strains measured at the bottom flanges were almost two times the strain level at the top flanges, confirming the location of the neutral axis for the fully composite section. The distance from the bottom flange to the neutral axis (13.25 in.) is 1.7 times the distance for the top flange (7.75 in.).

The deflection under the applied load during service load testing with the load at Load Position 2 is shown in Fig. 5.14, including the theoretical deflection curve. All three experimental curves disagree with the theoretical curve. As with Specimen 4, it is suspected that the experimental deflection behavior with the load at Load Position 2 was affected by the ultimate load test at Load Position 1; in this failure there was complete yielding of the steel beams at midspan. So the greater experimental deflections, shown in Fig. 5.14, are reasonable considering the extent of damage (i.e., complete yielding of the steel beams) that occurred at midspan. Thus, the deflection at Load Position 2 would have been significantly less during the service and ultimate load tests, if failure at midspan (Load Position 1) had not occurred first.

Figures 5.13 and 5.14 confirm that strain and deflection data were reproducible at both load positions. Furthermore, strains and deflections increased linearly with load and exhibited similar behavior. Therefore, only deflection data will be presented in the remainder of this section.

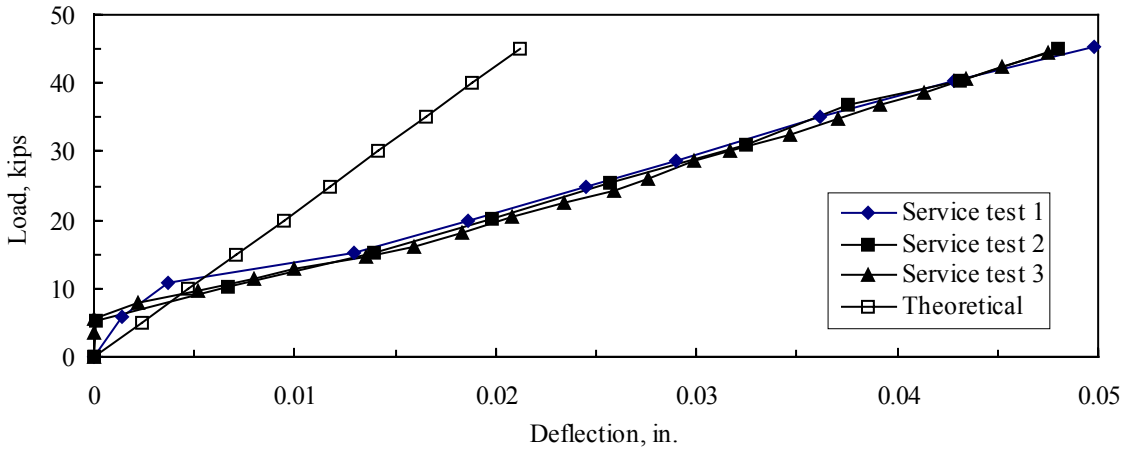

Figure 5.14. Deflections under load during service load testing at Load Position 2 on Specimen 5.

Illustrated in Fig. 5.15 are the deflections under the load during ultimate load testing at both load positions. The ultimate loads and corresponding maximum deflections were as follows: 126.3 kips and 5.57 in. at Load Position 1 and 171.3 kips and 0.94 in. at Load Position 2. Excellent ductility of the Concrete Arch System is indicated by the deflection curve for the load at Load Position 1.

The ultimate load at Load Position 2 was 1.36 times that at Load Position 1; therefore, unlike Specimen 4, the ultimate load was greater near the end of the specimen than at midspan. That is because the transverse restraint of this system is much better than that offered by the system in Specimen 4. This was demonstrated by a flexural failure that occurred at Load Position 1 before the wheel footprint was able to punch through the concrete arch. Since flexure does not play a major role near a support, failure did not occur at Load Position 2 until the concrete arch failed in punching shear. Hence, a greater ultimate load was achieved.

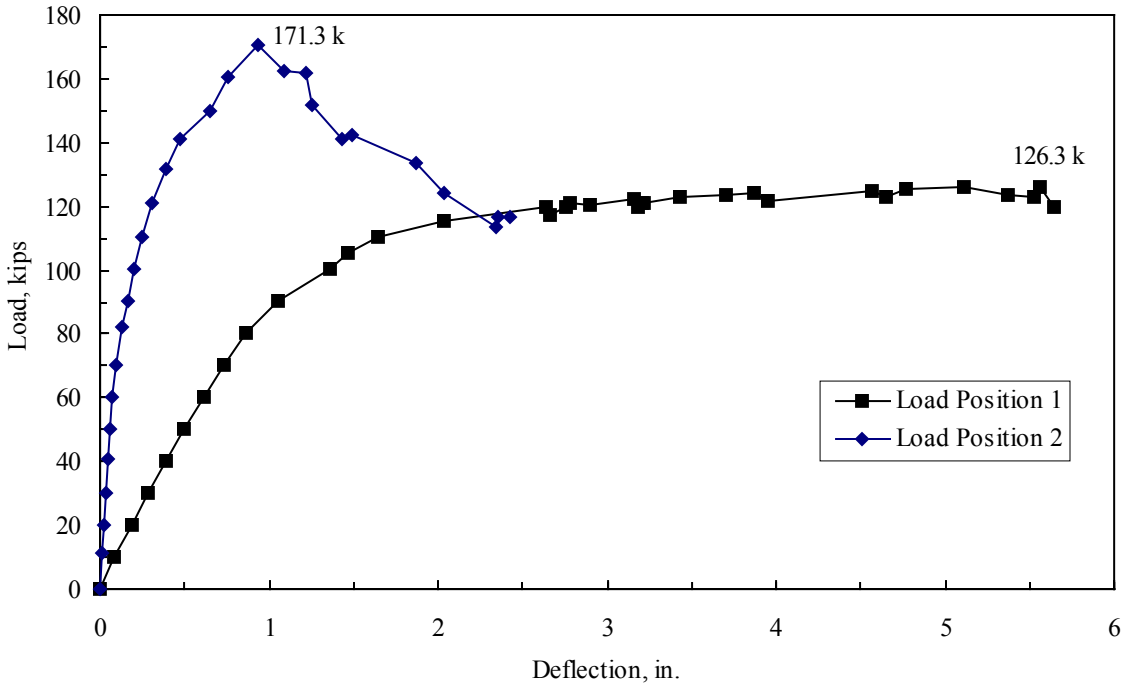

Figure 5.15. Deflections under load during ultimate load testing of Specimen 5.

The comparison of the experimental ultimate moment capacity, $M_{u(exp)}$, to the theoretical ultimate moment capacity, $M_{u(theo)}$, shown in Table 5.4, verifies that it was a flexural failure; the specimen reached its ultimate moment capacity before punching occurred. Since the beams were simply supported when the concrete was placed, the moment due to selfweight was not included in the experimental ultimate moment capacity. The theoretical moment capacity was calculated using both beams and an effective slab width equal to the full width of the specimen.

Table 5.4. Comparison of ultimate moment capacity for Specimen 5.

Load Position	Ultimate Load (kips)	$M_{u(exp)}$ (ft-kips)	$M_{u(theo)}$ (ft-kips)	$M_{u(exp)}/M_{u(theo)}$
1	126.3	1057.8	1087.5	0.973

In comparing Specimens 4 and 5, the ultimate load at Load Position 1 was 1.17 times greater for Specimen 4, yet its theoretical ultimate moment capacity was 1.32 times greater. The difference being that Specimen 5 attained its ultimate moment capacity and Specimen 4 did not. Despite a larger volume of concrete in Specimen 5, its ultimate moment capacity was less because of its smaller overall depth.

After failing the specimen in flexure, another failure test was performed at Load Position 1 to determine the amount of additional load the concrete arch could sustain until a punching shear failure occurred. Support blocks were placed underneath both steel beams to prevent deflection beyond that associated with the flexure failure. During reloading, the steel beams began resting on the support blocks at an approximate load of 130 kips, which is close to the flexural failure load of 126.3 kips. From this point, an additional load of 112 kips was applied until shear punching and longitudinal splitting of the top of the concrete arch occurred. The total failure load was then 242 kips. At a total load of 177 kips, a weld connecting one of the steel straps to a bottom flange broke and longitudinal splitting of the top of the arch was noticeable.

The failure pattern resulting from this test is illustrated in Fig. 5.16a. The longitudinal crack shown in the photograph extends approximately 16 ft. to the West end of the specimen (opposite of Load Position 2) and was the reason for not performing a third test near this end. A photograph of the punching shear failure at Load Position 2 is shown in Fig. 5.16b; in this end view, a typical vertical crack, associated with splitting of the top of the arch may be seen. Longitudinal splitting initiated the punching failure just as it did during the second failure test at Load Position 1. Note the vertical crack ends at the reinforcing bar which is identified in the photograph.

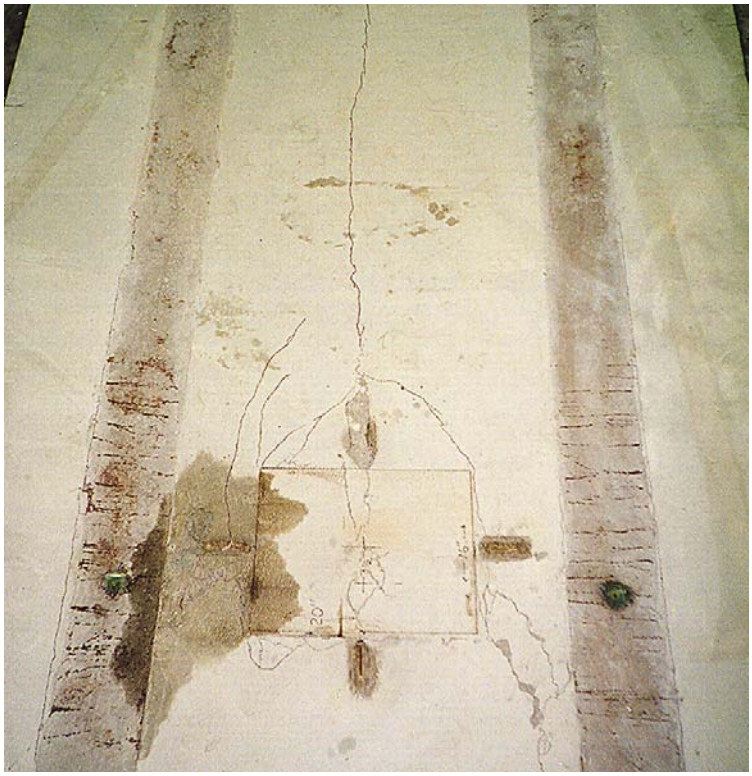

a. Top view of failure pattern at Load Position 1

b. End view of failure pattern at Load Position 2

Figure 5.16. Photograph of failure patterns in Specimen 5.

Longitudinal splitting could be prevented or at least delayed, if steel reinforcement was appropriately placed to resist the transverse tension forces developed at the top of the concrete arch. The purpose of the existing reinforcement in Specimen 5 was to resist transverse tension forces developed during horizontal shear transfer while confining the concrete around the ASC holes. Nonetheless, this reinforcement could be utilized more efficiently by positioning it lower thus, making it more effective in resisting the transverse tension forces caused by a load applied between the steel beams. As shown in Fig. 3.4, the ASC reinforcement is currently located 3 in. from the top. Lowering the reinforcement would be especially desirable for use in a system with larger beam spacings, since splitting would probably occur at a lesser load.

A section of the pipe (stay-in-place form) directly below Load Position 1 was removed to view the failure pattern of the underside of the arch. For more details on the failure pattern at Load Position 1, refer to Reference 14.

To check the serviceability of the Concrete Arch System, the deflections under the load, at both load positions, are compared to the maximum allowable live load deflection (L/800) as specified by AASHTO [1] (see Table 5.5). The deflections at the various loads were measured during the ultimate load test. It is shown that all service load deflections are less than allowable.

Based on the results presented and discussed in this section, it can be concluded that the Concrete Arch System (i.e., Specimen 5) could be used in bridges on low-volume roads. It met serviceability requirements and the failure loads were much greater than the factored wheel load. The system exhibited a lateral restraint that was more than sufficient. The

Table 5.5. Comparison of Specimen 5 deflections to the maximum allowable.

Load Position	Deflections under the load (in.)			
	Nominal wheel load (16 kips)	Factored wheel load (45 kips)	Ultimate load (see Fig. 5.11)	Allowable (L/800)
1	0.152	0.433	5.567	0.503
2	0.016	0.049	0.936	0.503

concrete arch was able to sustain additional load after the specimen attained its ultimate moment capacity. Specimen 5 was easier to construct than Specimen 4.

5.3 Push-out Specimen Fatigue Results

The test program and summary of the test results for each specimen are listed as a group corresponding to series SH1, SH2, and SH3 in Tables 5.6, 5.7, and 5.8, respectively. The results presented in these tables consist of the number of cycles to failure from fatigue tests as well as the ultimate strength values from static tests. In Tables 5.6 and 5.7, the maximum load levels are expressed in terms of a percentage of the average ultimate static strength; while in Table 5.8, the maximum load levels are expressed in terms of a percentage of the ultimate static strength based only on specimen SH3-4.

In Table 5.6, note that specimen SH1-1 was initially tested in fatigue with a maximum load equal to 50 kips. The test was stopped before failure at 1.5 million cycles before any indication of an increase in slip. The specimen was then tested statically, which exhibited a similar slip characteristic compared to the specimens SH1-3 and SH1-8, which were not loaded in fatigue (Fig. 5.17). The load-slip curves exhibited a nearly linear stiffness phase, and a phase where the slip increases with a corresponding slight decrease in the load. Also, all three specimens maintained over 80 percent of the maximum load at a slip of 0.3 in.

Table 5.6. Summary of series SH1 test results.

Specimen	Loading	Minimum load (lb.)	Maximum load (lb.)	% of static strength	Cycles to failure	Ultimate static strength, (lb.)
1	Fatigue	2,000	50,000	64	1,500,000[a]	81,065
2	Fatigue	2,000	62,000	80	10,970	-
3	Static	-	-	-	-	74,728
4	Fatigue	2,000	57,000	73	27,950	-
5	Fatigue	2,000	54,000	69	75,610	-
6	Fatigue	2,000	57,000	73	11,380	-
7	Fatigue	2,000	70,000	90	450	-
8	Static	-	-	-	-	80,784
9	Fatigue	2,000	62,000	80	1,750	-
10	Fatigue	2,000	54,000	69	181,980	-
11	Fatigue	2,000	62,000	80	11,730	-
12[b]	Fatigue	2,000	54,000	69	1,030	-

[a] Fatigue test was stopped before failure and specimen statically loaded to failure.

[b] Data were not used in the evaluation as mentioned in Section 5.3.3.

Table 5.7. Summary of series SH2 test results.

Specimen	Loading	Minimum load (lb.)	Maximum load (lb.)	% of static strength	Cycles to failure	Ultimate static strength (lb.)
1	Static	-	-	-	-	94,525
2	Fatigue	2,000	83,000	84	6,430	-
3	Fatigue	2,000	72,000	73	697,180	-
4	Fatigue	2,000	76,000	77	55,670	-
5	Static	-	-	-	-	104,020
6	Fatigue	2,000	83,000	84	1,650	-
7	Fatigue	2,000	83,000	84	190	-
8	Fatigue	2,000	72,000	73	339,810	-
9	Fatigue	2,000	76,000	77	120,960	-

Table 5.8. Summary of series SH3 test results.

Specimen	Loading	Minimum load (lb.)	Maximum load (lb.)	% of static strength	Cycles to failure	Ultimate static strength, (lb.)
1[b]	Fatigue	2,000	68,500	72	420	-
2	Fatigue	2,000	79,000	83	12,250	-
3	Fatigue	2,000	72,500	76	95,700	-
4	Static	-	-	-	-	95,098
5	Fatigue	2,000	68,500	72	920,080	-
6	Static	-	-	-	-	N/A[a]

[a] Result has been neglected due to premature failure during the testing.

[b] Data were not used in the evaluation as mentioned in Section 5.3.3.

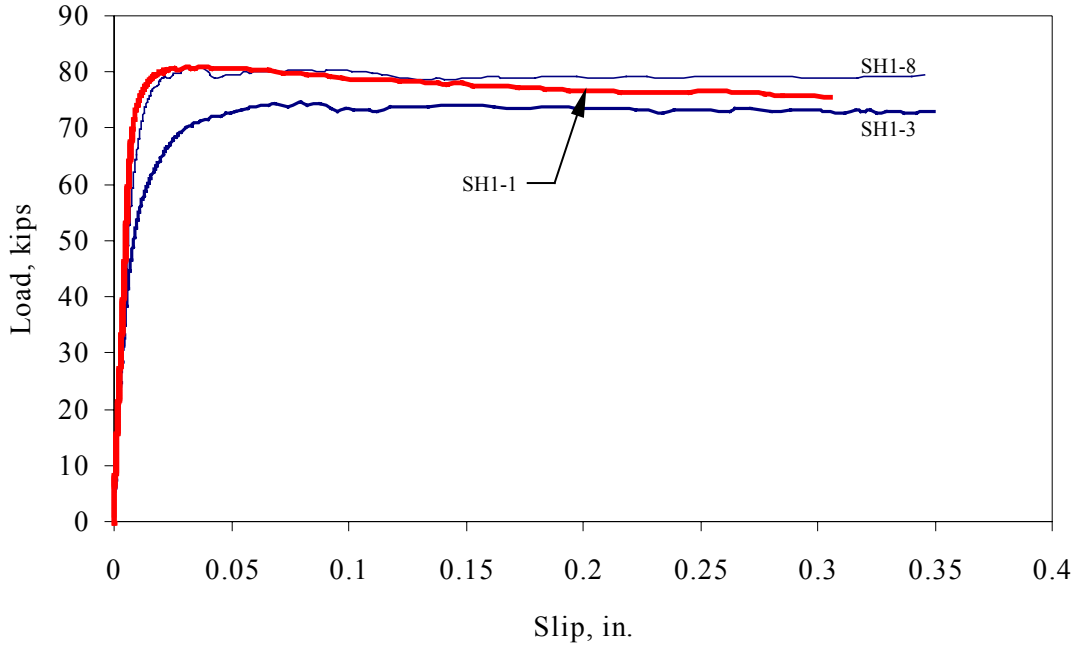

Figure 5.17. Static load-slip curves for series SH1.

Data from specimen SH1-12 were also not used in the evaluation of the connection performance. Upon examination of the reinforcing bars placed through the shear holes, all bars, except for the one in specimen SH1-12, were bent. This suggests that the reinforcing bars of specimen SH1-12 were not properly placed in the shear holes before the concrete was poured (Fig. 5.18). Since the reinforcing bars were held against the shear plate by soft wire loops, it is possible that the bars to were knocked loose by the concrete during pouring. This is probably the reason specimen SH1-12 failed prematurely, compared to the other specimens tested at the same load level.

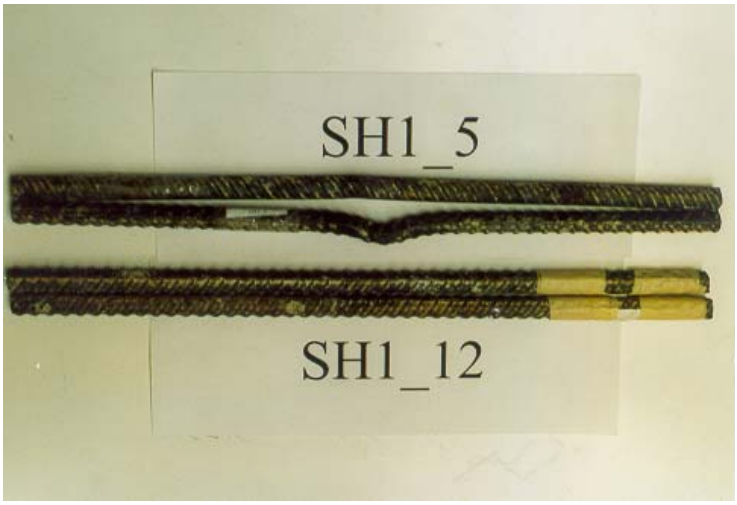

Figure 5.18. Reinforcing bars from specimens SH1-5 and SH1-12.

In Table 5.8, note that the data of specimen SH3-1 were also not used in the evaluation. It was noticed that specimen SH3-1 exhibited a large amount of separation between the shear plate and the concrete blocks after testing, which was not seen in other specimens (Fig. 5.19). Prior to testing, the steel plate of SH3-1 may not have been properly cast in the concrete, leaving the left side of the steel plate lower than the right side. In addition, previous research conducted at Iowa State University [17] showed that the ASC exhibited separation averaging 25 percent of the slip. But the separation of specimen SH3-1 was more than half the interface slip, which according to Yam [27] will affect the behavior of the connector.

For specimen SH3-6, results have been neglected because the 2 in. x 2 in. angle on the left concrete block was not in place due to a premature crack in the concrete while the test was still in progress (Fig. 5.20).

Figure 5.19. Photograph of specimen SH3-1 after failure.

Figure 5.20. Photograph of specimen SH3-6 during testing.

5.3.1 Static Tests

In Fig. 5.21, the load-slip curves for all three series of the static tests are presented. For series SH1 and SH2, the load-slip curves are the average of the load-slip curves for the individual specimens, which are presented in Reference 21. While the load-slip curve of series SH3 is the load-slip curves for the specimen SH3-4. For all specimens, the difference between the two individual slip readings was less than ± 20 percent.

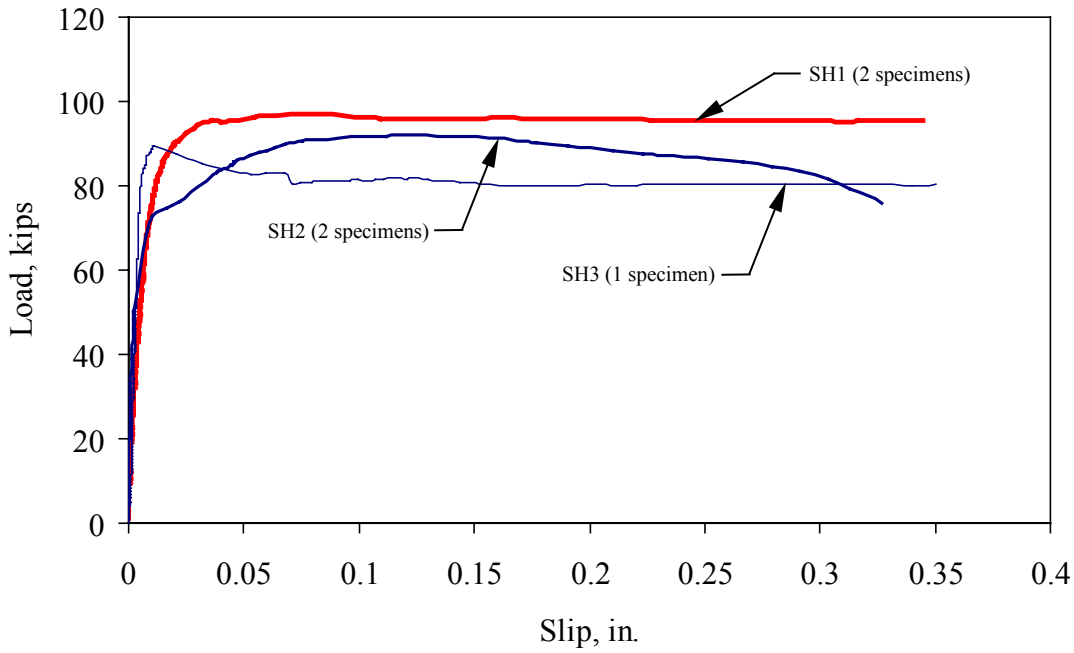

Figure 5.21. Static load-slip curves.

Although as previously noted, the same type and strength of concrete was ordered each time, the concrete strength differed from series SH1 to series SH2 and SH3. Therefore, the curves in Fig. 5.21 are based on a normalized concrete strength of 6,000 psi. Since shear

is the main mechanism of failure, the $\sqrt{f_c^{'}}$ is used to convert the measured value to the normalized value. This is done by using the following expression:

$$\text{Normalized value} = \text{Measured value} \times \left[\frac{6{,}000 \text{ psi}}{f_c^{'}} \right]^{1/2}$$

where f_c' is the actual concrete compressive strength in psi and 6,000 psi is the desired concrete compressive strength. Normalizing the concrete strengths allows for a direct comparison of the variables in the various series.

After normalizing the experimental results, the maximum loads for all three series were within 10 percent of each other. When compared to series SH1, series SH2 and SH3 showed a slightly stiffer connection. Since only too specimens were tested statically in series SH1 and SH2, and one in SH3, there were too few specimens to make conclusions as to the behavior of the connector. However, the curves suggest that the alignment of the shear holes and placement of the reinforcing bars through the full-circle shear holes have minimal effect on the strength and behavior of the connector, compared to variables such as the shear hole diameter, the amount of transverse reinforcement, the number of shear holes, and the concrete compressive strength.

All three curves exhibited an almost linear stiffness phase at the beginning of the test, with over 80 percent of the maximum load maintained at a slip of 0.3 in. This is in agreement with the results obtained from previous tests at Iowa State University [10,17]. Table 5.9 shows the comparison of the experimental and predicted static strength of ASC, based on the proposed equation from the previous investigation at Iowa State University [10].

The experimentally determined static strength of the connector for all three series was within ± 10 percent of the prediction.

Table 5.9. Experimental and predicted (based on the Ref. 10) static strength of ASC.

Series	q_{test}, kips	q_{pred}, kips	$\frac{q_{test}}{q_{pred}}$
SH1	77.76	81.69	0.95
SH2	99.27	92.18	1.07
SH3	95.10	94.05	1.01

5.3.2 Fatigue Tests

Typical slip-cycle curves for specimens tested in fatigue are presented in Fig. 5.22. In general, for specimens tested at the low maximum load level (69 percent of the ultimate static strength), the fatigue slip-cycle curves exhibited three separate phases of slip characteristics. The first phase was a gradual increase of slip at the beginning of the fatigue test. The second phase was a nearly level slip curve with little increase in slip until near failure, and the last phase was a sharp increase in the rate of slip as specimens reached failure (Fig. 5.22a). Unlike the specimens tested at low maximum load level, the second phase was not clearly defined for specimens tested at high maximum load level (80 percent of ultimate static strength) (Fig. 5.22b). Having observed these types of slip characteristics on the first few specimens, it was possible to predict impending failure of the other specimens. The fatigue slip-cycle curves for all of the individual specimens are presented in Reference 22.

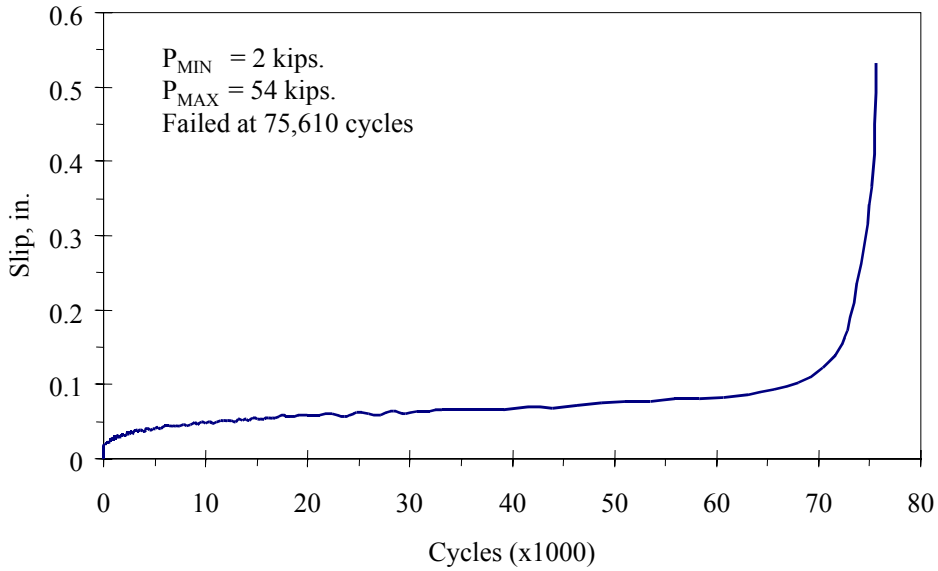

a. Typical fatigue slip-cycle curve for low load level (SH1-5 at 69 percent).

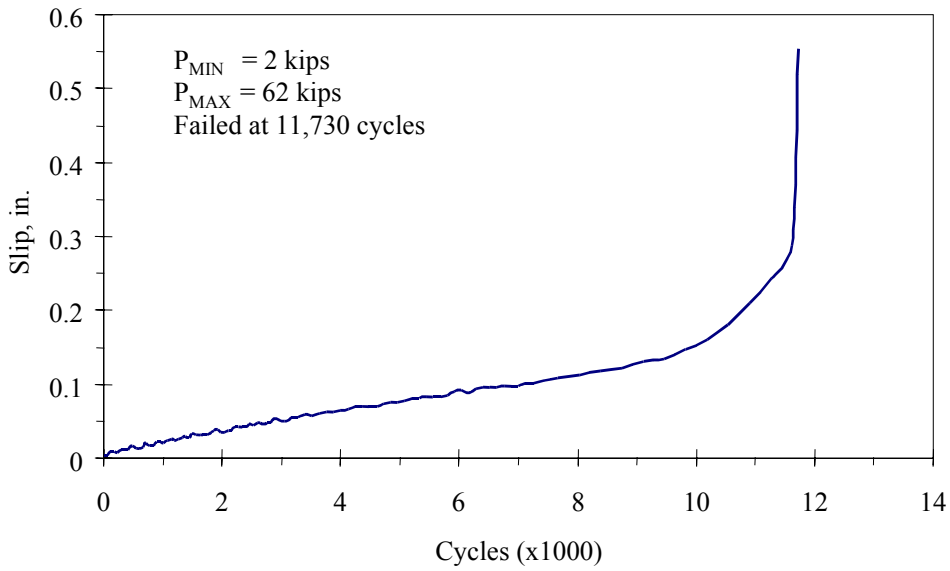

b. Typical fatigue slip-cycle curve for high load level (SH1-11 at 80 percent).

Figure 5.22 . Comparison of fatigue slip-cycle curves.

5.3.3 Failure Mechanisms

Inspection of the failed specimens revealed that the failure mechanisms did not follow any typical pattern. However, the failure mechanisms generally involved initial failure of the concrete in the high stress area around the reinforcing bar placed through the shear hole (Fig. 5.23). The highly stressed concrete area is due to the diagonal traction force and transverse pressure induced by the reinforcing bar under loading. The failure of specimen SH2-7 provided the opportunity to examine the concrete dowels after failure; Fig. 5.24 shows that the concrete dowels failed in double shear through the shear holes.

Examining the reinforcing bars placed through the shear holes revealed that the reinforcing bars were bent, except for specimen SH1-12 for reasons previously explained in Section 5.3. Bending of the reinforcing bars suggested that shear transfer by the reinforcing bars continued to provide shear resistance after the failure of the concrete dowels which assists in the redistribution of load in the ultimate state.

5.3.4 Evaluation of Fatigue Test Results

The results of the fatigue tests were plotted on S-N curves logarithmically, and have a mathematical form of:

$$\log N = \log A + B \log S \qquad \text{(Eqn. 5.1)}$$

where, S = fatigue load expressed in terms of percent of the ultimate static strength.

N = number of cycles to failure.

A, B = empirical constants.

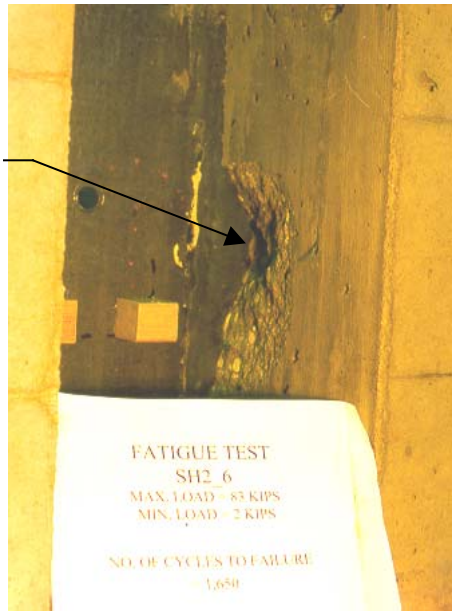

Figure 5.23. Failure of concrete in high stress area.

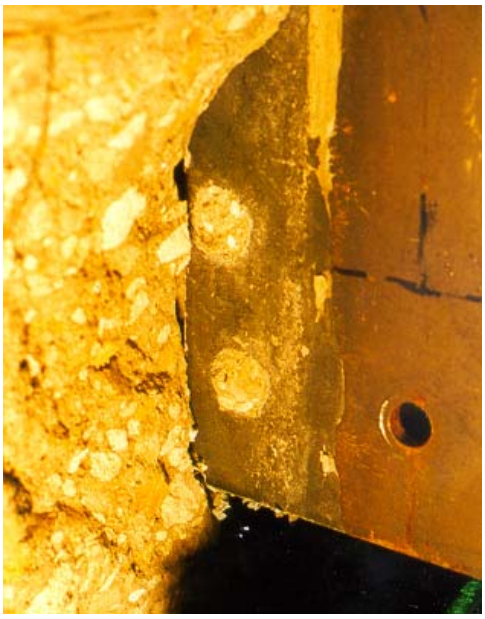

Figure 5.24. Photograph of concrete dowel failed in double shear (specimen SH2-7).

After many trials of curve fitting by the least square method, a simple linear regression analysis proved to be the best bit. The fatigue load, S, was expressed in terms of percentage of ultimate static strength, thus eliminating the strength and age differences between specimens.

The evaluations of the fatigue data are summarized in Table 5.10 and the S-N curves are plotted in Fig. 5.25. In Table 5.10, note that the data of specimen SH1-1 were not used in the evaluation of the connector in series SH1 because the specimen had not failed. As mentioned in Section 5.3, fabrication of specimen SH1-12 and SH3-1 were not consistent with other specimens. As a result, both of the specimens were not considered in the regression analysis for their respective series.

Using Eqn. 5.5, the calculated number of cycles for specimen tested in fatigue at 80 percent and 69 percent of the ultimate strength are 8,954 and 475,227 cycles, respectively.

Table 5.10. Results of regression analysis.

Series	Model	Eqn.	R^2
SH1	$\log N = 42.25 - 20.26 \log S$ [a]	(5.2)	0.852
SH2	$\log N = 85.26 - 42.72 \log S$	(5.3)	0.867
SH3	$\log N = 61.17 - 29.77 \log S$ [b]	(5.4)	0.979
SH1 + SH2 + SH3	$\log N = 55.05 - 26.85 \log S$ [c]	(5.5)	0.666

[a] SH1-1 and SH1-12 were not included in the model.

[b] SH3-1 was not included in the model.

[c] SH1-1, SH1-12 and SH3-1 were not included in the model.

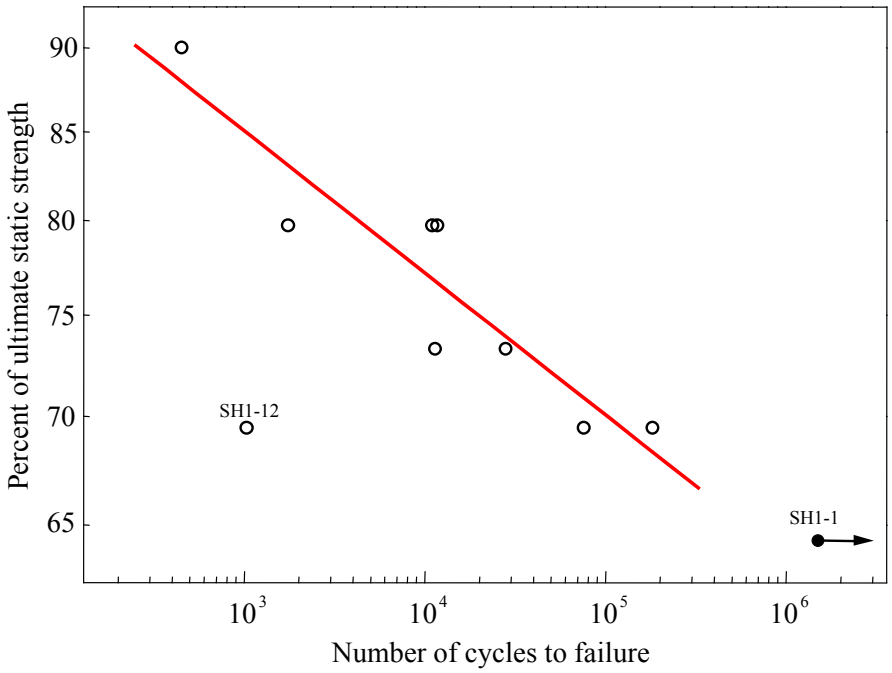

a. S-N curve for series SH1.

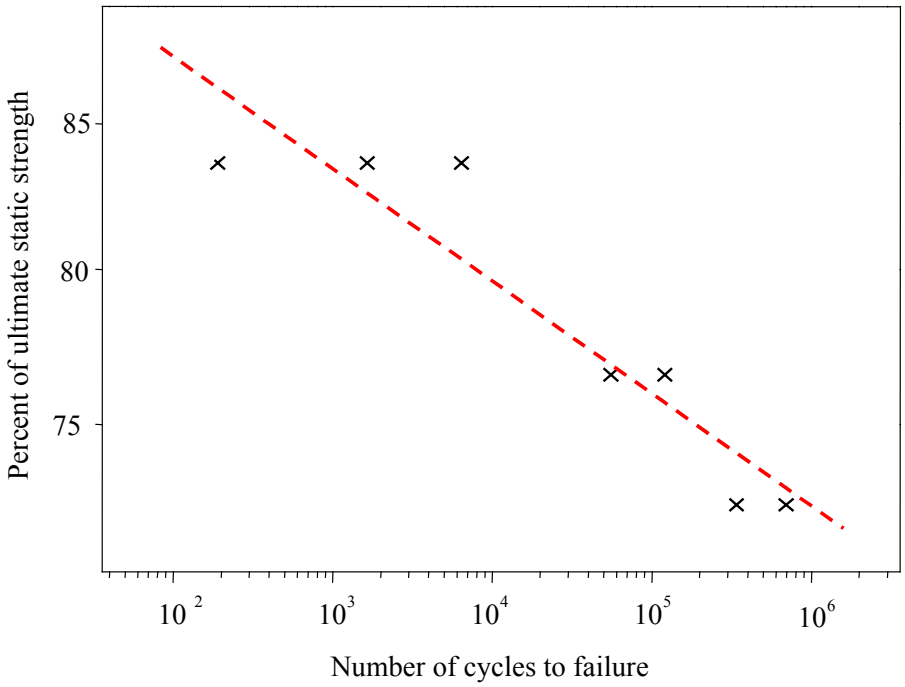

b. S-N curve for series SH2.

Figure 5.25. S-N curves.

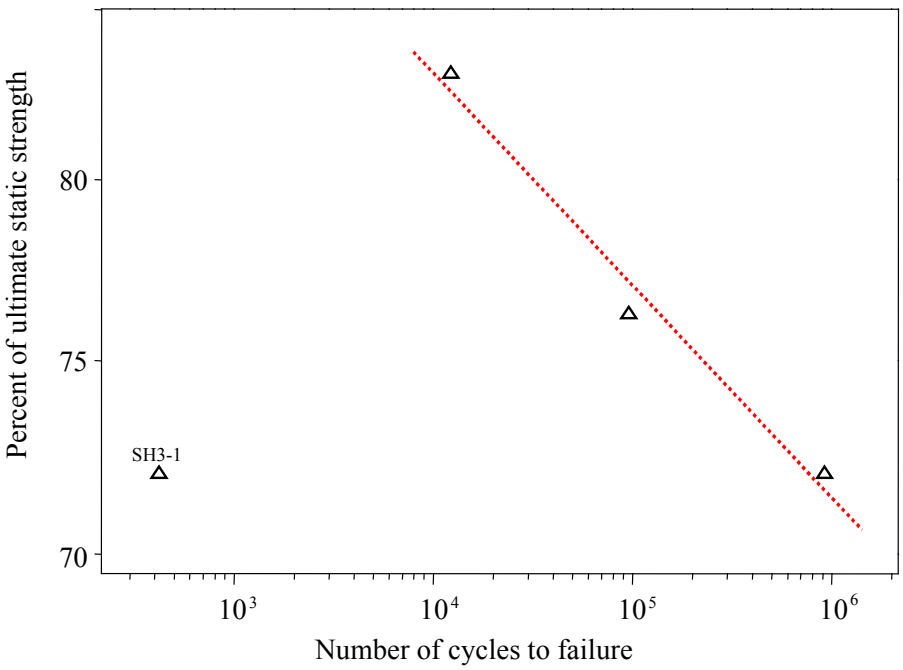

c. S-N curve for series SH3.

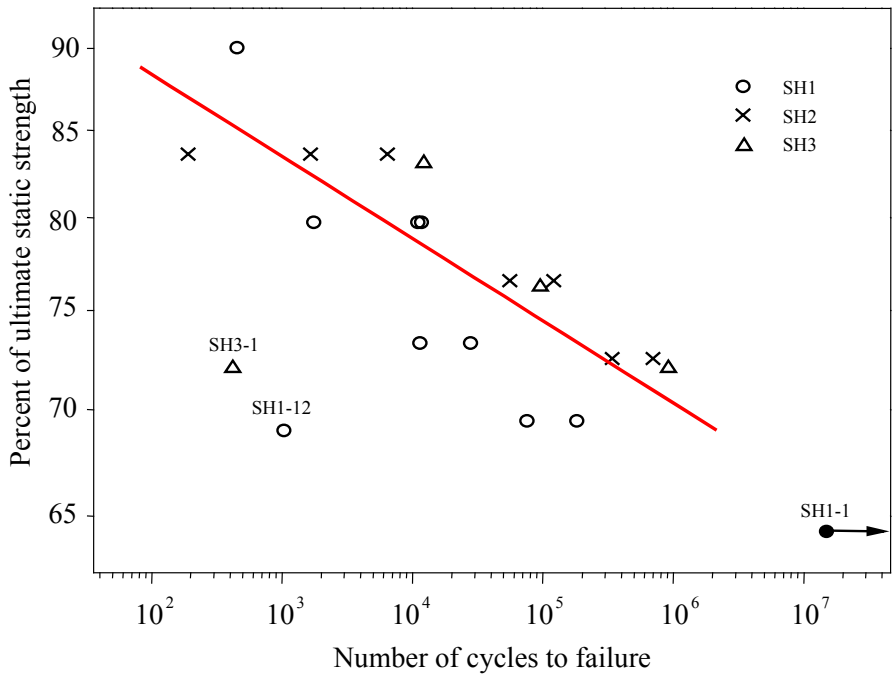

d. S-N curve for all three series.

Figure 5.25. Continued.

For comparison of the variables in the three series, curves for each series are shown in composite S-N curves in Fig. 5.26. The fatigue strength of series SH3 might not be as high as it is shown in the composite curves because the ultimate static strength of the series was determined using only specimen SH3-4 (Fig. 5.21). If higher ultimate static strength were determined by more specimens tested statically for series SH3, the S-N curve would shift downward.

The plots show that at the lower maximum load levels series SH2 has higher fatigue strength than series SH1. This infers that minimal strength was gained when the shear hole alignment was staggered. It also suggests that the best way to place the reinforcing bars

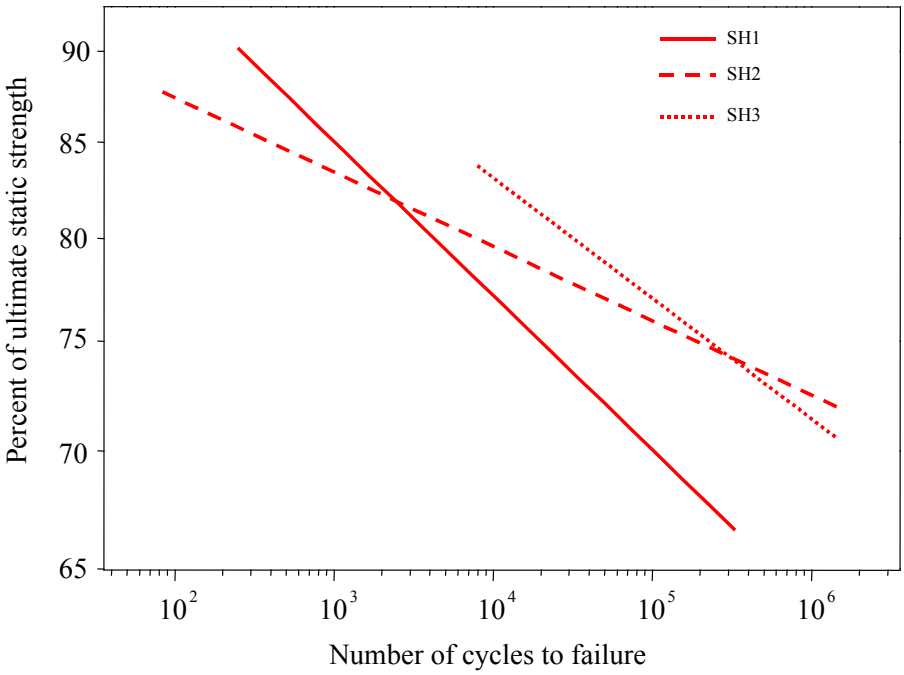

Figure 5.26. Composite S-N curves.

through the shear holes, in terms of the fatigue strength, is to use a full diameter hole as in the SH3 series test. In other words, shear holes at the edge of the shear plate for the series

SH1 need to be torched deeper than just the half-circle shear holes, for the reinforcing bar to perform more effectively.

5.3.5 Practical Design Implication

In order to relate the fatigue test results to typical design conditions, the following calculation was completed. The typical design conditions were assumed to be a single span bridge with a span length ranging from 30 to 80 ft, stringers spaced on 4.5 ft centers, and AASHTO H20 truck loading. The maximum horizontal shear found in a single span bridge varied between 34.51 kips and 35.31 kips for span lengths in the 30 to 80 ft range.

Based on a normalized concrete compressive strength of 3,000 psi, the concrete strength used in calculation, the normalized ultimate static strength of the connectors for series SH1, SH2, and SH3 is 70.0, 69.5, and 66.5 kips. respectively. To relate the typical design conditions to the fatigue test results, the horizontal shear, 35.31 kips, was expressed in terms of a percentage of the normalized ultimate static strength, which was 50.4, 51, and 53 percent for series SH1, SH2, and SH3, respectively.

Using the regression analysis model (for all three series combined), the fatigue strength of the ASC was determined to be 69 percent of the ultimate static strength at 500,000 cycles loading, the design criteria for low volume roads by AASHTO specification. This implies that the fatigue strength of the ASC was 16 percent higher than the horizontal shear in the assumed typical design conditions.

6. SUMMARY AND CONCLUSIONS

The summary and conclusions from the various tests completed in this part of the project are present in three sections: composite beam specimens, two-beam specimens, and fatigue push-out specimens.

6.1 Composite Beam Specimens

Three full-scale composite beam specimens were constructed and tested. Specimens 1 and 2 consisted of a W21x62 with its top flange and 1 in. of the web removed, resulting in an inverted T-beam. The top 2 1/2 in. of the remaining web was embedded into an 8 in. concrete slab. Specimen 3 was a W21x62 with its top flange embedded 3 1/4 in. into an 8 in. concrete slab.

All three specimens utilized the ASC. The ASC for Specimens 1 and 2 consisted of 1 1/4 in. diameter (torched) holes spaced on 3 in. centers; the exception to this was a half hole every 15 in. at the top of the inverted T-beam. Placed at the bottom of every half hole was a #4 reinforcing bar. Since the top flange was not removed in Specimen 3, the ASC was slightly modified from that used in Specimens 1 and 2. It consisted of a continuous line of 1 1/4 in. diameter holes spaced at 3 in. on centers, and the #4 reinforcing bars were placed at the bottom of every fifth hole (15 in. spacing).

An ultimate load test, following three service load tests, was performed on each specimen. Specimens 1 and 3 were loaded statically and Specimen 2 was loaded cyclically. The load was applied by two line loads across the slab width, each located 4 ft – 6 in. from midspan. Strains, deflections, and slip were measured during service and ultimate load

testing. The purpose of the composite beam tests was to further investigate the static and fatigue strength of the ASC.

From the service and ultimate load tests the following conclusions can be made about the ASC, with and without the top flange:

- The ASC was effective in creating full composite action during service level loading.
- Rigid behavior was exhibited by the ASC at service level conditions, however, at failure the ASC was ductile.
- The ASC was able to transmit the horizontal shear force required to develop the ultimate moment capacity, as intended by design, for both Specimens 1 and 3.
- With the top flange intact (i.e., Specimen 3), the ASC was able to develop a 7% greater moment than without a top flange (i.e.,, Specimen 1) and slip was considerably less at failure due to its ability to confine the concrete tightly around the holes.
- The ASC is not prone to fatigue problems since it provides a rigid connection at service level. While exhibiting little slip, the ASC withstood 464,000 cycles of a load coinciding with 75% of the specimen's ultimate moment capacity, which is more than adequate for a bridge on a low-volume road.

For the following reasons, one may want to use a complete-beam rather than one with the top flange removed (to obtain the desired beam depth):

- Better confinement of the concrete around the ASC holes is achieved with a top flange.
- Added cost and time to remove the top flange.

- Slight increase in flexural stiffness with the top flange.
- The top flange provides lateral stability to the steel beam during construction.

6.2 Two-beam Specimens

Two full-scale two-beam specimens, incorporating the ASC with other modifications to the BISB, were constructed and tested. Both specimens utilized the same ASC configuration as in Specimen 3. Specimen 4 represented a Steel-free Deck System, which is more of a modification of the conventional slab-on-girder system than that of the BISB. The system was constructed similar to Specimen 3 except the concrete slab was unreinforced. Specimen 5, representing a Concrete Arch System, was more directly related to the BISB than was Specimen 4 in that the steel beams were fully encased in concrete. The modifications to the BISB, offered by both systems, included the removal of concrete in tension and composite construction through the use of the ASC.

The two-beam testing program involved an investigation that focused on the behavior of a slab and beam system, rather than just the ASC. Tests were performed at three locations on Specimen 4 and at two locations on Specimen 5. Three service load tests and an ultimate load test was performed at each location. Loading consisted of a single concentrated load, representing a wheel load, applied between the steel beams (longitudinal centerline of the specimen). Strains and deflections were measured during service and ultimate load testing. The purpose of the tests was to determine the potential application of the bridge systems, represented by Specimens 4 and 5.

Based on the service and ultimate load tests, the following conclusions were made:

Steel-free Deck System:

- Service load deflections were less than allowable (L/800) according to AASHTO.
- Relative to the steel beams, the concrete slab deflected very little at service level conditions.
- Punching shear failures at all load positions indicated that the #5 reinforcing bars, spaced on 15 in. centers, provided the lateral restraint required to develop arching action in the concrete slab; therefore, additional reinforcement is not needed for strength purposes.
- Four #5 reinforcing bars, spaced on 3 in. centers and located at both ends of the specimen, provided adequate edge stiffening to maintain the arching action near a transverse free edge.
- A punching shear failure at midspan occurred shortly before the ultimate moment capacity was attained.
- Failure loads were much greater than the factored AASHTO wheel loads.
- The Steel-free Deck System, as represented by Specimen 4, has the potential for use as a bridge alternative on low-volume roads.

Concrete Arch System:

- Service load deflections were less than allowable (L/800) according to AASHTO.
- Relative deflection of the slab did not occur during service load testing nor did it occur during ultimate load testing.
- Failure at midspan occurred when the ultimate moment capacity was reached.

- While supporting the steel beams, the concrete arch was able to sustain additional load after the specimen attained its ultimate moment capacity. The resulting failure was by punching shear, initiated by longitudinal splitting at the top of the arch.
- Punching shear initiated by longitudinal splitting was also the mode of failure near the end of the specimen. It is suspected that this is a typical failure mode unless a flexural failure occurs first.
- Failure loads were much greater than the factored wheel load based on AASHTO.
- The Concrete Arch System offers excellent ductility and a lateral restraint that is more than sufficient.
- As represented by Specimen 4, the Concrete Arch System has the potential for use as a bridge alternative low-volume roads.

6.3 Fatigue Push-out Specimens

The ASC was investigated in an earlier study [10] to determine its static strength, behavior, and effectiveness in composite action. This study was undertaken to investigate the fatigue behavior of the connector.

The fatigue behavior of the connector was investigated using 27 push-out specimens. Six of the 27 push-out specimens were tested statically to determine the ultimate static strength of the connector. Fatigue tests were conducted at various load levels corresponding to various percentages of the ultimate static strength, to determine the relationship between the fatigue load and the fatigue life of the connector and to determine the slip of the connector during testing. Three different shear hole arrangements were investigated to

determine their effect on the fatigue strength, with variables such as alignment of shear holes and placement of reinforcing bars through the shear holes being evaluated.

The results of the static tests conducted were in good agreement with the previous investigation [10]. The experimentally determined static strength of the connector for all three series was within ± 10 percent of the predicted strength, based on the previously proposed relationship. Alignment of the shear holes and placement of the reinforcing bars through the full-circle shear holes has minimal effect on the static performance of the connector.

After testing to 1.5 million cycles at 64 percent of the ultimate static strength, specimen SH1-1 experienced less than 0.05 in. of slip and still exhibited slip characteristic similar to the specimens that were not loaded in fatigue. After the 1.5 million cycles, specimen SH1-1 was loaded statically to failure and maintained over 80 percent of its maximum load at a slip of 0.3 in.

The performance of the specimens under fatigue load was different between low and high maximum levels of load. At low maximum load levels, the connection exhibited three separate phases of slip characteristics: a gradual increase of slip, a region with little increase in slip, and a sharp increase in the rate of slip as specimens reached failure. Unlike the specimens tested at low maximum load level, the second phase was not clearly defined for specimens tested at high maximum load levels.

The failure mechanism of the specimens involved the failure of the concrete in the high stress area induced by the reinforcing bars through the shear holes, with the concrete dowels failing in double shear through the shear holes. The reinforcing bars placed through the shear holes continue to provide shear resistance after the failure of the concrete dowels.

The least square curve fit method was used to evaluate the fatigue test results. A mathematical model expressing the logarithm of the fatigue life as a linear function of the logarithm of the fatigue load was found to provide the best fit of the test data. The fatigue load was expressed in terms of the percentage of the ultimate static strength. The S-N curves indicated that the connectors gained minimal strength in fatigue when the shear hole alignment was staggered, and the reinforcing bars were included in the full-circle shear holes.

As a result of this investigation, the following conclusions can be made:

- The experimentally determined static strength of the ASC was within ± 10 percent of the predicted strength using the equation previously developed for the ultimate strength of ASC.
- Specimen SH1-1 showed that the shear connector underwent less than 0.05 in. (1.5 mm) of slip and still maintained its composite action, even after tested to 1.5 million cycles at 64 percent of the ultimate static strength.
- Under fatigue loading at low maximum load levels, the connection exhibited three separate phases of slip characteristics: a gradual increase of slip, a region with little increase in slip, and a sharp increase in the rate of slip as specimens reached failure. At high maximum load level, the second phase was not as clearly defined.
- Fatigue load of the connector is linearly related to its fatigue life logarithmically. The number of cycles attained for specimen tested in fatigue at 80 percent and 69 percent of the ultimate strength are 8,954 and 475,227 cycles, respectively.
- The S-N curves reveal that the connectors gained minimal strength when the shear hole alignment was staggered.

- The best way to place the reinforcing bars through the shear holes, to improve fatigue strength, is to use a full diameter hole (as in the SH3 series) which ensures that the reinforcement bar will develop double shear.
- If shear holes are torched at the edge of the web for the convenience of placing the reinforcing bars in the shear holes, they need to be cut deeper than just a half-circle shear hole.
- Fatigue strength of the ASC was 69 percent of the ultimate static strength at 500,000 cycles loading, which was approximately 16 percent higher than the horizontal shear found in a typical single span bridge.

7. RECOMMENDED RESEARCH

On the basis of the work completed in this phase of the investigation, the following two tasks would be logical in bringing this research to a successful, practical conclusion.

1. Sufficient laboratory research has been completed on the ASC so that it is ready for use in a demonstration bridge (i.e. develop the required composite connection between steel beams and the concrete deck using the ASC rather than the welded shear studs). Although the ASC could be used in any composite bridge, it is proposed that it be used in the Steel Beam Precast Units that were used in the Black Hawk Demonstration Bridge documented in Volume 1 of the final report for this investigation. The use of the ASC in the Steel Beam Precast Units would further simplify their fabrication. The bridge in which the ASC were employed would be instrumented and service load tested upon completion and periodically inspected and re-tested during the first two years of service.
2. The modifications proposed to the BISB systems shown in Fig. 1.1b (obtaining composite action between the steel beams and concrete and reducing the amount of concrete in tension) have been successfully tested in the laboratory. Prior to using this system in a demonstration bridge, the effects of increasing the distance between beams (which obviously would reduce the number of steel beams required in a given bridge) and lowering the holes associated with the ASC in the beam webs (to improve the resistance to transverse tension forces caused by loading between the steel beams) need to be investigated in the laboratory. Upon

completion of these few tests, a full scale demonstration bridge using the modified BISB concept should be designed and constructed. This bridge would be instrumented and service load tested upon completion and periodically re-tested during the first two years. All phases of construction would be videotaped and photographed for use by county engineers in training their crews to construct this type of bridge.

8. ACKNOWLEDGEMENTS

The study presented in this report was conducted by the Bridge Engineering Center under the auspices of the Engineering Research Institute of Iowa State University. The research was sponsored by the Project Development Division of the Iowa Department of Transportation and the Iowa Highway Research Board under Research Project TR-410.

The authors wish to thank the various Iowa DOT and county engineers who provided their input and support. In particular, we wish to thank the project advisory committee:

- Dennis J. Edgar: Assistant County Engineer Fayette County
- Robert L. Gumbert: County Engineer, Tama County (retired)
- Gerald D. Petermeier: County Engineer, Benton County (retired)
- Wallace C. Mook: Director of Public Works, Bettendorf
- Jim Witt: County Engineer, Cerro Gordo and Winnebago Counties

Special thanks are given to Doug Wood, Manager of the ISU Structural Engineering Laboratory. Thanks are also given to the following Civil Engineering graduate and undergraduate students for their assistance in various aspects of the project: Rick Boss, Peter Fanous, Melissa Leek, Chris Lundeen, Juli Manchester, Erik Raker, and Mike Williams.

9. REFERENCES

1. American Association of State Highway and Transportation Officials (AASHTO), LRFD Bridge Design Specifications, First Edition, Washington, D.C., 1994.

2. American Society of Civil Engineering, "1998 Report Card for America's Infrastructure", Washington, D.C., 1998.

3. Bakht, B., "Revisiting Arching in Deck Slabs", Canadian Journal of Civil Engineering, Vol. 23, pp. 973-981, 1996.

4. Bakht, B. and Agarwal, A.C., "Deck Slabs of Skew Bridges", Canadian Journal of Civil Engineering, Vol. 22, pp. 514-530, 1995.

5. Bakht, B. and Markovic, S., "Accounting for Internal Arching in Deck Slab Design", Journal-Institute of Engineering India Part CI, Vol. 67, No. 1, pp. 18-25, 1986.

6. Bakht, B., Mufti, A.A., and Jaeger, L.G., "Design Provisions for Steel-free Deck Slabs", Developments in Short and Medium Span Bridge Engineering '98. Limit States and LRFD Codes., 1998.

7. Bakht, B. and Selvadurai, A.P.S., "Performance of Steel-free Deck Slabs Under Simulted Wheel Loads", Second International Conference on Advanced Composite Materials in Bridges and Structures, Montreal, Canada, pp. 767-776, 1996.

8. King, D. C., Slutter, R. G., and Driscoll, G. C., Jr. "Fatigue Strength of 1/2-Inch Diameter Stud Shear Connectors", Highway Research Record, Highway Research Board, Washington, D.C., No 103, pp. 78-106, 1965.

9. Klaiber, F.W., Wipf, T.J., Phares, B.M., "Investigation of Two Bridge Alternatives for Low Volume Roads, Concept 1: Steel Beam Precast Units", Iowa Department of Transportation Project HR-382, ISU-ERI-Ames 97405, Iowa State University, Ames, Iowa, 1997.

10. Klaiber, F.W., Wipf, T.J., Reid, J.R., and Peterson, M.J., "Investigation of Two Bridge Alternatives for Low Volume Roads, Concept 2: Beam-in-Slab Bridge", Iowa Department of Transportation Project HR-382, ISU-ERI-Ames 97405, Iowa State University, Ames, Iowa, 1997.

11. Lehman, H.G., Lew, H.S. and Toprac, A.A., "Fatigue Strength of 3/4-Inch Studs in Lightweight Concrete", Texas Highway Department Project 3-5-64-76, Center for Highway Research, The University of Texas, Austin, Texas, May 1965.

12. Leonhardt E.F., Andra W., Andra H.P., Harre W., "New Improved Shear Connector With High Fatigue Strength for Composite Structures (Neues, vorteilhaftes Verbundmittel fur Stahlverbund--Tragwerke mit hoher Dauerfestigkeit)", Beton--Und Stahlbetonbau, Vol. 12, pp. 325-331, 1987.

13. Mufti et al., "Experimental Investigation of Fibre-reinforced Concrete Deck Slabs Without Internal Steel Reinforcement", Canadian Journal of Civil Engineering, Vol. 20, pp. 398-406, 1993.

14. Nauman, J.C., Testing an Alternative Shear Connector and the Modifications to a Beam-in-Slab-Bridge System, M.S. Thesis, Iowa State University, Ames, Iowa 1999.

15. Ontario Highway Bridge Design Code (OHBDC), Ministry of Transportation of Ontario, Downsview, Ontario, Canada, 1979, 1983 and 1992.

16. Peterson, M.J., Testing and Modifications of the Beam-in-Slab Bridge System for Use in Short-Span Low-Volume Bridges, M.S. Thesis, Iowa State University, Ames, Iowa, 1998.

17. Reid, J.W., Bridge Alternatives for Low-Volume County Roads, M.S. Thesis, Iowa State University, Ames, Iowa, 1997

18. Roberts, W.S. and Heywood, R.J., "Development and Testing of a New Shear Connector for Steel Concrete Composite Bridges", Proceedings, Fourth International Bridge Engineering Conference on Short and Medium Span Bridges. Developments in Short and Medium Span Bridge Engineering '94., pp. 137-145, 1994.

19. Roberts, W.S. and Heywood, R.J., "An Innovation to Increase the Competitiveness of Short Span Steel Concrete Composite Bridges", Proceedings, Fourth International Conference on Short and Medium Span Bridges. Developments in Short and Medium Span Bridge Engineering '94, Halifax, Novia Scotia, Canada, pp. 1160-1171, 1994.

20. Salmon, C.G. and Johnson, J. E., Steel Structures Design and Behavior, Fourth Edition., New York: HarperCollins College Publishers, 1996.

21. Slutter, R.G., and Fisher, J.W., "Fatigue Strength of Shear Connectors", Highway Research Record, Highway Research Board, Washington, D.C., No 147, pp. 65-88, 1966.

22. Siow, Y.S., Push-Out Fatigue Tests of the Alternate Shear Connector, M.S. Thesis, Iowa State University, Ames, Iowa, 1998.

23. Thurlimann, B., "Fatigue and Static Strength of Stud Shear Connectors", Jour. ACI, Vol. 30, No 12, pp. 1287-1302, June 1959.

24. Toprac, A.A., "Fatigue Strength of 3/4-Inch Stud Shear Connectors", Highway Research Record, Highway Research Board, Washington, D.C., No 103, pp. 53-77, 1965.

25. Wipf, T.J., Klaiber, F.W., Besser, D.M., and LaViolette, M.D., "Manual for Evaluation, Rehabilitation and Strengthening of Low Volume Bridges", Iowa Department of Transportation Project HR 323, ISU-ERI-Ames-93062, Iowa State University, Ames, Iowa, 1993.

26. Wipf, T.J., Klaiber, F.W., and Prabhakaran, A., "Evaluation of Bridge Replacement Alternatives for the County Bridge System", Iowa Department of Transportation Project HR-365, ISU-ERI-Ames 95403, Iowa State University, Ames, Iowa, 1994.

27. Yam, L.C.P. Design of Composite Steel-Concrete Structures, London: Surrey University Press, 1981.